UNIVERSITY OF CALIFORNIA,

IRVINE

# $IP_3$-Mediated $Ca^{2+}$ Signaling Deficit in Monogenic and Sporadic Forms of Autism Spectrum Disorders

DISSERTATION

submitted in partial satisfaction of the requirements

for the degree of

DOCTOR OF PHILOSOPHY
in Biomedical Sciences

by

Galina Schmunk

Dissertation Committee:

Professor J. Jay Gargus, MD, PhD, Chair
Department of Physiology & Biophysics, Department of Pediatrics

Professor Ian Parker, PhD, FRS
Department of Neurobiology and Behavior, Department of Physiology & Biophysics

Professor Michael D. Cahalan, PhD
Department of Physiology & Biophysics

2017

## DEDICATION

I dedicate this work to people with autism, their families, and caregivers.

**TABLE OF CONTENTS**

## LIST OF FIGURES

## LIST OF TABLES

## LIST OF ABBREVIATIONS

| | |
|---|---|
| AD | Alzheimer's disease |
| ADHD | attention deficit hyperactivity disorder |
| ADOS | Autism Diagnostic Observation Schedule |
| ADP | adenosine diphosphate |
| ASD | autism spectrum disorders |
| ATP | adenosine triphosphate |
| $Ca^{2+}$ | calcium |
| CART | Center for Autism Research and Translation |
| CICR | $Ca^{2+}$-induced $Ca^{2+}$ release |
| EEG | electroencephalogram |
| EGTA | ethylene glycol-bis(β-aminoethyl ether)-N,N,N',N'-tetraacetic acid |
| EPSC | excitatory postsynaptic current |
| ER | endoplasmic reticulum |
| FLIPR | fluorometric imaging plate reader |
| FXS | fragile X syndrome |
| GPCR | G protein-coupled receptor |
| $IP_3$ | inositol 1,4,5-trisphosphate |
| $IP_3R$ | inositol 1,4,5-trisphosphate receptor |
| LTD | long-term depression |
| LTP | long-term potentiation |
| PLC | phospholipase C |
| PWS | Prader-Willi syndrome |
| RyR | ryanodine receptor |
| SCA | spinocerebellar ataxia |
| TSC | tuberous sclerosis syndrome |
| UDP | uridine diphosphate |
| UTP | uridine triphosphate |

**ACKNOWLEDGMENTS**

I would like to express my deepest gratitude to my advisor and committee chair, Dr. J. Jay Gargus for his continuous support of my scientific curiosity and extracurricular endeavors. His scientific insights about molecular mechanisms of autism spectrum disorders and guidance in the field of genetic syndromes have been an integral part of my development as a scientist.

I would like to express my deep appreciation to my co-mentor and committee member, Dr. Ian Parker, for gracefully providing me with a "foster lab family" to develop into a careful and thorough scientist, and generously sharing his time, energy, and scientific insights about biophysics, $IP_3$ receptors, and $Ca^{2+}$ imaging.

Special thanks go to Dr. Michael Cahalan, my committee member and the Chair of the Physiology and Biophysics department, for his help and advice throughout my graduate school.

I would like to thank Kyle Ellefsen, who as a good friend was always willing to help and give his best suggestions. It would have been a lot of lonely evenings in the lab without him. Many thanks to other lab members, Divya Swaminathan, Jeffrey Lock, Ian Smith, Lu Forrest, Angelo Demuro, and George Dickinson, and the members of my other group, David Ferguson, Rachel Nguyen, and Kenny Kumar.

I thank my husband, David Schmunk, for his continuous support and encouragement. If not for him, I would not have courage to start this amazing trip called "grad school". I thank my immediate family in Russia and the acquired one across the United States. Deep appreciation goes to my friends, Marina Shmunk, Irene Vorontsova, Carley Karsten and Irina Ushach for their words of wisdom, support, and heartfelt laughter.

I thank Nature Publishing Group for first accepting my papers and then their permission to reprint them in chapter 2 and 4 of this dissertation. I also thank all co-authors who contributed to the work.

This work was supported by The Thompson Family Foundation through a generous gift to The UCI Center for Autism Research and Translation (to J.J. Gargus) through The Center for Autism and Neurodevelopmental Disorders, an entrepreneurial public-private partnership, and National Institutes of Health grant GM048071 (to Ian Parker).

## CURRICULUM VITAE

### EDUCATION

2011 –2017 **PhD in Biomedical Sciences, University of California, Irvine**

- Program in Cellular and Molecular Biology, Department of Physiology and Biophysics

2009 (2007) **M.S. (B.S.), Mendeleev University of Chemical Technology, Moscow**

- Chemical Engineering (major: Small Organic Synthesis and Chemistry of Dyes). Thesis title: "Development of oligomer synthesis methods based on (R)-2 ((1R, 2S)-2-aminocyclohexyl) butanoic acid"

### WORK EXPERIENCE

2013 – 2017 **PhD student; project on $IP_3$-mediated calcium signaling in autism spectrum disorders**

- Profs. J. Jay Gargus and Ian Parker – University of California, Irvine

2012 – 2013 **PhD student; project on the Kv1.3 potassium channel function and its role in colorectal cancer and obesity**

- Prof. K. George Chandy – University of California, Irvine

2009 – 2010 **Pharm-Sintez**, Chemist, Moscow, Russia

- Synthesis, isolation and purification of a synthetic growth hormone inhibitor Octreotide

2008 – 2009 **Undergraduate researcher; synthesis and analysis of gamma aminoacids**

- Prof. S. H. Gellman – University of Wisconsin, Madison.

### PATENTS

1. Defective calcium signaling as a tool in autism spectrum disorders, Appl. No. 62/035,412; UC Ref. 2014-805-1. Inventors: J.J. Gargus, **G. Schmunk**, I. Parker, I. Smith

## PUBLICATIONS

1. **Schmunk, G**., Nguyen, R. L., Ferguson, D. L., Kumar, K., Parker, I. & Gargus, J. J. High-throughput screen detects calcium signaling dysfunction in typical sporadic autism spectrum disorder. *Scientific Reports,* **7,** 40740 (2017).
2. **Schmunk, G**., Boubion, B. J., Smith, I. F., Parker, I. & Gargus, J. J. Shared functional defect in $IP_3R$-mediated calcium signaling in diverse monogenic autism syndromes. *Transl. Psychiatry* **5,** e643 (2015).
3. Gargus, J. J. & **Schmunk, G**. in *Compr. Guid. to Autism* (Vinood B. Patel, Victor R. Preedy, C. R. M.) 1285–1312 (Springer Science+Business Media New York, 2014).
4. **Schmunk, G**. & Gargus, J. J. Channelopathy pathogenesis in autism spectrum disorders. *Front. Genet.* **4,** 222 (2013).
5. Upadhyay, S. K., Eckel-Mahan, K. L., Mirbolooki, M. R., Tjong, I., Griffey, S. M., **Schmunk, G**., Koehne, A., Halbout, B., Iadonato, S., Pedersen, B., Borrelli, E., Wang, P., Mukherjee, J., Sassone-Corsi, P. & Chandy, K. G.. Selective Kv1.3 channel blocker as therapeutic for obesity and insulin resistance. *Proc. Natl. Acad. Sci. U. S. A.* **110,** E2239–2248 (2013).
6. Nguyen, H. M., Galea, C. A., **Schmunk, G**., Smith, B. J., Edwards, R. A., Norton, R. S. & Chandy, K. G.. Intracellular trafficking of the KV1.3 potassium channel is regulated by the prodomain of a matrix metalloprotease. *J. Biol. Chem.* **288,** 6451–6464 (2013).

## INVITED TALKS

1. "Calcium signaling defects in monogenic models of ASD and in sporadic autism". UCI Center for Autism Research and Translation Symposium, Irvine, CA, Dec. 2015
2. "Reduced $IP_3$-mediated calcium signaling in autism spectrum disorder", selected abstract for a data blitz presentation, Society for General Physiologists, Woods Hole, MA, Sep. 2015
3. "Reduced $IP_3$-mediated calcium signaling in autism spectrum disorders in the context of fragile X and tuberous sclerosis syndromes". Gordon Research Conference/Seminar, selected speaker, Newry, ME, June 2015
4. "Calcium signaling defects in monogenic models of ASD in the context of fragile X and tuberous sclerosis syndromes". UCI Center for Autism Research and Translation Symposium, Irvine, CA, Nov. 2014

## CONFERENCE POSTER ABSTRACTS

1. **Galina Schmunk**, Rachel L. Nguyen, Kenny Kumar, David L. Ferguson, Ian Parker, J. Jay Gargus. "$IP_3$-mediated $Ca^{2+}$ signaling biomarker for typical non-syndromic forms of autism spectrum disorders" – Advances and Breakthroughs in Calcium Signaling, Honolulu, April 2016

2. **Galina Schmunk**, Rachel L. Nguyen, Kenny Kumar, David Ferguson, Ian Parker, J. Jay Gargus. "Typical non-syndromic forms of autism spectrum disorders share the same reduced $IP_3$-mediated $Ca^{2+}$ signaling originally identified in rare syndromic forms" – Biophysical Society 59th Annual Meeting, March 2016

3. **Galina Schmunk**, Rachel L. Nguyen, Kenny Kumar, Dave Ferguson, Ian Parker, J.Jay Gargus. "Reduced $IP_3$-mediated $Ca^{2+}$ signaling in syndromic and non-syndromic forms of autism spectrum disorders" – Society of General Physiologists meeting, 69th annual meeting, September 2015

4. **Galina Schmunk**, Bryan J. Boubion, Ian F. Smith, Ian Parker, J. Jay Gargus. "Reduced $IP_3$-mediated $Ca^{2+}$ signaling in autism spectrum disorders in the context of fragile X and tuberous sclerosis syndromes" – Gordon Research Conference, June 2015

5. **Galina Schmunk**, Bryan J. Boubion, Ian F. Smith, Ian Parker, J. Jay Gargus. "$IP_3$-mediated $Ca^{2+}$ signaling defects in autism spectrum disorders" – ICTS Clinical Translational Research Day, UCI, May 2015.

6. **Galina Schmunk**, Bryan J. Boubion, Ian F. Smith, Ian Parker, J. Jay Gargus. "Reduced $IP_3$-mediated $Ca^{2+}$ signaling in autism spectrum disorders in the context of fragile X and tuberous sclerosis syndromes" – Biophysical Society 59th Annual Meeting, Feb. 2015

**ABSTRACT OF THE DISSERTATION**

$IP_3$-Mediated $Ca^{2+}$ Signaling Deficit in Monogenic and Sporadic Forms of Autism Spectrum Disorders

By

Galina Schmunk

Doctor of Philosophy in Biomedical Sciences

University of California, Irvine, 2017

Professor John Jay Gargus, Chair

Autism spectrum disorder (ASD) affects 2% of children and is characterized by impaired social and communication skills together with repetitive, stereotypic behavior. The pathophysiology of ASD is complex due to genetic and environmental heterogeneity, complicating the development of therapies and making diagnosis challenging. Growing evidence supports a role of disrupted $Ca^{2+}$ signaling in ASD. I developed and applied a high-throughput fluorometric imaging plate reader (FLIPR) assay to monitor agonist-evoked $Ca^{2+}$ signals in human primary skin fibroblasts. My results indicate that $IP_3$ -mediated $Ca^{2+}$ release from the endoplasmic reticulum in response to activation of purinergic receptors is significantly depressed in subjects with sporadic, as well as rare syndromic forms of ASD. This was apparent in $Ca^{2+}$ signals evoked by G protein-coupled receptors and by photoreleased $IP_3$ at the levels of both

global and local elementary $Ca^{2+}$ events, suggesting fundamental defects in $IP_3R$ channel activity in ASD.

Given the ubiquitous involvement of $IP_3R$-mediated $Ca^{2+}$ signaling in neuronal excitability, synaptic plasticity, gene expression and neurodevelopment, I further expanded my findings to a murine model of FXS. Activation of the $IP_3$ cascade *via* plasma membrane metabotropic receptors did not reveal any $Ca^{2+}$ signaling deficits in neurons from mice with the *FMR1* gene deletion. Glial cells from FXS mice did not demonstrate any sizable difference in response to GPCR activation, or $IP_3$ UV flash uncaging as compared with wild type. Finally, mouse fibroblasts from FXS mice assayed with the high-throughput screen FLIPR, analogous to what was used on the human skin fibroblasts, did not reveal any difference in the $IP_3$-mediated $Ca^{2+}$ release compared with wild type mice. These findings highlight divergence between animal models and human conditions, and show inadequacy of the murine model in studying the effect of the *FMR1* gene mutation on $IP_3$ signaling cascade.

In conclusion, my findings suggest that deficits in $IP_3$-mediated $Ca^{2+}$ signaling represent a convergent function shared across the spectrum of autistic disorders – whether caused by rare highly penetrant mutations or sporadic forms – and hold promise as a biomarker for diagnosis and novel drug discovery. This work also highlights potential pharmaceutical targets, and identifies $Ca^{2+}$ screening in human skin fibroblasts as a promising technique for early detection of individuals susceptible to ASD.

# Chapter 1. Introduction

## *1.1 Autism spectrum disorder.*

Autism spectrum disorder (ASD) is a complex neurodevelopmental disorder with three core behavioral features: 1) qualitative impairment in social skills, 2) delayed or disordered language and communication skills, and 3) restricted and repetitive behaviors. With the May 2013 publication of the American Psychiatric Association Diagnostic and Statistical Manual (DSM-5), all autism subtypes, including Asperger's Disorder and Pervasive Developmental Disorder Not Otherwise Specified (PDD-NOS) were merged into one umbrella diagnosis of ASD (Association 2016). The symptoms are highly variable and often co-exist with other neuropsychiatric disorders, such as developmental delay, epilepsy, hyperactivity, and attention deficit hyperactivity disorder (ADHD). The most recent report from the Centers for Disease Control and Prevention estimates ASD prevalence to be 1 in 68 of children (Blumberg and Bramlett 2013), a sharp 29% increase from the preceding estimate of 1 in 88 in 2008 and a 64% increase from 1 in 110 in 2006. ASD prevalence estimates vary by gender and racial/ethnic group, with boys being more than 4 times more affected than girls, and non-Hispanic white children being 30% more likely to be diagnosed with ASD than non-Hispanic black children and 50% more likely than Hispanic children (Autism and Developmental Disabilities Monitoring Network Surveillance Year 2010 Principal Investigators 2014).

Symptoms of autism typically start between the second and third year of life and cause problems of a wide range in various areas of development. The symptoms and severity vary widely across autistic individuals, complicating diagnosis of this complex spectrum

encompassing many phenotypes and co-morbidities, and giving rise to a tragic "diagnostic odyssey" that delays diagnosis, and hence treatment, until the typical mean age of 5yrs (Pringle et al. 2012). Early diagnosis is critical for optimal intervention (Anderson, Liang, and Lord 2014; MacDonald et al. 2014), and accurate diagnosis is crucial in order to exclude other potential conditions which may require different therapies. However, objective quantifiable biochemical markers of this disease have been very hard to come by, delaying the age of diagnosis.

Diagnosis of ASD is made based on questionnaires and behavioral tests, relying on parent observations and comprehensive evaluation by psychologists, pediatricians, psychiatrists, and speech therapists (for a recent review, see (Constantino and Charman 2015)). ASD diagnosis for research studies is stricter, more complex, time consuming and quantitative, but even at this most refined level ASD remains a group of developmental disorders that are only behaviorally, not yet pathophysiologically, defined (Filipek 2013).

There is a great need for new therapeutics targeted against the core deficits in ASD (Ghosh et al. 2013). Currently there are no approved pharmaceutical drugs to target communication and social deficits and repetitive behavior. Currently available treatments focus on non-core symptoms of ASD and other co-morbidities, such as seizures, ADHD, depression, and sleep disorders. Drug development has proven to be problematic because of our limited understanding of the pathophysiology of ASD, the heterogeneity of symptoms, current lack of physiologically defined biomarkers and difficulties in modeling the disease *in vitro* and *in vivo*.

### *1.2 Genetic architecture of ASD.*

The high heritability of ASD, calculated from concordance for monozygotic and dizygotic twins and siblings, ranges from 50% to 90% (Bailey et al. 1995; Folstein and Rutter 1977; De Rubeis and Buxbaum 2015), suggesting that information about the molecular basis of the disease may be hidden in DNA sequence variations. That, and an unusually high incidence of the disorder in several monogenic syndromes, led many scientists in the field to believe that a handful of "autism genes" may be found, contributing to the development of so-called monogenic models of ASD. Monogenic risk models assume that one highly penetrant *de novo* gene mutation, or a limited number of moderately penetrant mutations, are sufficient to cause ASD. The causal role of single genes is most obvious in rare, highly penetrant Mendelian (monogenic) syndromes. Among monogenic syndromes that are highly co-morbid with ASD, significant early discoveries included the identification of the *FMR1* gene as a cause of fragile X syndrome (FXS) (Fu et al. 1991), the *MECP2* gene as a cause of Rett syndrome (Amir et al. 1999), and demonstration that mutations in either *TSC1* (hamartin) (Slegtenhorst et al. 1997) or *TSC2* (tuberin) (Consortium 1993) genes cause tuberous sclerosis syndromes 1 and 2 (TSC1 and TSC2). Our understanding of the etiology of ASD has been greatly advanced by studies of syndromic forms of ASD caused by rare single gene mutations (Wang, Berry-Kravis, and Hagerman 2010; Yu and Berry-Kravis 2014; Ghosh et al. 2013). These individual syndromes are rare, each accounting for less than 1% of all ASD cases. However, high co-morbidity with ASD, ranging from 40% to 80% (de la Torre-Ubieta et al. 2016), makes them attractive models for studying ASD. Indeed, recent advances in our understanding of FXS, Rett syndrome, and TSC provided insight into the pathophysiology of these conditions, offered a tractable system

for better understanding of the underlying molecular mechanisms and genetic architecture of ASD, and the development of animal models that can be extrapolated into other forms of ASD. Here I will concentrate on two particular syndromic forms of ASD, fragile X and tuberous sclerosis syndromes, because a large proportion of the work in this thesis was conducted using these monogenic forms of ASD.

FXS is the most common monogenic cause of ASD (Coffee et al. 2009), and is a widely used and well characterized model of ASD. It results from large (>200) expansion of a CGG repeat on the fragile X mental retardation (*FMR1*) gene, resulting in methylation and translational silencing of its corresponding protein, the fragile X mental retardation protein (FMRP). FMRP, being a polyribosome-associated RNA binding protein, has been shown to affect the translation of several hundreds of mRNA transcripts (Darnell et al. 2011), each with their own "downstream" biology. The loss of FMRP leads to substantial cognitive functional impairment and intracellular signaling defects both in humans and in mice. Several *FMR1* knockout mouse lines are available, providing a platform for behavioral testing and as a source of tissues and cells.

Another important syndromic form of ASD is TSC, caused by dominant mutations in one of two genes, hamartin (*TSC1*) or tuberin (*TSC2*) and leading to ASD-like behaviors, seizures, intellectual disability, brain tumors and characteristic skin lesions. The protein products of these two genes heteromultimerize to regulate mammalian target of rapamycin (mTOR), an integrative regulator of $Ca^{2+}$ signaling and mitochondrial function created by a large multidomain protein kinase that regulates cell growth and metabolism in response to environmental signals (Ramanathan and Schreiber 2009).

Rapid development of sequencing technologies made it possible to dramatically decrease costs of DNA sequencing – dropping from ~$500 million for the first sequenced human genome to $1,000 per full genome sequence (https://www.genome.gov/27565109/the-cost-of-sequencing-a-human-genome/). The era of gene hunting in different diseases thus began. The possibility to sequence and analyze billions of base pairs both cheaply and accurately allowed the performance of large-scale, unbiased genome-wide searches necessary for complex heterogeneous disorders such as ASD and permitted the identification of hundreds, if not thousands of genes implicated in ASD. A handful of other monogenic syndromes have been identified, together with over 800 individual genes contributing to susceptibility for autism (Anney et al. 2010; Uddin et al. 2014; O'Roak, Vives, Girirajan, et al. 2012; O'Roak, Vives, Fu, et al. 2012). These findings indicate that although one highly penetrant mutation is enough to cause ASD (Geschwind and State 2015; O'Roak et al. 2011), this is very rare, and the number of potentially contributory genes is too large to be of diagnostic utility. Although highly heritable, the *polygenic* pattern of ASD inheritance (De Rubeis and Buxbaum 2015) implies that heterogeneous, weakly penetrant genetic variants – either arising *de novo* or inherited from parents – act in combination with environmental risk factors to cause ASD (Gaugler et al. 2014; Klei et al. 2012). The field has thus begun to migrate from the study of single genes and monogenic disorders, such as FXS and TSC, to envisaging how numerous susceptibility factors may converge on a common functional signaling pathway, such as excitation/inhibition (Bateup et al. 2013; Gibson et al. 2008; Nelson and Valakh 2015; Rubenstein and Merzenich 2003), synaptic transmission (Deng, Sojka, and Klyachko 2011; Gilman et al. 2011; Südhof 2008) or $Ca^{2+}$ homeostasis (Group and Consortium 2013; Laumonnier et al. 2006; Palmieri et al. 2010;

Schmunk and Gargus 2013) to exert their deleterious effects. This has led to a convergence hypothesis (Zeida´n-Chulia et al. 2013; Lu et al. 2012; Sakai et al. 2011), proposing that key hubs within signaling pathways may be a point of convergence for many of the mutated genes. The largest GWAS to date of single nucleotide polymorphisms (SNPs) in a European cohort of over 30,000 psychiatric cases and a similar number of control subjects revealed that alterations in several common $Ca^{2+}$ channel genes are associated with five neurological disorders, including schizophrenia, bipolar disorder, major depression, ADHD and ASD (Group and Consortium 2013). Only 4 of the ~25,000 human loci were associated with neuropsychiatric disease at "genome-wide significance" — with a probability of chance false positive association being less than 5 in 100 million ($p<5\times10^{-8}$). Among them were genes encoding $Ca^{2+}$ channel subunits – *CACNA1C*, and the accessory $Ca^{2+}$ channel subunit *CACNB2*. Mutations in the *CACNA1C* gene are associated with Timothy syndrome – an autosomal dominant syndromic disease involving heart, brain, immune and skin cells. Remarkably, over 80% also have ASD (Splawski et al. 2004; Splawski et al. 2006). The voltage-gated $Ca^{2+}$ channel family where *CACNA1C* belongs is well-recognized to cause channelopathy diseases. Two close paralogs of this gene, *CACNA1S* and *CACNA1A,* also have highly penetrant, simple dominant mutant alleles that cause, respectively, the skeletal muscle diseases hypokalemic periodic paralysis and malignant hyperthermia (Maclennan and Zvaritch 2011), and the neurological diseases hemiplegic migraine, episodic ataxia and spinocerebellar ataxia (Gargus 2009; Pietrobon 2010)

Furthermore, numerous genetic studies have implicated "weak" genetic mutations in $Ca^{2+}$ channels and $Ca^{2+}$-associated proteins with increased susceptibility to ASD (Gargus 2009; Palmieri et al. 2010; Lawrence et al. 2010; Lu et al. 2012; Ripke et al. 2013; Zeida´n-Chulia et

al. 2013). Those "weak" loci do not neatly segregate with ASD in a family, but instead appear to contribute susceptibility to ASD pathogenesis. The first example of such a paralog is the gene *CACNA1H.* In families with familial ASD, several affected subjects are observed to carry the mutant allele, however, not all with the allele manifest diagnosable ASD. The "risk allele" simply is shown to cluster in such cases of familial ASD (Splawski et al. 2006). *CACNA1G,* another $Ca^{2+}$ channel alpha subunit paralog, was found to be associated with ASD in male multiplex families in the Autism Genetic Resource Exchange cohort (Strom et al. 2010). The same family of voltage-gated $Ca^{2+}$ channels was again found to contain SNPs in *CACNA1I* and *CACNA1C* in a subsequent larger study (Lu et al. 2012). Several sequencing studies have identified exon-disrupting copy-number variations in a $Ca^{2+}$ channel accessory subunit *CACNA2D3* among recurrent CNV hotspots in ASD (Girirajan et al. 2013), and identified *de novo* rare alleles in alpha subunit loci *CACNA1D* and *CACNA1E* as "top *de novo* risk mutations" for ASD (O'Roak, Vives, Girirajan, et al. 2012). Table 1.8.1 summarizes $Ca^{2+}$ channels and their subunits in which mutations have been implicated in ASD.

Taken together, these findings strongly implicate $Ca^{2+}$ signaling as an emerging molecular target implicated in pathogenesis of ASD.

### *1.3 $Ca^{2+}$ signaling.*

$Ca^{2+}$ signaling is one of the most universal and ancient of cellular signals (Berridge 1997a). It is a versatile and well-preserved biological messenger system, known to regulate an array of cellular functions ranging from membrane potential, ion transporters, kinases, transcription factors and even cell morphology. Deregulation of intracellular $Ca^{2+}$ signaling outside of its

normal spatial and temporal boundaries can lead to detrimental downstream changes in $Ca^{2+}$-dependent signaling processes and ultimately cellular death. Intracellular $Ca^{2+}$ signaling events govern and orchestrate cellular functions ranging from conception (Berridge 1993) to necrosis and apoptosis (Berridge, Lipp, and Bootman 2000).

$Ca^{2+}$ homeostasis and signaling events are tightly regulated by an exquisite array of $Ca^{2+}$-permeable ion channels, transporters, and exchangers located in the plasmalemmal and intracellular membranes, as well as a plethora of regulatory/accessory proteins and molecules (Berridge 2016; Berridge 2009; Berridge, Lipp, and Bootman 2000). A combination of these proteins and factors unique for each cell type provides highly customizable "$Ca^{2+}$ toolkit" for downstream signal transduction, catering to the specific needs of each cell. This variety ensures that the speed, amplitude, duration, and spatial-temporal pattern of intracellular $Ca^{2+}$ events tailor to each cell's unique and dynamic physiological needs.

$Ca^{2+}$ passively enters the cytoplasm across the plasma membrane and is cleared from the cytoplasm to a level far below extracellular levels by a host of ion pumps and carriers driven by metabolic energy. Intracellular $Ca^{2+}$ concentration is kept between 50 and 100 nM by a host of $Ca^{2+}$ pumps located on the plasmalemmal and ER/SR membranes and by $Ca^{2+}$-binding proteins. The cytosolic $Ca^{2+}$ concentration is ~10,000 fold lower than concentrations of 2 mM found extracellularly, or 0.5-1.0 mM within the lumen of ER/sarcoplasmic reticulum (SR). The resulting concentration gradients create a strong driving force for $Ca^{2+}$ flux into the cytosol. Cytosolic $Ca^{2+}$ signals thus originate by the release of $Ca^{2+}$ from organellar stores through intracellular ion channels and by extracellular $Ca^{2+}$ entering through ion channels across the plasma membrane.

The intracellular $Ca^{2+}$ stores can be rapidly released via intrinsic ER channels, the inositol 1,4,5-trisphosphate receptors ($IP_3Rs$) and the ryanodine receptors (RyRs). Once released, this $Ca^{2+}$ activates a host of kinases, ion channels and transcription factors, and then is resequestered *via* the ER's $Ca^{2+}$ ATPase pump (SERCA) and cleared out of the cell via plasma membrane $Ca^{2+}$ ATPase (PMCA) (Di Leva et al. 2008).

Given that proper functioning of the $Ca^{2+}$ signaling pathway is critical for many cellular functions, it is not surprising that perturbations in this system cause profound downstream defects. Disrupted functioning of ER $Ca^{2+}$ release channels is observed in several cognitive disorders including Alzheimer's (Stutzmann et al. 2004; Ito et al. 1994; Stutzmann et al. 2006), Huntington's disease (Bezprozvanny 2011), and amyotrophic lateral sclerosis (Van Den Bosch et al. 2006).

### *1.4 $IP_3$ $Ca^{2+}$ signaling.*

$IP_3Rs$ are a family of $Ca^{2+}$-permeable ion channels ubiquitously and predominantly expressed in the ER membrane of nearly all known cells (for an exhaustive review see (Foskett et al. 2007)). Functional $IP_3Rs$ are tetramers, with each subunit consisting of a large cytosolic N-terminus, six transmembrane domains containing the ion channel pore, and a short cytosolic C-terminus (Foskett et al. 2007). In mammals, the $IP_3R$ family is comprised of three separate gene products ($IP_3Rs$ types 1-3) and a number of splice variants (Foskett et al. 2007). At the protein level, $IP_3R$ isoforms are 60-80% homologous, and their functional domains are similar. However, different isotypes have different affinity for $IP_3$ and $Ca^{2+}$, and are differentially modulated by ATP, cAMP and protein kinases. Different forms of $IP_3Rs$ exhibit distinct and

overlapping expression patterns with most cell types expressing more than one isoform.

$IP_3$-mediated $Ca^{2+}$ signal transduction is typically initiated by stimulation of cell surface receptors linked to the activation of phospholipase C isoforms β or γ (PLC- β/γ) (Berridge 1993). PLC-β is activated following stimulation of G-protein coupled receptors linked to the heterotrimeric Gq family proteins (GPCRs) (Berridge 1997a), whereas PLC-γ is turned on by phosphorylation in response to tyrosine kinase-linked (Clandinin, DeModena, and Sternberg 1998) cell surface receptor stimulation. Activation of PLC leads to the generation of inositol 1,4,5-trisphosphate ($IP_3$) and diacylglycerol (DAG) following hydrolysis of phosphatidylinositol 4,5-bisphosphate ($PIP_2$). $IP_3$ liberated from the inner leaflet of the plasmalemma diffuses into the cytoplasm and binds to $IP_3$Rs located in the ER membrane. The $IP_3$R forms a $Ca^{2+}$ -permeable channel in the membrane of the ER, and its opening allows the release into the cytosol of $Ca^{2+}$ sequestered within the ER (Berridge 1997b; Bootman, Berridge, and Lipp 1997; Parker and Yao 1996). Opening of the $IP_3$R channel requires binding of $IP_3$ together with $Ca^{2+}$ to receptor sites on the cytosolic face. Gating by $Ca^{2+}$ is biphasic, such that small elevations of cytosolic $Ca^{2+}$ induce channel opening, whereas larger elevations cause inactivation (Bezprozvanny, Watras, and Ehrlich 1991; Foskett et al. 2007). The positive feedback by $Ca^{2+}$ underlies the process known as $Ca^{2+}$-induced $Ca^{2+}$ release (CICR), whereby $Ca^{2+}$ is released in a regenerative manner that may remain restricted to a cluster of $IP_3$Rs, producing local $Ca^{2+}$ signals known as $Ca^{2+}$ puffs (Fig. 1..1) (Yao, Choi, and Parker 1995), or may propagate throughout the cell as a saltatory wave involving the recruitment of multiple puff sites by successive cycles of $Ca^{2+}$ diffusion and CICR. Thus, $IP_3$-mediated $Ca^{2+}$ signaling represents a hierarchy of $Ca^{2+}$ events of differing magnitudes (Lipp and Niggli 1996; Parker, Choi, and Yao

1996), and the spatial patterning and distribution of $IP_3Rs$ is critical to proper cellular function (Fig. 1.9.1). The spatial and temporal localization of $Ca^{2+}$ signaling ensures high specificity of cellular responses.

In the mammalian brain, different isoforms of $IP_3Rs$ have distinct expression patterns depending on the brain region and developmental state. $IP_3R$ type 1 is predominantly expressed in neurons, especially in Purkinje cells in the cerebellum. $IP_3R$ type 3 demonstrates predominantly a neuronal pattern of expression that does not overlap with the $IP_3R1$. For instance, Purkinje cells in the cerebellum are highly enriched in $IP_3R1$, but have low or undetectable levels of $IP_3R3$, but granule cells of the cerebellum and many regions of the medulla display moderately high levels of $IP_3R3$, whereas $IP_3R1$ is virtually undetectable in these regions. $IP_3R1$ expression levels are the highest in cerebellar Purkinje neurons, where $IP_3$-mediated $Ca^{2+}$ signaling is necessary for induction of long-term depression (LTP), a candidate mechanism for the cellular basis of motor learning (Inoue et al. 1998). Interestingly, cerebellar dysfunction has been repeatedly implicated in the pathogenesis of ASD (Wang, Kloth, and Badura 2014).

In neurons, $IP_3R$-mediated $Ca^{2+}$ release is involved in crucial functions – including synaptic plasticity and memory (Inoue et al. 1998; Rose & Konnerth 2001), neuronal excitability (Hernandez-Lopez et al. 2000; Stutzmann, LaFerla, and Parker 2003), neurotransmitter release (Li et al. 1998; Diamant, Schwartz, and Atlas 1990), axon growth (Gomez and Spitzer 1999) and long-term changes in gene expression (Li et al. 1998) - highlighting the central integrating position played by $IP_3Rs$ (Patterson, Boehning, and Snyder 2004). $IP_3$-induced $Ca^{2+}$ response in neurons propagates along the dendrite as a wave and is different from action potential-induced

$Ca^{2+}$ fluctuations in both temporal and spatial aspects. Unlike brief spike-evoked $Ca^{2+}$ signals that occur throughout the cell, $IP_3$-mediated events start at a local proximal dendrite and then spread to the soma as a $Ca^{2+}$ wave. This was first observed in hippocampal neurons (Shirasaki, Harata, and Akaike 1994; Jaffe and Brown 1994). Subsequently, $IP_3$-mediated $Ca^{2+}$ waves were observed and characterized in other brain regions – cortical pyramidal neurons and midbrain dopamine neurons, suggesting a ubiquitous role of $IP_3$ signaling throughout the brain (Morikawa et al. 2000; Larkum et al. 2003).

In the cerebellum, $IP_3$-mediated $Ca^{2+}$ release is critical for induction of long-term depression (Khodakhah and Armstrong 1997), a form of synaptic plasticity, which is thought to be an important cellular mechanism for motor learning and coordination. In cerebellar Purkinje cells that are especially enriched in $IP_3$Rs, repetitive parallel fiber stimulation triggers metabotropic glutamate receptor (mGluR) activation and subsequent $IP_3$-mediated $Ca^{2+}$ release from the ER (Takechi, Eilers, and Konnerth 1998; Yuzaki and Mikoshiba 1992). Because both $IP_3$ and $Ca^{2+}$ are required for the initial $IP_3$R activation, some cytoplasmic $Ca^{2+}$ is necessary. If the concentration of $IP_3$ is high, even low basal $Ca^{2+}$ concentration is enough, however, at lower $IP_3$ concentrations an additional source of $Ca^{2+}$ is required. This dual requirement for the two messengers is met by two inputs to the Purkinje neurons: the climbing fiber input strongly depolarizes Purkinje cells to generate a $Ca^{2+}$ signal via plasmalemmal channels, whereas parallel fiber inputs activate the mGluRs to produce $IP_3$. Thus maximal activation of $Ca^{2+}$ release via $IP_3$Rs depends on the timing of co-activation and serves as a coincidence detector for these two types of inputs (Sarkisov and Wang 2008). Consistent with the role of $IP_3$R1 in cerebellar long-term depression (LTD), LTD is completely abolished in mice with a genetic

deletion of $IP_3Rs$ (Inoue et al. 1998).

In cortical pyramidal neurons $IP_3R$ activation is a key signaling hub downstream of mGluRs (Inoue et al. 1998; Berridge 1993), where it leads to a brief hyperpolarization followed by a more prolonged depolarization (El-Hassar et al. 2011; Stutzmann, LaFerla, and Parker 2003). The initial outward current results from the opening of small conductance $Ca^{2+}$-activated $K^+$ channels (Chandy et al. 1998; Köhler et al. 1996). This current is proportional to the $Ca^{2+}$ signal amplitude (Stutzmann, LaFerla, and Parker 2003); and can be triggered directly by intracellular uncaging of $IP_3$ (El-Hassar et al. 2011; Stutzmann, LaFerla, and Parker 2003). As a result, $IP_3$-evoked $Ca^{2+}$ release transiently hyperpolarizes the cell and briefly depresses neuronal excitability, leading to a reduction in firing frequency (Stutzmann, LaFerla, and Parker 2003). Suppressed $IP_3$-mediated $Ca^{2+}$ release from the internal stores diminishes the inhibitory $K^+$ conductance, and produces neuronal hyperexcitability (Repicky and Broadie 2009; Bateup et al. 2011), consistent with observations following mGluR stimulation of ASD-model neurons (Repicky and Broadie 2009; Bateup et al. 2011).

In hippocampal CA1 slices, brief pre-treatment with group 1 mGluR agonists has been shown to facilitate the induction of long-term potentiation (LTP), that manifests in an enhanced magnitude and stability of LTP (Cohen and Abraham 1996). However, stronger activation of the group 1 mGluRs induces LTD (Palmer et al. 1997; Oliet, Malenka, and Nicoll 1997). Application of a group 1 mGluR agonist *acutely* reversibly depressed excitatory postsynaptic currents (EPSCs) in rat slices. Intriguingly, this effect was age-dependent and strongest in neonatal rats, as the EPSCs were significantly decreased in adolescent animals (day 12-30) and almost completely abrogated in adults (age >80 days) (Baskys and Malenka 1991), highlighting

an important neurodevelopmental role played early in life by the $IP_3$ $Ca^{2+}$ signaling.

### *1.5 Neurological and physiological consequences of genetic deletion of $IP_3$Rs in mice*

#### 1.5.1 $IP_3$R type 1.

Genetic manipulation of a gene of interest in laboratory rodents has long been an invaluable tool in determining that gene's function. Knockout mouse models of all three $IP_3$R isoforms have been generated, with the most studied being the *ITPR1* knockout. Mice with homozygous deletion of *ITPR1* suffer from severe ataxia and epilepsy and most of them die *in utero* or before the weaning age (Matsumoto and Nagata 1999; Matsumoto et al. 1996). Interestingly, the *in utero* lethality rate was reduced when the genetic background was shifted from widely used C57Bl/6 to CD-1 strain. After birth, the $IP_3$R1 knockout mice exhibit truncal ataxia on postnatal day 7 and tonic-clonic epileptic seizures starting on postnatal day 13 or 14. Anti-convulsants such as pentobarbital eliminate the seizures, while leaving ataxia intact, suggesting distinct features responsible for each phenotype. Neuroanatomical analysis of the $IP_3$R1 knockout brains has shown no detectable malformations in the cerebellum with Purkinje cell numbers, with morphological properties and arborization all being unaffected (Matsumoto and Nagata 1999). Electrophysiological studies further failed to reveal any abnormalities in the membrane excitability of Purkinje cells, the number or strength of parallel fiber or climbing fiber inputs. However, subsequent studies demonstrated that LTD was completely abolished in Purkinje cells (Inoue et al. 1998). Cerebellar LTD is commonly accepted as a molecular basis of cerebellar motor learning and the development of motor coordination, suggesting that the lack of $IP_3$R1 is responsible for the ataxic phenotype of the knockout mice.

$IP_3R1$-deficient mice also show impairments in hippocampal synaptic plasticity. In the CA1 hippocampal neurons of $IP_3R1$ knockout mice, the mean magnitude of the LTP or LTD induced by a standard tetanus of low-frequency stimulation (standard protocol for LTP and LTD induction, respectively) were unaffected in the knockout animals. However, when a short tetanus (10 pulses at 100 Hz) was used to induce LTP, the mean magnitude of the resulting LTP was significantly greater in mutant mice than in wild-type mice (Fujii et al. 2000). Depotentiation (DP) and LTP suppression are also attenuated in the CA1 hippocampal neurons of $IP_3R1$ knockout mice (Fujii et al. 2000). These results suggest that, unlike in Purkinje cells, in hippocampal CA1 neurons the $IP_3R1$ is involved in LTP, DP, and LTP suppression but is not essential for LTD. In addition, deletion of $IP_3R1$ results in a lack of heterosynaptic LTD in the CA1 region of the hippocampus, indicating the contribution of $IP_3R1$ to input specificity.

Whereas homozygous $IP_3R1$ mice demonstrate these profound phenotypes, heterozygous mice demonstrate only subtle motor coordination deficits, observed when tested with a rotarod (Ogura, Matsumoto, and Mikoshiba 2001).

### 1.5.2 $IP_3R$ type 2.

$IP_3R$ type 2 receptor in the brain is predominantly expressed in astrocytes (Zhang et al. 2014). *ITPR2* loss in astrocytes was reported to lead to the apparent loss of all astrocytic $Ca^{2+}$ signaling (but also see (Srinivasan et al. 2015)), however, it was not accompanied by any gross deficits in behavioral (Petravicz, Boyt, and McCarthy 2014) or neurological functions (Petravicz, Fiacco, and McCarthy 2008; Agulhon, Fiacco, and McCarthy 2010). Interestingly, contrary to Petravicz *et al*. findings that used astrocyte-specific *ITPR2* knockout, a global knockout of the receptor

was associated with depressive-like behavior in mice, presumably mediated by a lack of ATP signaling from astrocytes (Cao et al. 2013). Another study implicated a role of the $IP_3R2$ signaling in synapse elimination, again mediated by astrocytic ATP release (Yang et al. 2016). Moreover, other groups have demonstrated an apparent effect of *ITPR2* knockout on cortical plasticity in response to whisker stimulation, possibly through perturbed release of d-serine from astrocytes (Takata et al. 2011), potentiation of visual responses in excitatory neurons of the primary visual cortex (Chen et al. 2012), and modulation of neural network activity (Wang et al. 2012). Astrocytic $Ca^{2+}$ signaling mediated via $IP_3R2$ was implicated in $K^+$ uptake by astrocytes, leading to decreased extracellular $K^+$ concentrations and as a result hyperpolarization of neurons and reduced excitatory synaptic activity. In conclusion, the vast majority of *ITPR2* knockout studies concentrated on astrocytes as a predominant cell type expressing this receptor in the brain. However, the apparent discrepancy between findings from studies utilizing cell-type specific and global knockouts suggest that the role of $IP_3R$ type is not limited to astrocytes, and may play a role in more subtle neurological functions fine-tuning brain activity.

In 2014 the presence of homozygous missense *ITPR2* mutations was identified in five human subjects from a consanguineous family. Interestingly, anhidrosis (inability to sweat) and severe heat intolerance as a result were the only reported phenotype in these patients. Upon clinical investigation, no other abnormalities were observed, with body growth, as well as teeth, hair, nails and skin all normal. No neurological abnormalities were reported, suggesting that at least in humans the complete loss of $IP_3R2$ does not lead to any detrimental consequences beyond inability to produce sweat (Klar et al. 2014).

### 1.5.3 $IP_3R$ type 3.

From the standpoint of neurophysiology, mice with a genetic deletion of *ITPR3,* dubbed a "mouse with bad hair and poor taste", are largely unexciting (Tordoff and Ellis 2013). $IP_3R3$ regulates hair shedding in mice (Sato-Miyaoka et al. 2012) and is responsible for the tufted locus – a locus responsible for irregular hair growth pattern – of the BTBR mouse model of polygenic autism with several sporadic mutations (Tordoff and Ellis 2013; Ellis, Tordoff, and Parker 2013). It would be tempting to suggest a causative link between the *ITPR3* mutation and the autism phenotype in the BTBR mice, however the currently available scientific evidence indicates that the role of $IP_3R3$, at least in mice, is limited to the taste perception and hair loss only.

## *1.6 $IP_3$ $Ca^{2+}$ signaling and its disruption in neurological diseases*

### 1.6.1 Spinocerebellar ataxia.

A straightforward example of dysregulation of $IP_3$-mediated $Ca^{2+}$ signaling is seen in spinocerebellar ataxias (SCA), a group of neurodegenerative disorders characterized by problems in coordination of movement affecting legs, hands, and eyes. While there are many types of SCA, several of them have strong connection to $Ca^{2+}$ signaling abnormalities that eventually funnel onto an $IP_3$ pathway. One unifying feature of this group of neurodegenerative disorders is widespread Purkinje cell death mediated by dysregulated $IP_3$-mediated $Ca^{2+}$ signaling. Heterozygous deletions in *ITPR1*, a gene encoding $IP_3R1$, were identified in several unrelated families affected with SCA types 15 (SCA15) (Van De Leemput et al. 2007), an autosomal dominant disease. The same study showed that the affected patients with confirmed

*ITPR1* deletion had decreased amounts of $IP_3R1$ at a protein level, unlike a family member who does not carry the deletion, suggesting haploinsufficiency and decreased function of $IP_3R$ in the pathogenesis of the disease. A large deletion and a point mutation in *ITPR1* were subsequently identified in two additional families (Hara et al. 2008), solidifying the causative pathogenic role of *ITPR1* haploinsufficiency in SCA. Gene mutations causative for SCA16 were mapped to a locus overlapping with that of SCA15, that also contains *ITPR1* heterozygous deletion (Iwaki et al. 2008). It is worth noting that SCA16 was initially mapped to chromosome 8q (Miyoshi et al. 2001), but later additional studies established the linkage to 3p, where *ITPR1* resides, making SCA16 and SCA15 virtually the same disorder (Bezprozvanny 2011). Additional heterozygous missense mutations in *ITPR1* have been identified in SCA29 (Sasaki et al. 2015; Huang et al. 2012), which is clinically distinguished from SCA15 by early onset of symptoms.

SCA type 2 and 3 (SCA2 and SCA3) are autosomal dominant disorders that are caused by an expansion of unstable CAG repeats that encode polyglutamine tract expansions (polyQ) in genes encoding ataxin 2 and 3, respectively. Multiple lines of evidence suggest perturbed $Ca^{2+}$ release from the ER in both of these disorders. Pull-down and co-immunoprecipitation have revealed that the mutated ataxin-2 specifically associates with the COOH-terminal domain of $IP_3R1$, while the wild type form of it did not form such associations (Liu et al. 2009). In lipid bilayer experiments, the mutated attaxin-2 increased the sensitivity of $IP_3Rs$ to $IP_3$, dramatically increasing its activation. In cultured Purkinje cells, expression of mutant ataxin-2 also facilitated $Ca^{2+}$ release in response to mGluR activation. Finally, prolonged treatment of mutant mice with dantrolene, an antagonist of the ryanodine receptor, another channel on the ER that magnifies $IP_3$-initiated $Ca^{2+}$ release, ameliorated Purkinje cell loss in cerebellum and improved

performance in aged mice on the rotarod test (Liu et al. 2009). Similar results were obtained with a mutant ataxin-3 protein, suggesting that the polyglutamine repeat on ataxin proteins may be a unifying theme in several types of ataxia and it contributes to its pathogenesis by facilitation of binding to $IP_3R$ and increase in its sensitivity to $IP_3$ (Chen et al. 2008).

### 1.6.2 Huntington's disease.

In Huntington's disease, a pathophysiological polyglutamine (polyQ) expansion in a protein, huntingtin, enhances its binding to the COOH-terminus of $IP_3R1$ and sensitizes it to $IP_3$ (Bezprozvanny 2011). This gives rise to larger $Ca^{2+}$ signals that disrupt neuronal function and induce cell death. In a mouse model of Huntington's disease, the increase in $IP_3$-mediated $Ca^{2+}$ release decreases ER store $Ca^{2+}$ levels, leading to overactivation of store-activated $Ca^{2+}$ entry and subsequent striatal synaptic loss (Wu et al. 2016). Genetic ablation of $IP_3R1$ and chemical treatment with $Li^+$, which leads to decrease in $IP_3$ signaling, reduce accumulation of mutant huntingtin proteins and ameliorates spine loss (Wu et al. 2016; Sarkar et al. 2008; Bauer et al. 2011).

### 1.6.3 Alzheimer's disease.

Alzheimer's disease (AD) is a devastating neurodegenerative disorder that progressively destroys neurons leading to a sharp decline in cognitive abilities. AD is driven by a release of soluble β-amyloid (Aβ) that forms Aβ oligomers toxic to neurons. Sustained upregulation of intracellular $Ca^{2+}$ levels was shown to initiate the disease early on and exacerbate the core features from amyloid plaque formation to synapse loss (for reviews, see (Mattson and Chan 2001; Stutzmann 2007)). Disrupted $IP_3$-mediated $Ca^{2+}$ signaling is a well-documented

contributing factor in this process, both in familial and sporadic forms. Sporadic forms of AD are more common among AD patients, have poorly defined etiology and strike later in life (>65 years). The familial form of AD (FAD) is an early-onset, less common form of the disease, contributing to less than 10% of reported cases. FAD is caused by an autosomal-dominant mutations in presenilin 1 (PS1), presenilin 2 (PS2), or amyloid precursor protein (APP) genes (Campion et al. 1999), with the mutations in presenilins being responsible for the majority of FAD cases. Despite relatively rare occurrence, the genetically defined architecture of FAD makes it a tractable model for studying this highly heterogeneous condition. Moreover, regardless of the type, AD progression follows the same steps in both familial and sporadic forms, with accelerated development in the FAD form. Mutant PS1 is the most common cause of FAD. The presenilin protein is a catalytic subunit of the gamma secretase complex located on the ER membrane that generates Aβ by cleaving APP. The first proposed mechanism of PS1 pathogenicity is that its mutant form cleaves APP preferentially into a longer and more amyloidogenic $A\beta_{42}$ form. Another role of the PS mutant protein in the pathophysiology of FAD is to increase $Ca^{2+}$ release from the intracellular stores, contributing to cytotoxicity and neuronal death (Mak et al. 2015; Stutzmann et al. 2004; Leissring et al. 1999). This effect has been shown in cultured neuronal-like PC12 cells expressing mutant PS1 (Guo et al. 1996), in cultured primary neurons from PS1 knockin mice (Chan et al. 2000; Guo et al. 1999) and in brain slices from young, adult, and aged mutant PS1 knockin mice (Stutzmann et al. 2006). The exact mechanism of such increases is still debated, but proposed causes include abnormal elevation of the ER $Ca^{2+}$ stores (Leissring et al. 2001), gain-of-function enhancement of $IP_3R$ gating by presenilin proteins (Mak et al. 2015), and enhanced ryanodine receptor recruitment

consequent to initial $IP_3R$ activation (Stutzmann et al. 2006). Cheung et al. have shown that several FAD PS mutations have a gain-of-function effect on $IP_3Rs$, leading to a high open probability burst mode of these channels, thus enhancing $Ca^{2+}$ signaling (Cheung et al. 2010). There are two important implications of such increased sensitivity. Under normal physiological conditions (when PS is not mutated), the mean channel open time is too short (~10 ms) to recruit neighboring $IP_3Rs$ and RyR and induce $Ca^{2+}$-induced $Ca^{2+}$ release. However, given that in the presence of the mutant PS the $IP_3R$ channel has a propensity to dwell in a longer open time with burst activity (>200ms), the resulting $Ca^{2+}$ release will recruit spatially segregated RyR, inducing CICR. As a result, the initial increase in $Ca^{2+}$ store release will be further amplified by downstream players and will lead to cytotoxicity. Secondly, taking into consideration $IP_3R$'s sensitivity to both $IP_3$ and $Ca^{2+}$, the channel's increased sensitivity to $IP_3$ potentiates the channel's opening in response to increase in intracellular $Ca^{2+}$ due to RyR activation, leading to a self-propagating loop. Consistent with this, in mutant PS mice increasing basal intracellular $Ca^{2+}$ *via* RyR is enough to induce $IP_3R$-mediated $Ca^{2+}$ release (Goussakov, Miller, and Stutzmann 2010).

To further support the calciumopathy phenotype in AD, exaggerated $IP_3$-mediated $Ca^{2+}$ signaling was observed in non-neuronal cells from symptomatic (Hirashima et al. 1996; Ito et al. 1994) and pre-symptomatic AD patients (Etcheberrigaray et al. 1998), as well as in neurons from mouse models of AD (Stutzmann et al. 2004).

Both familial and sporadic forms of AD are believed to be caused by pathologic actions of Aβ protein oligomers. Among other cytotoxic effects of Aβ that are beyond the scope of the present introduction section, the role of Aβ is to stimulate the $IP_3$ production to release $Ca^{2+}$ from the

ER (Mattson and Chan 2001). The neurotoxic effect of Aβ oligomers *via* $Ca^{2+}$ release from the intracellular stores was demonstrated with a bath application of Aβ to neuronal cultures (Ferreiro, Oliveira, and Pereira 2004). Pre-incubation of cells with dantrolene or xestospongin C, inhibitors of RyRs and $IP_3Rs$, respectively, prevented $Ca^{2+}$ release and protected cells from the apoptotic cell death. A different set of experiments on human neuroblastoma SH-SY5Y cell culture produced similar results, demonstrating $Ca^{2+}$ release from intracellular stores upon bath application of Aβ that was partially blocked by caffeine, an $IP_3R$ antagonist (Jensen et al. 2013). Interestingly, when these experiments were done on permeabilized chicken DT40 TKO cells that are void of any $IP_3Rs$, the $Ca^{2+}$ release in response to Aβ remained and was not different from the WT DT40 cells (Jensen et al. 2013), implicating other molecular players besides $IP_3Rs$. Another line of evidence supporting the cytotoxic effect of Aβ was obtained from injecting oligomers directly into frog oocytes. Such injections of Aβ led to $Ca^{2+}$ increase due to both $Ca^{2+}$ entry across the plasma membrane and $Ca^{2+}$ release from intracellular stores (Demuro and Parker 2013). In these experiments, $Ca^{2+}$ release could be inhibited by application of caffeine, heparin, or pretreatment with pertussis toxin that blocks G-protein-mediated activation of phospholipase C. Furthermore, incubation of oocytes with lithium to block the inositol monophosphatase enzyme involved in *de novo* synthesis of inositol and hence depleting the inositol phospholipid pools rescued oocytes from Aβ-mediated cytotoxicity and death, as did co-injection with EGTA to buffer intracellular $Ca^{2+}$ levels (Demuro and Parker 2013). These findings establish that one of the roles of the Aβ in the pathogenesis of AD is in its ability to evoke intracellular $Ca^{2+}$ release. Sustained and prolonged increase in intracellular $Ca^{2+}$ levels is neurotoxic and leads to neuronal cell death and, as a result, memory loss. An important

confirmation of the $Ca^{2+}$ signaling disruption in the AD came from *in vivo* findings that genetic reduction of $IP_3R1$ in several mouse models of familial AD reduces pathogeniety of the condition (Shilling et al. 2014).

### *1.7 Conclusions*

In light of the crucial roles of $IP_3$-mediated $Ca^{2+}$ signaling in regulating normal neuronal development and function, as well as in pathogenesis of several neurological diseases, I hypothesize that the $IP_3$ receptor acts as a signaling 'hub' where many genes that are altered in ASD converge to exert their deleterious effect. My overall goal was to investigate if $IP_3$-mediated $Ca^{2+}$ signaling is altered in ASD and to elucidate downstream consequences of such abnormalities relevant to ASD phenotypes.

## *1.8 Tables*

### Table 1.8.1 $Ca^{2+}$ channels and $Ca^{2+}$ channel subunits implicated in ASD.

| *Protein* | *Description* | *Normal function* | *Disease association* |
|---|---|---|---|
| **CACNA1C** | Voltage-regulated L-type calcium channel, alpha 1C subunit | Regulates entry of Ca2+ into excitable cells: muscle contraction, hormone/neurotransmitter release, gene expression, cell cycle | Timothy Syndrome, ASD, psychiatric diseases |
| **CACNA1D** | Voltage-regulated calcium channel, alpha 1D subunit | High-voltage activated, long-lasting calcium activity | Sinoatrial node dysfunction and deafness, ASD, psychiatric diseases |
| **CACNA1E** | Voltage-regulated R-type calcium channel, alpha 1E subunit | High-voltage activated, rapidly inactivating | ASD, psychiatric diseases |
| **CACNA1F** | Voltage-regulated L-type calcium channel, alpha 1F subunit | Regulates entry of Ca2+ into excitable cells: muscle contraction, hormone/neurotransmitter release, gene expression, cell cycle | ASD and X-linked congenital stationary night blindness |
| **CACNA1G** | Voltage-regulated T-type calcium channel, alpha 1G subunit | Regulates entry of Ca2+ into excitable cells: muscle contraction, hormone/neurotransmitter release, gene expression, cell cycle | ASD; intellectual disability; juvenile myoclonic epilepsy |
| **CACNA1H** | Voltage-regulated T-type calcium channel, alpha 1H subunit | Regulates neuronal and cardiac pacemaker activity | Familial autism; childhood absence epilepsy |
| **CACNA1I** | Voltage-regulated T-type calcium channel, alpha 1I subunit | Characterized by a slower activation and inactivation compared to other T-channels | Possibly implicated ASD |
| **CACNA2D3** | Voltage-regulated calcium channel, alpha 2/delta 3 subunit | Accessory calcium channel subunit; regulates entry of Ca2+ into excitable cells | ASD |
| **CACNA2D4** | Voltage-regulated calcium channel, alpha 2/delta 4 subunit | Accessory calcium channel subunit; regulates entry of Ca2+ into excitable cells | Gene deletion along with CACNA1C leads to ASD |
| **CACNB2** | Accessory calcium channel beta-2 subunit | Contributes to the function of calcium channels. Modulates voltage dependence of activation and inactivation and controls trafficking of the calcium channel family. | ASD, psychiatric diseases |

### *1.9 Figures*

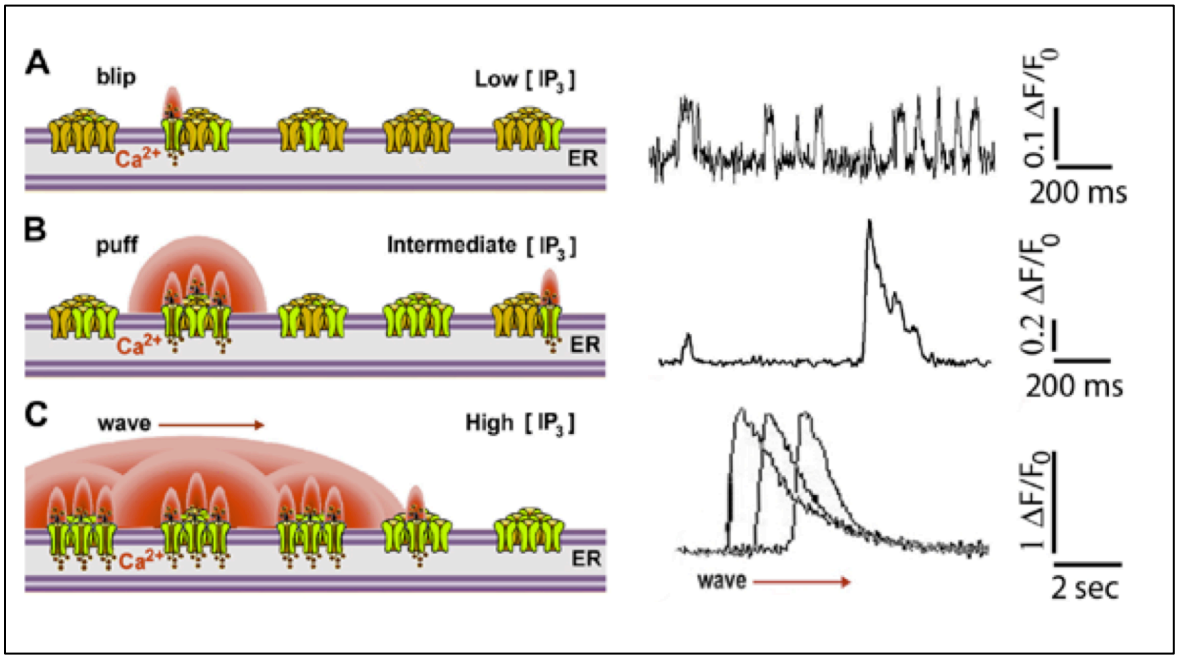


**Figure 1.9. 1 Local and global $Ca^{2+}$ signaling events**

Hierarchical organization of $Ca^{2+}$ signals; from fundamental single-channel events ('blips'; **A**), to elementary events ('puffs'; **B**) and global waves (**C**). Cartoons on the left illustrate the proposed spatial organization of $IP_3R$ channels in the ER membrane that gives rise to these events, and traces at right are representative experimental fluorescence traces of blips, puff and wave. Note differences in amplitude and time scales.

## Chapter 2. $Ca^{2+}$ signaling abnormalities in human subjects with various monogenic and sporadic forms of ASD

### *2.1 Introduction*

Autism Spectrum Disorder (ASD) is a common complex polygenic disorder characterized by difficulties in social interaction, communication and restricted, repetitive behaviors. The symptoms and severity vary widely across autistic individuals, complicating diagnosis of this complex spectrum and giving rise to a tragic "diagnostic odyssey" that delays diagnosis, and hence treatment, until the typical mean age of 5yrs (Pringle et al. 2012). Diagnosis of ASD is made based on questionnaires and behavioral tests, relying on parent observations and comprehensive evaluation by psychologists, pediatricians, psychiatrists, and speech therapists (Constantino and Charman 2015). The current lack of biomarkers and molecular targets makes diagnosis, study and treatment of ASD a challenging task. Moreover, early diagnosis is critical for optimal intervention (Anderson, Liang, and Lord 2014; MacDonald et al. 2014), and accurate diagnosis is crucial in order to exclude other potential conditions which may require different therapies.

A wealth of genetic data now implicate a host of genes encoding ion channels and associated intracellular $Ca^{2+}$ signaling proteins in the molecular architecture of ASD (Group and Consortium 2013; Lu et al. 2012; Palmieri et al. 2010; Schmunk and Gargus 2013), placing $Ca^{2+}$ homeostasis at a central node. Cytosolic $Ca^{2+}$ homeostasis involves ion flux from intracellular organellar stores, as well as transport across the plasma membrane. Diseases of the intracellular organelles are an emerging area of medicine. Several prototypes are already well developed for

neurogenetic diseases of mitochondria and the lysosomes (Lim, Li, and Raben 2014; Valenti et al. 2014; Wallace, Fan, and Procaccio 2010; Weinreb 2013), and increasing evidence implicates the ER (Roussel et al. 2013). $Ca^{2+}$ release from $IP_3Rs$ has been shown to be altered in cognitive disorders including Alzheimer's (Smith et al. 2005; Stutzmann et al. 2004) and Huntington's diseases (Bezprozvanny 2011), and $IP_3Rs$ have recently been identified among the genes affected by rare *de novo* copy number variations in ASD patients (Gilman et al. 2011). I focus on $Ca^{2+}$ signaling as a compelling potential root defect in the disorder, in light of the growing genetic evidence supporting its role in susceptibility to ASD (Group and Consortium 2013; Lu et al. 2012; Palmieri et al. 2010; Schmunk and Gargus 2013) , and its ubiquitous participation in cellular functions as diverse as neuronal excitability (Hernandez-Lopez et al. 2000; Stutzmann, LaFerla, and Parker 2003), neurotransmitter release (Li et al. 1998; Diamant, Schwartz, and Atlas 1990), cell secretion (Berridge and Patel 1968; Fain and Berridge 1979), gene expression, and apoptosis (Pinton et al. 2008; La Rovere et al. 2016).

### *2.2 Materials and Methods*

#### 2.2.1 Materials.

Fluo-8 AM was purchased from AAT Bioquest, diluted in DMSO (Sigma D2650) to a stock concentration of 2 mM and frozen as 25 µl aliquots until needed. On the day of the experiment the Fluo-8 AM solution was thawed and diluted with an equal volume of 20% Pluronic F-127 (Molecular Probes, P6867) prepared in DMSO. Adenosine triphosphate (ATP), adenosine diphosphate (ADP), uridine triphosphate (UTP) and uridine diphosphate (UDP) were purchased from Sigma Aldrich, diluted in water to a stock concentration of 100 mM and frozen as 50 µl

aliquots until needed. MRS 2365 (supplied pre-dissolved at a concentration of 10mM) was purchased from Tocris. Ionomycin was purchased from Life Technologies, diluted in DMSO to 1 mM and frozen as 10 µl aliquots until needed.

### 2.2.2 Subject fibroblast cell lines.

All methods were carried out in accordance with relevant guidelines and regulations, and all experimental protocols were approved by UCI Institutional Review Board (IRB) review. Skin fibroblast cultures were obtained from sporadic ASD subjects enrolled into the UCI Center for Autism Research and Translation (CART). All CART-derived cell lines reported here were from subjects who were referred with a clinical diagnosis of ASD. Three such subjects had Prader-Willi syndrome and are classified as such. CART subjects underwent a full day of testing to develop their deep phenotype, including skin biopsy, all obtained with informed consent and assent. Age-appropriate research-grade ADOS and IQ tests were administered, followed by a set of high-density EEG studies, a sleep study and preparation for a follow-up at home 5-day sleep study with accelerometers and app-assisted parent sleep and behavior logging. Metabolomic studies of blood, urine, saliva and volatile metabolites in breath were obtained, as well as blood from the subject and family members for whole genome sequencing. Only those subjects with validated ADOS scores in the "Autism" or the "Autism Spectrum Disorder" ranges were selected for study (Table 2.5.1). Fibroblast cell lines were established from punch skin biopsy (2-3 mm) explants and frozen at passage 5 in liquid nitrogen for long-term storage.

Primary, untransformed skin biopsy fibroblast cultures from neurotypical controls and monogenic forms of ASD (fragile X syndrome, tuberous sclerosis, Rett, and one with Prader-

Willi syndrome) were obtained from Coriell cell biorepository.

Fibroblast were cultured in Dulbecco's Modified Eagle's Media (Gibco, 11965-092) supplemented with 20% (v/v) fetal bovine serum without antibiotics at 37 °C in a humidified incubator gassed with 95% air and 5% $CO_2$, and used for up to 15 passages. Cells were studied at passages 10-15. For $Ca^{2+}$ signaling studies, cells were detached with $Ca^{2+}$- and $Mg^{2+}$-free 0.25% trypsin-EDTA (Life Technologies), harvested in normal growth media and sub-cultured on FLIPR 96 well plates for 2 days to provide standardized conditions prior to imaging studies.

### 2.2.3 High-throughput $Ca^{2+}$ imaging.

Skin fibroblasts were seeded in clear-bottom black 96-well plates (Greiner Bio One T-3026-16) at 1 x $10^4$ cells per well and grown to confluency. On the day of the experiment, cells were loaded by incubation with 2 μM of the membrane-permeant $Ca^{2+}$ indicator Fluo-8 AM (Takada, Furuya, and Sokabe 2014) in standard buffer solution (130 mM NaCl, 2 mM $CaCl_2$, 5 mM KCl, 10 mM glucose, 0.45 mM $KH_2PO_4$, 0.4 mM $Na_2HPO_4$, 8 mM $MgSO_4$, 4.2 mM $NaHCO_3$, 20 mM HEPES and 10 μM probenecid, pH 7.4 at the room temperature) with 0.1% fetal bovine serum for 1 h at 37 °C, then washed with a $Ca^{2+}$ -free HBSS solution (120 mM NaCl, 4 mM KCl, 2 mM $MgCl_2$, 10 mM glucose, 10 mM HEPES, 1 mM EGTA, pH 7.4 at the room temperature) once. The solution was replaced with 100 μl of fresh $Ca^{2+}$ -free HBSS solution in each well and cells were allowed to equilibrate for 5 minutes prior to assay with a fluorometric imaging plate reader (FLIPR; Molecular Devices, Sunnyvale, CA). A basal read of fluorescence in each well (470–495 nm excitation and 515–575 nm emission, expressed in arbitrary units; AU) was read for 2 seconds at 0.4 s exposure time. Next, 100 μl of 2x ATP (to 100 μM final concentration) or 100 μl

of 2x ionomycin (to 1 μM final concentration) in $Ca^{2+}$ -free HBSS was added to a given well. Only a single recording was obtained from each well. Ionomycin-induced fluorescence changes from wells without prior addition of ATP were used to normalize ATP-evoked responses. Recordings were performed in triplicate. Each experiment was repeated on at least two independent days.

### 2.2.4 Whole-cell $Ca^{2+}$ imaging.

Cells seeded in glass-bottomed dishes were loaded for imaging using membrane-permeant esters of Fluo-8 and caged i-$IP_3$ (ci-$IP_3$ (Smith, Wiltgen, and Parker 2009; Ellefsen et al. 2014)). Briefly, cells were incubated at room temperature in HEPES-buffered saline (2.5 mM $CaCl_2$, 120 mM NaCl, 4 mM KCl, 2 mM $MgCl_2$, 10 mM glucose, 10 mM HEPES) containing 1 μM ci-$IP_3$/PM for 45 mins, after which 4 μM Fluo-8 AM was added to the loading solution for further 45 minutes before washing three times with the saline solution. $[Ca^{2+}]_i$ changes were imaged using a Nikon Eclipse microscope system with a 40x (NA=1.30) oil objective. Fluo-8 fluorescence was excited by 488 nm laser light, and emitted fluorescence (l > 510 nm) was imaged at 30 frames $sec^{-1}$ using an electron-multiplied CCD Camera iXon DU897 (Andor). A single flash of UV light (350-400 nm) from an arc lamp focused to uniformly illuminate a region slightly larger than the imaging field was used to uncage i-$IP_3$, a metabolically stable isopropylidene analogue of $IP_3$, which evoked activity persisting for a few minutes. Image data were acquired as stack .nd2 files using Nikon Elements for offline analysis. Fluorescence signals are expressed as a ratio ($\Delta F/F_0$) of changes in fluorescence ($\Delta F$) relative to the mean resting fluorescence at the same region before stimulation ($F_0$). Recordings were performed in triplicate,

and the measurement outcomes were compared using Mann-Whitney test.

### 2.2.5 Imaging local $Ca^{2+}$ events.

For experiments studying local $Ca^{2+}$ signals, cells were incubated at room temperature in HEPES buffer containing 1 μM ci-$IP_3$/PM and 4 μM Cal-520 for one hour (Ellefsen et al. 2014), washed and further incubated with 10 μM EGTA AM for an hour. Cells were then washed three times and remained in buffer for 30 min to allow for de-esterification of loaded reagents. $[Ca^{2+}]_i$ signals were imaged using the Nikon Eclipse microscope system described above, but now utilizing an Apo TIRF 100x (NA=1.49) oil objective. The imaging region on the camera sensor was cropped to 128 x 512 pixels (20.48 x 81.92 μm) to enable rapid (129 frames per second) imaging. Cal-520 fluorescence (l> 510 nm) was excited by 488 nm laser light within an evanescent field extending a few hundred nanometers into the cells. Image acquisition and processing was as described above for whole-cell imaging, except that local events were identified and analyzed using a custom-written algorithm based on MatLab (Ellefsen et al. 2014).

### 2.2.6 Western blot analysis.

Cell lines were grown in triplicates and lysed in mammalian protein extraction reagent (Thermo Scientific) with complete mini protease inhibitor cocktail tablets (Roche) and phosphatase 2 inhibitor cocktail (Sigma-Aldrich). Lysates were subsequently centrifuged at 14,000 rpm for 15 minutes at $+4^0$C. Protein levels in the cell lysate were measured using the Bradford method (Bradford 1976). 20 μg of protein was loaded per well with 5% β-mercaptoethanol on 3%–8% gradient tris-acetate gels with tris-acetate SDS running buffer (Invitrogen) and separated by electrophoresis at 130V. Proteins were transferred at 50 mA for 6

hours to 0.2 μm nitrocellulose membranes, which were blocked in 5% nonfat milk in tris-buffered saline supplemented with 0.1% tween-20 for 1 hr. Membranes were probed overnight at $+4^0$C with the following primary antibodies: rabbit polyclonal anti-$IP_3R1$ (Millipore, AB5882), rabbit polyclonal anti-$IP_3R2$ (LifeSpan Biosciences, LS-C24911), mouse monoclonal anti-$IP_3R3$ (BD Transduction Laboratories, 610312), rabbit polyclonal anti-$IP_3R1/2/3$ (Santa-Cruz Biotechnology, sc-28613), rabbit polyclonal anti-beta actin (Abcam, ab8227). Membranes were then incubated, as appropriate, with goat anti-rabbit (1:5,000, Sigma-Aldrich) or goat anti-mouse (1:5,000, Sigma-Aldrich) HRP-conjugated secondary antibodies for 1 hr. Bands were visualized by an ImageQuant LAS 4000 imager (GE Healthcare) using peroxidase substrate for enhanced chemiluminescence (ECL Prime; Amersham). Levels of protein expression were quantified via densitometry analysis using ImageJ, and are expressed normalized to actin levels.

**2.2.7 Data processing and analysis.**

The peak change in fluorescence amplitude (ΔF) in each well was normalized to the basal fluorescence of that well before stimulation ($F_0$) after subtraction of the camera black offset level. Mean ATP responses from triplicate wells were further normalized to the triplicate-average $\Delta F/F_0$ of the ionomycin response from each corresponding cell line from the same plate to express the ATP-releasable $Ca^{2+}$ pool as a proportion of the total cellular $Ca^{2+}$ store content. To mitigate plate-to-plate and day-to-day variability, mean ATP/ionomycin responses for each cell line from individual wells were divided by the ATP/ionomycin ratio of a reference cell line (GM03440) (mean of triplicates) included on each plate. All data are presented as mean $\pm$ 1 s.e.m.. Mann-Whitney test was used to determine statistical significance of the findings.

OriginPro 2015 (Origin Lab Corp., Northampton, Massachusetts) was used for data analysis and graph plotting.

### *2.3 Results*

#### 2.3.1 Agonist-induced $Ca^{2+}$ signaling is depressed in FXS and TS fibroblasts.

To screen for defects in $IP_3$-mediated signaling associated with ASD, I used a fluorometric imaging plate reader (FLIPR) to monitor cytosolic $Ca^{2+}$ changes in fibroblasts (Table 2.5.1) loaded with the $Ca^{2+}$-sensitive fluorescent indicator Fluo-8. Primary skin fibroblasts derived from five FXS males and five ethnicity- and age-matched unaffected male donors were grown to confluency on 96 well plates. Cells were stimulated by application of ATP to activate purinergic P2Y receptors (Fine, Cole, and Davidson 1989; Solini et al. 1999) and thereby evoke GPCR-mediated intracellular $Ca^{2+}$ release through $IP_3$Rs. Recordings were made in $Ca^{2+}$ -free extracellular solution to exclude complication from $Ca^{2+}$ influx through plasmalemmal channels. Different concentrations of ATP were applied to individual wells containing FXS and matched control cells. Fig. 2.6.1a (top panel) illustrates representative results, showing smaller ATP-evoked $Ca^{2+}$ signals in FXS cells. To determine whether differences in ATP-evoked signals may result from differences in filling of ER $Ca^{2+}$ stores, I recorded signals evoked in separate wells by application of 1 μM ionomycin in $Ca^{2+}$ -free medium to completely liberate all intracellular $Ca^{2+}$ stores (Fig. 2.6.1a, lower panel). No significant difference was observed between mean ionomycin-evoked $Ca^{2+}$ signals in FXS and control cells (Fig. 2.6.1b), suggesting that there is no systematic defect in ER $Ca^{2+}$ store filling in FXS cells. To normalize for differences in store content among different cell lines and experimental days, I expressed ATP-evoked signals as a

percentage of the ionomycin response obtained in parallel measurements in the same 96 well plate for each given cell line. Mean normalized $Ca^{2+}$ signals evoked by 100 μM ATP were significantly depressed in all five FXS fibroblast lines in comparison with their matched controls (Fig. 2.6.1c). A similar depression was observed at lower concentrations of ATP, pooling data across all 5 FXS and control cell lines (Fig. 2.6.1d). These results were consistently reproducible across different experimental days and matched cell pairs (total of 12 paired trials).

I further extended these findings to another genetic disorder with high co-morbidity with ASD, tuberous sclerosis (TS), caused by mutations in either of two distinct and independent genes – hamartin (*TSC1*) or tuberin (*TSC2*). Fig. 2.6.2 shows data obtained by FLIPR screening in the same way as performed for Fig. 2.6.1. Three cell lines derived from TS patients demonstrated a consistent and highly significant deficit in ATP-evoked $Ca^{2+}$ signals as compared with matched controls (Figs. 2.6.2 a,b,c), but without any appreciable difference in intracellular $Ca^{2+}$ store content as assessed by ionomycin application (Fig. 2.6.2a, lower panel). These findings were consistently replicated on different experimental days (total of 6 paired trials).

The diminished $Ca^{2+}$ signals in FXS and TS cells could result from lower expression levels of $IP_3R$ proteins. To investigate this, I performed western blot analysis on four cell lines selected as showing pronounced defects in $Ca^{2+}$ signaling (FXS-2, FXS-4, TS1-B, and TS2), together with three matched control lines (Ctr-2, Ctr-3, Ctr-4), using antibodies specific to type 1, 2 and 3 $IP_3Rs$ as well as a non type-specific antibody (Fig. 2.6.3a). My results showed an overall slight decrease in $IP_3R$ expression across all isotypes in FXS and TS cells relative to their matched controls (Fig. 2.6.3b). However, in all cases the depression of $IP_3R$ expression was much smaller than the corresponding depression of $Ca^{2+}$ signaling as measured in the FLIPR experiments, and

there was little or no correlation between $IP_3R$ expression and $Ca^{2+}$ signaling in the TS and FXS cells after normalizing relative to their matched controls (Fig. 2.6.3b).

### 2.3.2 Optimizing and expanding the FLIPR assay to include CART subjects.

For this part of the project, I decided to capitalize on a rich database of patients with sporadic ASD, as well as several forms of monogenic syndromes that were recruited through University of California Center for Autism Research and Translation (CART). All enrolled patients undergo a whole day of testing, including confirmation of the ASD diagnosis using a gold standard, Autism Diagnostic Observation Schedule (ADOS) test, deep phenotyping and genome-sequencing. Before running the $Ca^{2+}$ screening assay on the newly obtained fibroblast cultures, I sought to evaluate the extent to which factors including the source, culture initiation, and storage conditions of fibroblast cell lines might affect the FLIPR $Ca^{2+}$ signaling results. The same patient who had previously provided cell line GM24529 to Coriell cell biorepository was enrolled and re-biopsied at CART. The resulting cell line (AU0239-0201) was derived from the same individual with a two-year interval between sampling. Cell cultures were initiated, maintained and stored independently either at CART, exactly as for all of the other sporadic ASD samples; or at the Coriell cell biorepository, as were a majority of syndromic ASD cell lines and all of the controls. When run simultaneously on the same plate, both cell lines demonstrated closely similar responses to ATP that were not statistically different when normalized to the ionomycin response (Fig. 2.6.4).

Next I wanted to determine if CART sporadic ASD patients demonstrate a similar deficit in $Ca^{2+}$ signaling as FXS and TS patients. Representative fluorescence traces illustrating ATP

responses in fibroblasts from two neurotypical controls and one with FXS, as well as one from an enrolled subject with typical, sporadic ASD are shown in Fig. 2.6.5a. The grey dashed line shows the fluorescence signal change upon addition of vehicle only. I quantified fluorescence signals as a ratio ($\Delta F/F_0$) of the fluorescence change ($\Delta F$) at each well, after subtracting the change resulting from addition of vehicle alone, relative to the basal fluorescence ($F_0$) before stimulation. Fig. 2.6.5b shows $\Delta F/F_0$ values (mean of measurements from three plotted replicate wells) from these cell lines in response to 100 μM ATP.

Peak ionomycin response amplitudes, normalized to the basal fluorescence ($\Delta F/F_0$) from the same ASD and control cells as shown in Fig. 2.6.5d were closely similar in ASD and control cell lines. To account for any differences between individual cell lines in the $Ca^{2+}$ store filling across different 96-well plates and different days and to keep the data consistent with the previous findings, I present all ATP-induced $Ca^{2+}$ signals as a percentage of the ionomycin response evoked in parallel wells on the same plate (Fig. 2.6.5e). $Ca^{2+}$ signals with amplitudes comparable to that evoked by ATP were obtained with 100 μM uridine triphosphate (UTP), an agonist that, like ATP, primarily activates P2Y receptors (Fig. 2.6.5f).

In order to parse types of P2Y receptors responsible for the ATP-mediated $Ca^{2+}$ release, I used several purinergic agonists. While UTP evoked a robust and consistent $Ca^{2+}$ response (Fig. 2.6.6a), diphosphates – adenosine diphosphate (ADP) and uridine diphosphate (UDP), and MRS 2365, a selective P2Y1 agonist, all failed to evoke appreciable $Ca^{2+}$ signals at concentrations of 100 μM (Fig. 2.6.6). These data suggest that the receptors being activated by the FLIPR screening procedure are of the P2Y2, or a combination of P2Y4 and P2Y11, receptor class (Burnstock et al. 2016; Erb and Weisman 2012), concordant with reported expression of P2Y2

and P2Y4 in human dermal fibroblasts (Solini et al. 2003).

In addition to normalizing ATP-evoked $Ca^{2+}$ signals relative to ionomycin responses, I further sought to mitigate the day-to-day variability typical of high-throughput functional screens such as FLIPR (Elkins et al. 2013) by expressing ionomycin-normalized responses from each cell line as a percentage of the mean response in triplicate measurements from a "reference" cell line (the control line GM03440) included on the same plate. I chose this cell line as a reference because it demonstrated a robust $Ca^{2+}$ response and had a low passage number (P4) at the time of deposition at Coriell cell biorepository, similar to the passage number (P5) at which CART-derived cells were frozen down. Moreover, this line has been widely used in >20 published studies (Coriell 2016). Normalizing to the reference cell line reduced day-to-day variability in ATP-evoked $Ca^{2+}$ responses among individual cell lines by an average of 38%, measured using three different cell lines each run on four independent days. For each run a mean value was taken from triplicates and the variability between runs was calculated as the coefficient of variation (CV: standard deviation divided by the mean across the four runs). Respective values of CV for the three lines before and after normalization were: 0.81/0.33 (59% reduction in variability); 1.21/1.08 (11% reduction); 0.44/0.24 (45% reduction).

### 2.3.3 ATP-evoked $Ca^{2+}$ signals are depressed in fibroblasts from other monogenic and sporadic ASD subjects.

Monogenic syndromes represent just a small fraction of all ASD cases, with the majority being sporadic, or polygenic (for a review, see (de la Torre-Ubieta et al. 2016)). To determine whether the $IP_3$-signaling defect I observe is a common feature of ASD, or is unique to single-

gene mutations, I decided to expand my observations to fibroblasts from subjects with sporadic forms of ASD as well as two further monogenic syndromes (Prader-Willi syndrome, PWS; and Rett syndrome, Rett). Fig. 2.6.7 presents ATP-evoked $Ca^{2+}$ responses in fibroblasts from multiple sporadic ASD subjects as well as those from control, PWS, FXS, TSC and Rett syndromes, after normalizing each as a percentage of the $Ca^{2+}$ response to the mean reference cell line included in each plate. Data points (dots) show measurements from individual subjects as means of triplicates; grey bars indicate means of N subjects with error bars showing ± 1 s.e.m. Consistent with my previous findings, ATP-evoked $Ca^{2+}$ responses in cells from individuals with PWS and Rett were, on average, substantially reduced (to about 33% and 62%) as compared with the mean response in cells from control neurotypical individuals.

Most importantly, the mean response from cell lines from sporadic ASD subjects was also considerably depressed relative to controls (Fig. 2.6.7). A majority of the ASD cells gave very small or no detectable responses, and all control cells gave responses above the mean of the ASD cells. One ASD cell line consistently gave remarkably discrepant ATP responses, with a mean amplitude close to that evoked by ionomycin (75%) and almost seven times greater than the control average (Fig. 2.6.7, circled data point). That subject was shown to carry a chromosomal deletion and for the present I exclude that cell line from the statistical analysis. The mean response of the remaining 22 cell lines from subjects with sporadic ASD was 28% ± 7% s.e.m. of the reference cell line as compared to 87% ± 14% for the controls; a reduction to about 31%. However, despite the smaller average response, $Ca^{2+}$ signal amplitudes among the cell lines from subjects with sporadic ASD displayed a much wider spread than the controls, and six of the ASD subjects had cell responses that overlapped those of the controls. This high variability and

skewed, non-normal Gaussian distribution points to considerable heterogeneity of $Ca^{2+}$ signaling among the cohort of sporadic ASD subjects.

### 2.3.4 ROC curves discriminate between ASD subjects and controls.

To assess the robustness of the difference between cell lines from subjects with sporadic ASD and controls, I generated receiver operating characteristic (ROC) curves (Fig. 2.6.8); a metric that is widely used to evaluate parameters to separate affected from unaffected individuals for diagnostic purposes (Metz 1978; Hanley and McNeil 1982). The ROC curve expresses the accuracy of a test in terms of two measures – sensitivity and specificity – in this case comparing the $Ca^{2+}$ signaling assay against the ADOS assessment as a 'gold standard' for diagnosis of ASD. Thus, sensitivity refers to the proportion of subjects who are correctly identified by the assay as having ASD (true positive): a highly sensitive test best assures that affected people will be identified. Specificity refers to the true-negative rate: here, the proportion of subjects without ASD who are correctly identified as not having the condition. At any given $Ca^{2+}$ signaling value, the sensitivity and the specificity are calculated from a ratio of people who are disease positive (true positive) or disease negative (false positive) at that threshold. For example, it is apparent from Fig. 2.6.7 that a low $Ca^{2+}$ signal cutoff value would exclusively capture subjects with ASD, but would not capture all of the affected subjects. As the signaling cutoff is increased, more ASD subjects are captured, so the *sensitivity* increases, but the number of unaffected controls captured increases, thereby decreasing the *specificity*. The ROC curve therefore essentially describes the compromise between sensitivity and specificity of a test at varying threshold cutoff values.

After sorting all subjects by their $Ca^{2+}$ signaling normalized to the reference cell line (as was done for Fig. 2.6.7), I generated an ROC curve by plotting sensitivity (true positive rate) against 1-specificity (false positive rate) at each test value for individuals with syndromic ASD (FXS, TSC1 and TSC2, Rett and Prader-Willi syndromes) as shown in Fig. 2.6.8a. The area under the ROC curve (AUC) is a useful tool to compare the utility of a biomarker. It represents the overall probability that the correct diagnostic status (ASD *vs* unaffected in my case) will be accurately identified in a randomly chosen individual, with an AUC of 1 having a perfect predictive value and 0.5 being no better than random. The ROC generated for syndromic ASD resulted in a robust AUC of 0.86, a value considered an excellent discriminant in predicting disease status (Hosmer and Lemeshow 2000).

Notably, my current cohort of subjects with sporadic ASD yielded an ROC curve (Fig. 2.6.8b) closely resembling that of syndromic ASD, with a similar AUC of 0.83. An ROC curve pooling individuals with both syndromic and sporadic ASD (Fig. 2.6.8c) yielded an AUC of 0.84. The similarity of my findings between sporadic ASD subjects and those with diverse monogenic syndromes suggests a common underlying signaling deficit across different forms of ASD. Using a cutoff value at 40% of the "reference" cell-normalized ATP-evoked $Ca^{2+}$ signal achieved 73% sensitivity and 100% specificity for discriminating between pooled ASD subjects and controls, irrespective of their genetic background (Fig. 2.6.8c). These findings indicate that $Ca^{2+}$ signaling may be a new promising biomarker target in ASD.

### 2.3.5 $IP_3$-induced $Ca^{2+}$ release is reduced in FXS and TS cells.

The FLIPR screen is a high-throughput, low-resolution $Ca^{2+}$ signaling assay that allows

investigation of many different cell lines at the same time, however, it provides little information on *how* those signals may be arising and what is the difference between individual cells' responses. To discriminate whether the observed deficits in ATP-induced $Ca^{2+}$ signals in ASD cell lines arose through defects in any of the intermediate steps from binding to purinergic GPCR receptors to generation of $IP_3$, or at the level of $IP_3$-mediated $Ca^{2+}$ liberation itself, I circumvented upstream GPCR signaling by loading cells with a caged analogue of $IP_3$ (ci-$IP_3$) (Smith, Wiltgen, and Parker 2009). UV flash photolysis of ci-$IP_3$ to photorelease physiologically active i-$IP_3$ then allowed us to directly evoke $Ca^{2+}$ liberation through $IP_3$Rs in a graded manner by regulating flash duration and intensity to control the amount of i-$IP_3$ that was photoreleased.

I chose one cell line from a FXS patient and one cell line from a patient with TS. Fig. 2.6.9a illustrates images obtained by epifluorescence microscopy of FXS and control fibroblasts loaded with Fluo-8 and caged i-$IP_3$ by incubation with membrane-permeant esters of these compounds. Fig. 2.6.9b shows superimposed fluorescence ratio ($\Delta F/F_o$) traces measured from several representative FXS-2 (GM09497) and matched control Ctr-2 (GM02912) cells in response to uniform photolysis flashes. Concordant with my observations of defects in ATP-induced global $Ca^{2+}$ signals, global cytosolic $Ca^{2+}$ responses evoked by equivalent photorelease of i-$IP_3$ in these FXS cells were smaller than in control cells (Fig. 2.6.9c); and displayed a longer time to peak (Fig. 2.6.9d) and slower rate of rise (Fig. 2.6.9e). Similar results were obtained from two other FXS-Ctr cell pairs (FXS-1/Ctr-1: 20.7±3.9/44.6±12.2 $\%\Delta F/F_0$, FXS-3/Ctr-3: 20.1±4.8/156.8±17.3). Moreover, I observed a consistent proportional depression of $Ca^{2+}$ signals for different relative UV flash strengths corresponding to photorelease of different i-$IP_3$ concentrations (25% flash strength, pooled FXS response 61% of control; 50% flash, 65% of

control; 100% flash, 74% of control: n = 13-17 cells for each flash duration).

TS cells also showed depressed and slowed $Ca^{2+}$ responses to photoreleased i-$IP_3$. Measurements from the matched TS1-B (GM06149) and Ctr-3 Ctr-3 (GM03440) cell lines (Fig. 2.6.9f) revealed a pronounced deficit in average $Ca^{2+}$ signal amplitudes (Fig. 2.6.9g); and again the time to peak was lengthened (Fig. 2.6.9h) and the rate of rise slowed (Fig. 2.6.9i). These differences were apparent employing two different relative UV flash strengths (15% flash strength, TS response 18% of control; 25% flash, 20% of control: n = 13-15 cells for each flash duration).

### 2.3.6 $IP_3$ signaling is affected at the level of local events.

$IP_3$-mediated cellular $Ca^{2+}$ signaling is organized as a hierarchy, wherein global, cell-wide signals, such as those discussed above, arise by recruitment of local, 'elementary' events involving individual $IP_3R$ channels or clusters of small numbers of $IP_3Rs$ (Yao and Parker 1993; Yao, Choi, and Parker 1995). I therefore imaged these elementary events to elucidate how deficits in the global $Ca^{2+}$ signals in FXS and TS cells may arise at the level of local $IP_3R$ clusters. I selected one FXS (FXS-3) fibroblast line, one TS1 (TS1-B) line, and a common control (Ctr-3) cell line matched to both. $Ca^{2+}$ release from individual sites was resolved utilizing total internal reflection fluorescence (TIRF) microscopy of Cal-520 (a $Ca^{2+}$ indicator that was shown to be superior to Fluo-8 in detecting local $Ca^{2+}$ signals (Lock, Parker, and Smith 2015)), in conjunction with cytosolic loading of the slow $Ca^{2+}$ buffer EGTA to inhibit $Ca^{2+}$ wave propagation (Dargan and Parker 2003). This technique captures in real time the duration and magnitude of the underlying $Ca^{2+}$ flux, providing a close approximation of the channel gating

kinetics as would be recorded by electrophysiological patch-clamp recordings (Parker and Smith 2010). $Ca^{2+}$ release evoked by spatially uniform photolysis of ci-$IP_3$ across the imaging field was apparent as localized fluorescent transients of varying amplitudes, arising at numerous discrete sites widely distributed across the cell body (Fig. 2.6.10a). Representative fluorescence traces illustrating responses at several sites (marked by large circles in Fig. 2.6.10a) are shown in Fig. 2.6.10b; and Figs. 2.6.10c,d respectively illustrate the time course and spatial distribution of selected individual events.

To quantify differences in elementary $Ca^{2+}$ events between the cell lines I utilized a custom-written, automated algorithm (Ellefsen et al. 2014) to detect events and measure their amplitudes and durations (Fig. 2.6.10e) A striking difference between control and ASD lines was apparent in the numbers of detected sites, with control cells showing on average 97 sites per imaging field, whereas FXS and TS cells showed only 12 and 29 sites, respectively (Fig. 2.6.11a). However, this could be a secondary effect of under-counting the number of release sites with very small $Ca^{2+}$ release. The mean frequency of events per site appeared higher in control cells than in both FXS and TS cells (Fig. 2.6.11b), but quantification was imprecise because many sites, particularly in the FXS and TS cells, showed only a single event. Using the latency between the UV flash and first event at each site as an alternative measure of the probability of event initiation (Dickinson, Swaminathan, and Parker 2012; Shuai et al. 2007) showed no significant difference among FXS, TS and control cell lines (Fig. 2.6.11c). Mean event amplitudes were also similar among the three cell lines (Fig. 2.6.11d). A second key difference between the control and FXS and TS cells was apparent in the durations of the local events. In all cell lines event durations were statistically distributed as single-exponentials, as expected for stochastic events.

However, the time constants fitted to these distributions were appreciably shorter in FXS and TS cells as compared with control cells (Fig. 2.6.11e).

### *2.4 Discussion*

I report abnormalities of $IP_3$-mediated $Ca^{2+}$ signaling in several distinct genetic models that display high co-morbidity with ASD – FXS, two genetically-distinct forms of TS (TS1 and TS2), Rett, and PWS. I also extend those findings to reveal a corresponding deficit in $IP_3$-mediated $Ca^{2+}$ release in cells from subjects with sporadic ASD, where each subject likely carries a unique sampling of genetic risk alleles. $Ca^{2+}$ responses evoked by agonist stimulation of GPCR-mediated $IP_3$ signaling were significantly smaller in fibroblasts derived from subjects with ASD, as compared with matched control cell lines. By using a high throughput assay to measure $Ca^{2+}$ signals evoked by ATP in fibroblasts from subjects with ASD and controls, I was able to derive an ROC curve that can discriminate subjects with ASD from unaffected controls with high sensitivity and specificity. Notably, this approach identifies subjects with highly heterogeneous sporadic forms of ASD as well as a spectrum of homogeneous monogenic syndromes caused by "major effect" mutations, and does so similarly well with both, pointing to a common signaling defect in the ubiquitous $IP_3$-mediated $Ca^{2+}$ signaling pathway. Even though the number of subjects used in this study was modest and the results need to be replicated with larger cohorts of ASD subjects and neurotypical controls, it serves as a proof of principle for the prospective utility of such testing.

In contrast, I found no significant differences in $Ca^{2+}$ liberation evoked by application of the $Ca^{2+}$ ionophore ionomycin, indicating that the diminished responses to $IP_3$ do not result from

diminished ER $Ca^{2+}$ store content. Moreover, $Ca^{2+}$ signals evoked by intracellular uncaging of i-$IP_3$ were depressed in FXS and TS cell lines, pointing to a deficit at the level of $Ca^{2+}$ liberation through $IP_3$Rs and not solely because of diminished GPCR-mediated production of $IP_3$. Finally, I conclude that the depression of $Ca^{2+}$ signals cannot be attributed entirely or substantially to reduced expression of $IP_3$R proteins, because mean agonist-evoked $Ca^{2+}$ responses across four FXS and TS lines were about 22% of matched controls, whereas western blots showed mean $IP_3$R levels to be about 80% of controls and uncorrelated with the extent of $Ca^{2+}$ signaling depression in these different cell lines.

By resolving $Ca^{2+}$ liberation during 'elementary', local signals evoked by photoreleased $IP_3$ (Yao, Choi, and Parker 1995), I further demonstrate that defects in global $Ca^{2+}$ signaling in these distinct ASD-associated models are reflected at the level of $Ca^{2+}$ release through individual and small clusters of $IP_3$Rs. In both FXS and TS cell lines I observed fewer sites of local $Ca^{2+}$ release as compared to a control cell line, and the durations of these events were shorter. Because functional sites are comprised of clusters of small numbers of individual $IP_3$Rs, the amplitude of the fluorescence signal at a site depends on the channel permeability, together with the number of active channels in the cluster (Yao, Choi, and Parker 1995). I observed similar amplitudes of local $Ca^{2+}$ signals across the cell lines, suggesting that the $Ca^{2+}$-permeation properties and cluster organization of $IP_3$Rs are not appreciably affected in FXS and TS. However, the shorter average duration of local events points to a modulation of $IP_3$R gating kinetics, and would lead to an overall decrease in amount of $Ca^{2+}$ released over time. Compounding this, I found the numbers of local $Ca^{2+}$ release sites within a cell to be dramatically lower in FXS and TS cells as compared with control cells (respectively, 87% and 70%), although it is possible that the short duration

events observed in the mutants may have contributed to undercounting their release sites. Taken together, these findings on local $IP_3$-mediated $Ca^{2+}$ signals indicate that the deleterious effects of single gene mutations are manifest at the level of the functional channel gating of $IP_3Rs$.

Fibroblasts are primary, untransformed cells that are readily obtained by skin biopsy. A patient-derived, cell-based assay such as I describe here has potential as a biomarker for early detection of children susceptible to ASD, before behavioral symptoms appear and when an earlier intervention has a better chance of improving outcome (Anderson, Liang, and Lord 2014; MacDonald et al. 2014). Although several blood-based biomarkers with high specificity and sensitivity have been proposed for ASD (Zaman et al. 2016; Pramparo et al. 2015; West et al. 2014), they are not currently suitable for high-throughput screening, and may be subject to alteration due to medication regimen, diet, lifestyle changes or other variables that would potentially complicate the read-out.

The current practice of testing new ASD treatments in biologically and behaviorally heterogeneous populations of ASD subjects is widely acknowledged to impede the identification of new drugs that would be effective in only a specific subgroup of "responders" (Berry-Kravis et al. 2012; Lozano, Martinez-Cerdeno, and Hagerman 2015). Therefore, there is hope that a set of biomarkers could independently stratify patient populations into distinct, biologically meaningful endophenotypes (Loth et al. 2016) to enable more robust clinical trials. Although limited to a modest cohort of subjects, my results already hint at such a stratification of $Ca^{2+}$ signal amplitudes among sporadic ASD subjects, which exhibit a much greater spread of signaling responses than controls, with a majority giving almost no response whereas others exhibit signals overlapping the control range.

## *2.5 Tables*

**Table 2.5.1 Skin fibroblast information for ASD subjects and controls.**

Controls are defined as apparently healthy individuals without any known neurodevelopmental disorders (Coriell cell biorepository). Cell lines starting with "GM#" were purchased from the Coriell cell biorepository; cell lines starting with "AU#" were established by UCI CART. The ASD diagnosis was established based on the results of administered appropriate version of ADOS. PDD-NOS = Pervasive Developmental Disorder-Not Otherwise Specified.

$Ca^{2+}$ signals are presented as percentage of the reference cell line (GM03440).

| *Monogenic ASD* | | | | | | *Sporadic ASD* | | | | | | *Control* | | | | | |
|---|---|---|---|---|---|---|---|---|---|---|---|---|---|---|---|---|---|
| **ID** | **Sex** | **Age** | **Ethnicity** | **Status** | **Ca2+ signal** | **ID** | **Sex** | **Age** | **Ethnicity** | **Status** | **Ca2+ signal** | **ID** | **Sex** | **Age** | **Ethnicity** | **Status** | **Ca2+ signal** |
| GM09497 | M | 28 | Caucasian | FXS | 33.4 | AU0001-0201 | M | 29 | Caucasian | Autism | 82.5 | GM00498 | M | 3 | N/A | Healthy | 104.8 |
| GM05848 | M | 4 | Caucasian | FXS | 10.8 | AU0027-0201 | F | 24 | Caucasian | Autism | 115.5 | GM01863 | M | 46 | Caucasian | Healthy | 58.5 |
| GM05185 | M | 26 | Caucasian | FXS | 11.7 | AU0027-0202 | M | 21 | Caucasian | Autism | 22.9 | GM02185 | M | 36 | Caucasian | Healthy | 107.8 |
| GM05131 | M | 3 | Caucasian | FXS | 25.3 | AU0078-0202 | F | 36 | Caucasian | Autism | 96.3 | GM02912 | M | 26 | Caucasian | Healthy | 64.3 |
| GM04026 | M | 35 | Caucasian | FXS | 31.4 | AU0120-0202 | M | 15 | Asian | Autism | 24.2 | GM03440 | M | 20 | Causasian | Healthy | 100.0 |
| GM04024 | M | 29 | Black | FXS | 113.0 | AU0197-0201 | M | 17 | Hispanic | PDD-NOS | 38.9 | GM04505 | F | 20 | N/A | Healthy | 110.6 |
| GM21890 | M | 19 | N/A | PWS | 82.7 | AU0197-0202 | F | 14 | Hispanic | PDD-NOS | 22.6 | GM05659 | M | 1 | Caucasian | Healthy | 40.8 |
| GM16548 | F | 5 | Caucasian | RETT | 34.2 | AU0236-0203 | F | 12 | Caucasian | Autism Spectrum | 7.2 | GM07492 | M | 17 | Caucasian | Healthy | 44.7 |
| GM07982 | F | 25 | Caucasian | RETT | 75.6 | AU0237-0201 | F | 13 | Caucasian | Autism | 686.6 | GM07753 | M | 17 | N/A | Healthy | 214.6 |
| GM06149 | M | 17 | Caucasian | TSC1 | 49.2 | AU0239-0201 | F | 16 | Caucasian | Autism | 21.3 | GM08399 | F | 19 | N/A | Healthy | 62.9 |
| GM06148 | M | 43 | Caucasian | TSC1 | 34.3 | AU0239-0203 | F | 6 | Caucasian | Autism Spectrum | 0.5 | GM23973 | M | 19 | Caucasian | Healthy | 42.7 |
| GM06121 | M | 22 | Caucasian | TSC2 | 22.8 | AU0243-0201 | M | 2 | Caucasian | Autism | 0.5 | GM23976 | M | 22 | Caucasian | Healthy | 93.0 |
| AU0240-0203 | M | 12 | Caucasian | PWS | 2.4 | AU0245-0201 | F | 20 | Caucasian | Autism | 68.4 | | | | | | |
| AU0244-0201 | M | 19 | Caucasian | PWS | 24.8 | AU0245-0202 | F | 18 | Caucasian | Autism Spectrum | 28.0 | | | | | | |
| AU0250-0202 | M | 11 | Caucasian | PWS | 16.4 | AU0249-0202 | F | 10 | Caucasian | Autism | 16.7 | | | | | | |
| | | | | | | AU0251-0202 | M | 8 | Hispanic | Autism | 40.6 | | | | | | |
| | | | | | | AU0251-0203 | M | 5 | Hispanic | Autism | 22.8 | | | | | | |
| | | | | | | AU0252-0201 | M | 4 | Asian | Autism | 20.6 | | | | | | |
| | | | | | | AU0254-0201 | M | 5 | Hispanic | Autism Spectrum | 0.3 | | | | | | |
| | | | | | | AU0254-0202 | F | 3 | Hispanic | Autism | 0.3 | | | | | | |
| | | | | | | AU0256-0201 | M | 5 | Caucasian | Autism | 0.2 | | | | | | |
| | | | | | | AU0256-0202 | M | 3 | Caucasian | Autism | 0.1 | | | | | | |
| | | | | | | AU0257-0202 | M | 3 | Asian | Autism | 1.2 | | | | | | |

## *2.6 Figures*

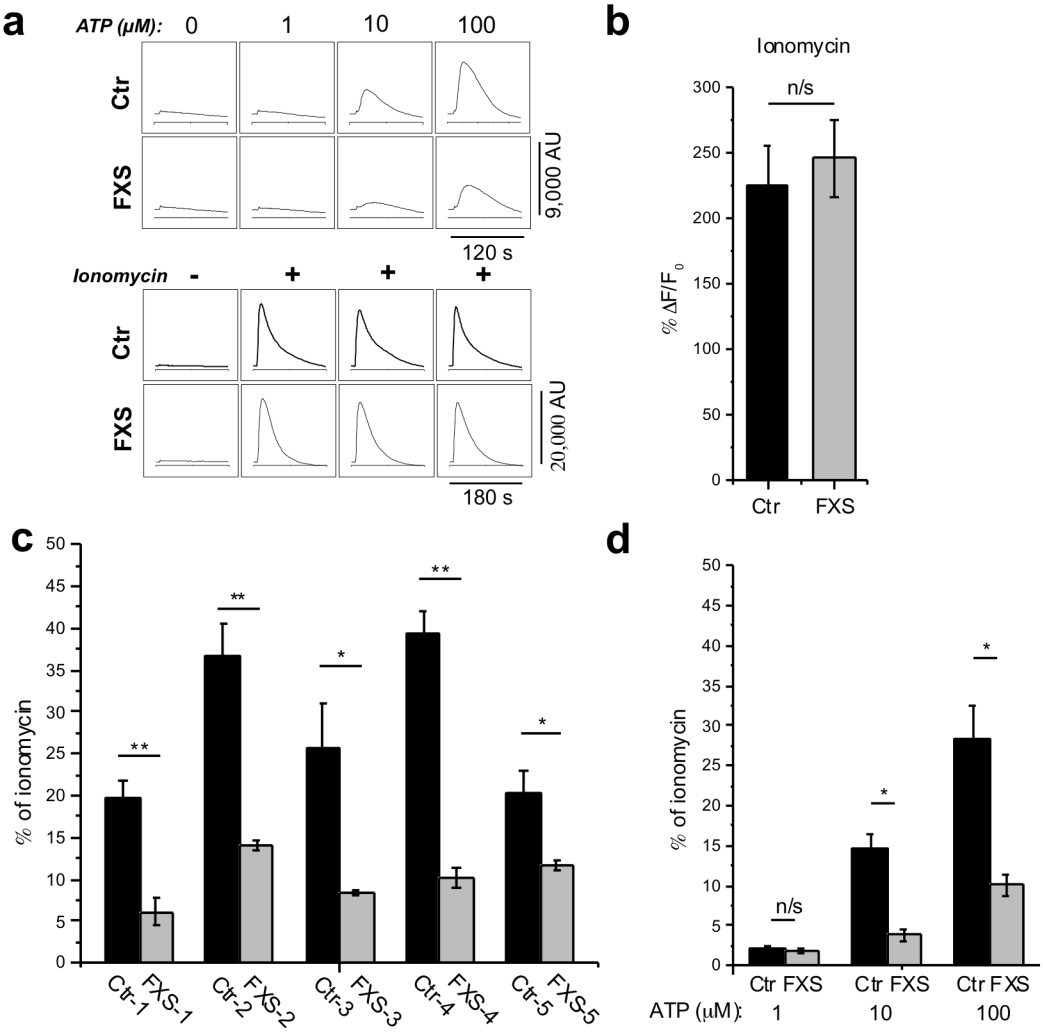


**Figure 2.6. 1 $Ca^{2+}$ responses to extracellular application of ATP in $Ca^{2+}$-free solution are depressed in human skin fibroblasts from FXS patients as compared with matched controls.**

**(a)** Representative FLIPR traces showing response to various concentrations of extracellular ATP (top panel) and to the $Ca^{2+}$ ionophore ionomycin (lower panel) in control (Ctr) and FXS

cells loaded with the $Ca^{2+}$ indicator Fluo-8. Traces show fluorescence in arbitrary units, and each recording was obtained from a separate well. **(b)** Peak $Ca^{2+}$ responses to 1 μM ionomycin in five control and five FXS cell lines. Bars show mean and s.e.m. of triplicate measurements. **(c)** Cells from five FXS cell lines (grey bars) and matched controls (black bars) were stimulated with 100 μM ATP in $Ca^{2+}$-free solution to stimulate $Ca^{2+}$ release from intracellular $Ca^{2+}$ stores. Recordings were performed in triplicate, averaged, and normalized with respect to corresponding ionomycin responses in $Ca^{2+}$-free solution. n=3 in each group. **(d)** Normalized $Ca^{2+}$ responses to various concentrations of ATP derived by combining results from 5 FXS and 5 matched controls. All data in this and following figures are presented as mean ± s.e.m.; * = p-value <0.05; ** = p <0.01 calculated from a two-sample Student's t-test.

Cell line numeration corresponds to Coriell IDs as follows: FXS-1 (GM05848), Ctr-1 (GM00498), FXS-2 (GM09497), Ctr-2 (GM02912), FXS-3 (GM05185), Ctr-3 (GM03440), FXS-4 (GM04026), Ctr-4 (GM02185), FXS-5 (GM05131), Ctr-5 (GM05659).

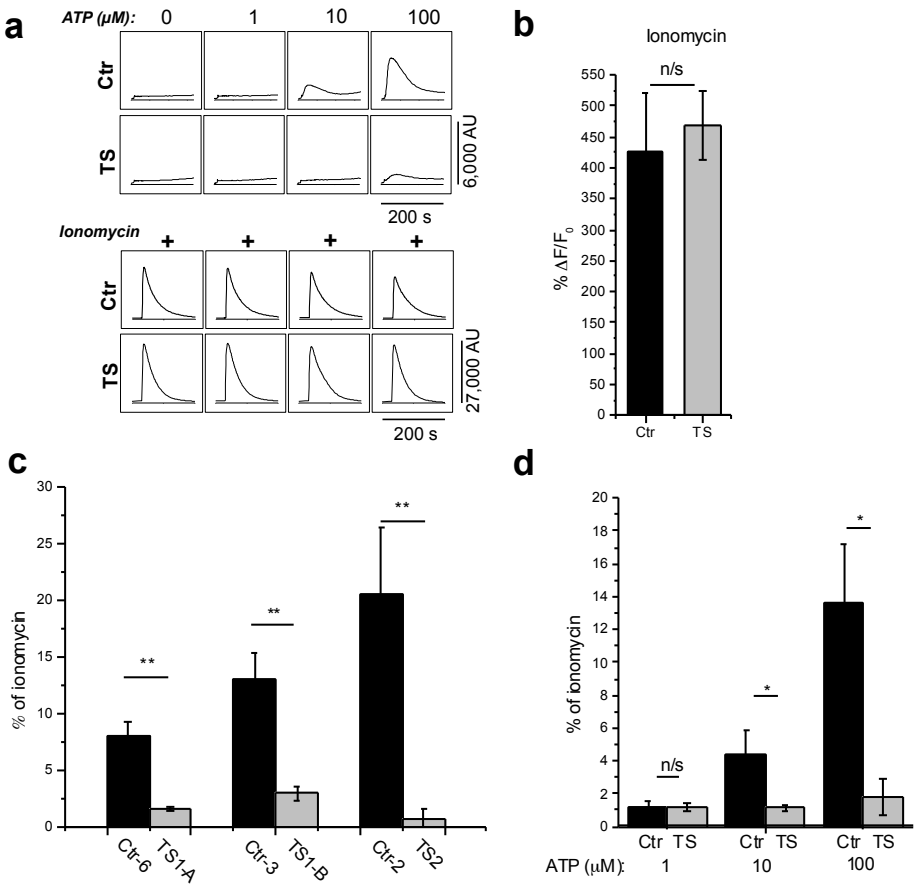


**Figure 2.6. 2 $Ca^{2+}$ responses to extracellular application of ATP in $Ca^{2+}$-free solution are strongly depressed in human skin fibroblasts from TS1 and TS2 patients compared with matched controls.**

**(a)** Representative FLIPR traces showing response to various concentrations of extracellular ATP (top panel) and to the $Ca^{2+}$ ionophore ionomycin (lower panel) in control (Ctr) and TS cells loaded with the $Ca^{2+}$ indicator Fluo-8. **(b)** Peak $Ca^{2+}$ responses to 1 μM ionomycin in three control and three TS cell lines. Bars show mean and s.e.m. of triplicate measurements. **(c)** Three cell lines from TS patients (grey bars) and matched controls (black bars) were stimulated with

100 μM ATP in $Ca^{2+}$-free solution to stimulate $Ca^{2+}$ release from intracellular $Ca^{2+}$ stores. Recordings were performed in triplicate, averaged, and normalized with respect to corresponding ionomycin responses in $Ca^{2+}$-free solution. **(d)** Normalized $Ca^{2+}$ responses to various concentrations of ATP derived by combining results from three TS and three matched controls. n=3 replicates in each group. All data in this and following figures are presented as mean ± s.e.m.; * = p-value <0.05; ** = p <0.01 calculated from a two-sample Student's t-test.

Cell line numeration corresponds to Coriell IDs as follows: FXS-1 TS1-A (GM06148), Ctr-6 (GM01863), TS1-B (GM06149), Ctr-3 (GM03440), TS2 (GM06121), Ctr-2 (GM02912).

**a**

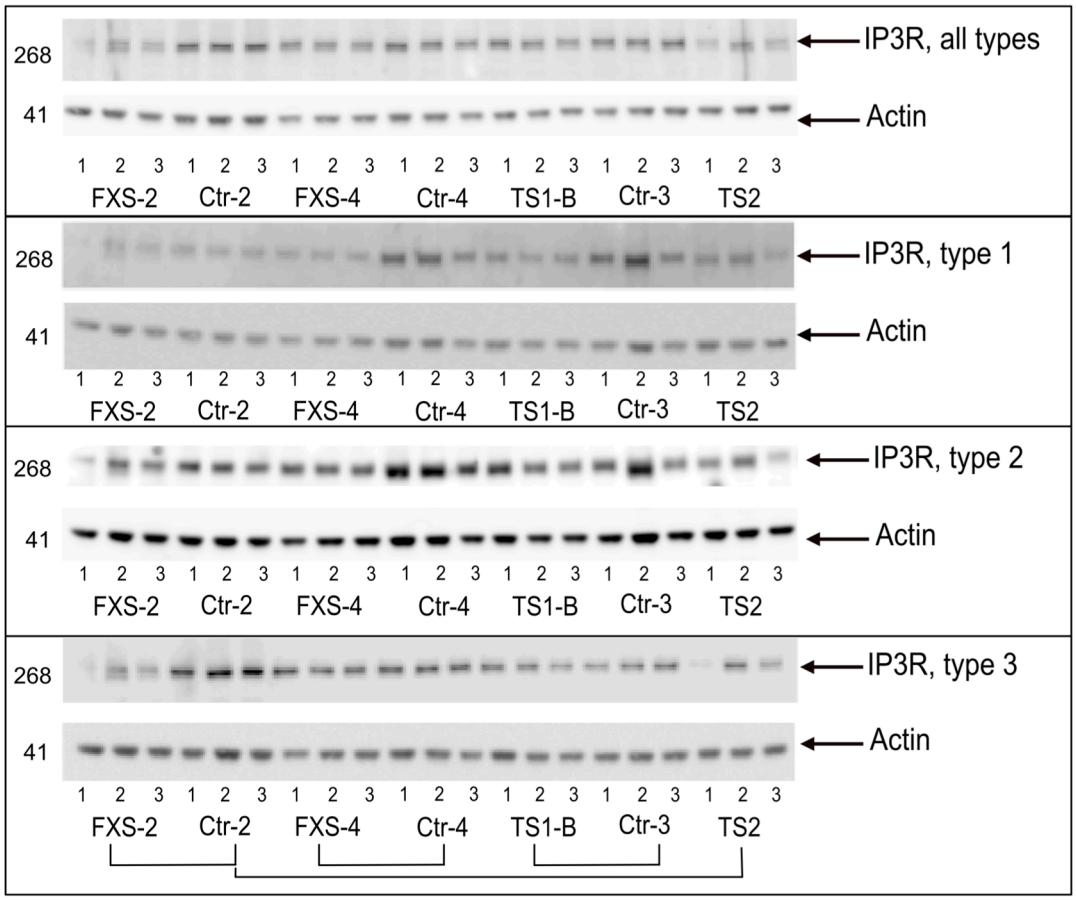
268
41
IP3R, all types
Actin
1 2 3 1 2 3 1 2 3 1 2 3 1 2 3 1 2 3 1 2 3
FXS-2 Ctr-2 FXS-4 Ctr-4 TS1-B Ctr-3 TS2
IP3R, type 1
IP3R, type 2
IP3R, type 3

**b**

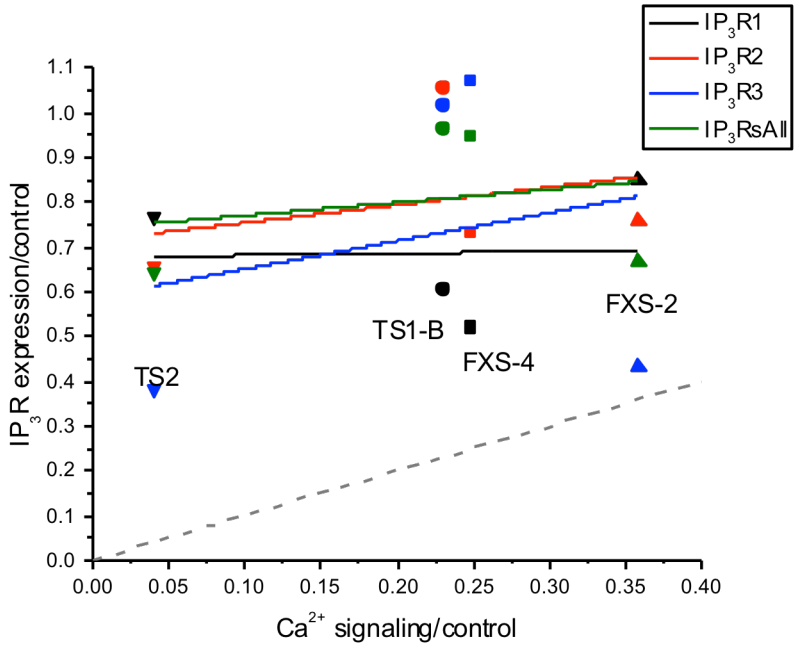
IP3R1
IP3R2
IP3R3
IP3RsAll
IP3R expression/control
Ca2+ signaling/control
0.0 0.1 0.2 0.3 0.4 0.5 0.6 0.7 0.8 0.9 1.0 1.1
0.00 0.05 0.10 0.15 0.20 0.25 0.30 0.35 0.40
FXS-2
TS1-B
FXS-4
TS2

**Figure 2.6. 3 $IP_3R$ protein level expression in FXS, TS and control cells.**

**(a)** Representative immunoblots of $IP_3R$ proteins in skin fibroblast cell lines FXS-2, Ctr-2, FXS-4, Ctr-4, TS1-B, Ctr-3 and TS2. Aliquots of protein lysates from cell lines grown in triplicates were subjected to SDS-tris-acetate electrophoresis and then immunoblotted with the indicated antibodies. All $IP_3R$ bands ran at a molecular mass of about 270 kD. Actin was used a loading control. The leftmost lane typically showed weak transfer onto the blot, and was excluded from quantitative analysis. **(b)** Scatter plot showing $IP_3R$ expression levels in TS and FXS cell lines determined by western blotting versus the mean ATP-evoked $Ca^{2+}$ signals in these cells relative to matched control cells. Different symbols represent different cell lines (TS2, downward arrow; TS1-B, circle; FXS-2, upward arrow; and FXS-4, square), and different colors represent $IP_3R$ expression levels as determined using antibodies for type 1 (black), type 2 (red), type 3 (blue) $IP_3Rs$, and a non type-specific antibody (green). All data are normalized relative to matched control cells. Solid lines are regression fits to data for $IP_3R1$ (black), $IP_3R2$ (red), $IP_3R3$ (blue), and total $IP_3Rs$ (green). The grey dashed line represents a one-to-one relationship between normalized $Ca^{2+}$ signal and normalized $IP_3R$ expression.

Cell line IDs correspond to Coriell numeration as follows: FXS-2 (GM09497), Ctr-2 (GM02912), Ctr-3 (GM03440), FXS-4 (GM04026), Ctr-4 (GM02185), TS1-B (GM06149), TS2 (GM06121).

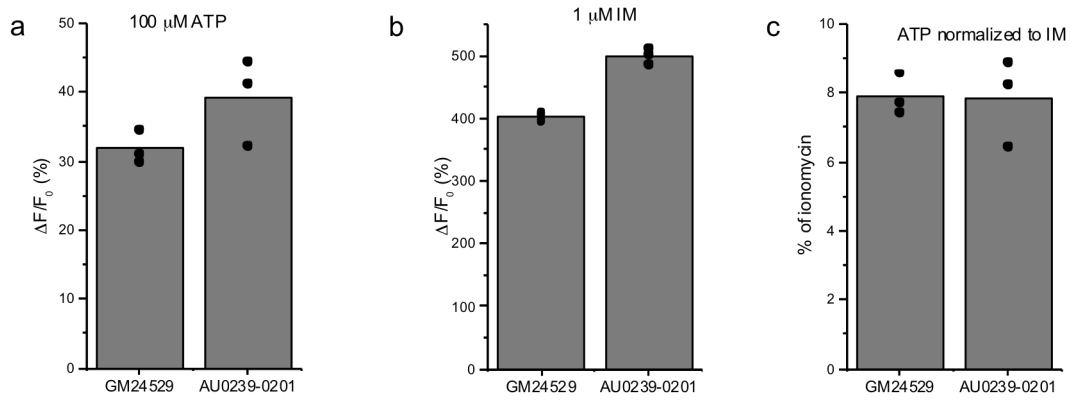


**Figure 2.6. 4 $Ca^{2+}$ response in two different fibroblast cell lines derived from the same patient.**

**(a)** Peak amplitude (ΔF) $Ca^{2+}$ response to 100 μM ATP normalized to the basal fluorescence ($F_0$) before stimulation. The data were calculated by subtracting vehicle addition peak response from peak trace value of each corresponding cell line. Bar graphs show mean of triplicate measurements. The cell line GM24529 was established by Coriell cell biorepository (Camden, New Jersey). The same patient was re-biopsied at CART, UC Irvine, and a cell culture (AU0239-0201) was established from an explant. Both cell lines were thawed from a liquid nitrogen long-term storage, passaged and plated for high-throughput $Ca^{2+}$ signaling in parallel. **(b)** Peak amplitude $Ca^{2+}$ response to 1 μM ionomycin normalized to the basal fluorescence before stimulation. **(c)** Peak ATP response for each cell line from (**a**) normalized to that of ionomycin response from (**b**). Bar graphs show mean of triplicate measurements from individual wells. Data points represent individual triplicate responses.

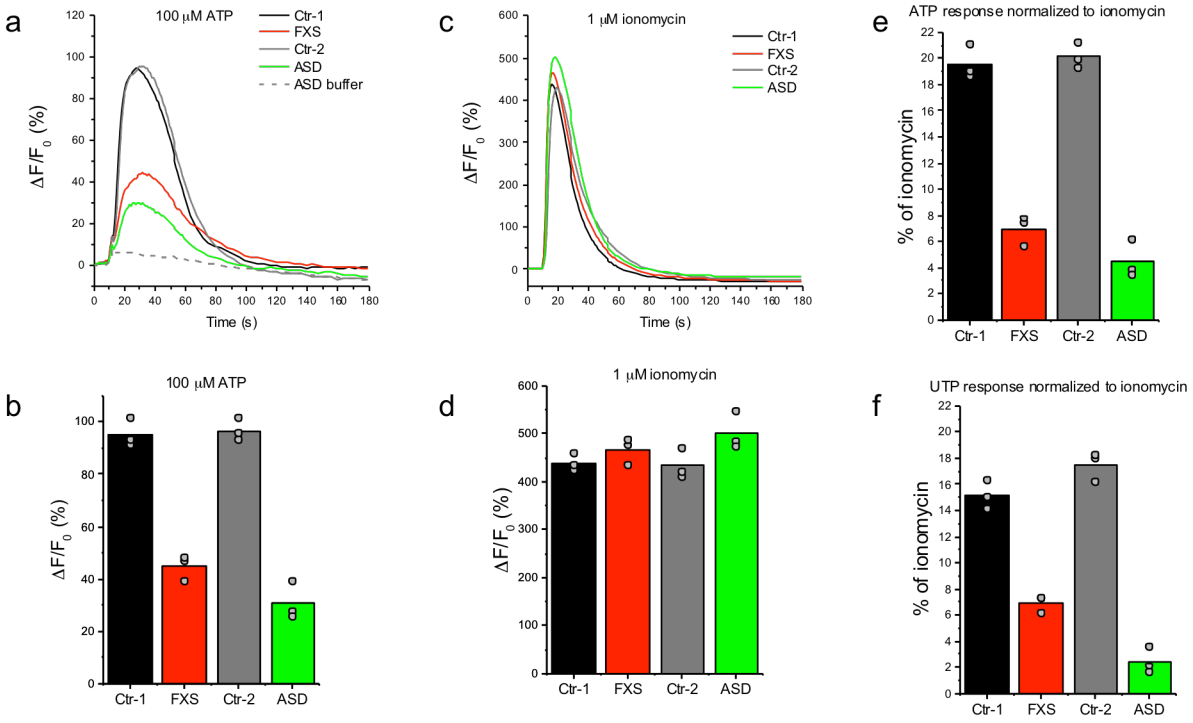


**Figure 2.6. 5 Representative $Ca^{2+}$ responses to extracellular application of purinergic agonists and ionomycin in absence of extracellular $Ca^{2+}$ in fibroblasts from ASD subjects and controls.**

**(a)** Representative FLIPR traces showing changes in Fluo-8 fluorescence over the basal fluorescence ($\Delta F/F_0$) in response to extracellular application of 100 μM ATP to fibroblast cell lines from two controls (black; GM03440 and grey; GM02912), one FXS (red; GM09497) and one sporadic ASD subject (green; AU0027-0202). Fluorescence changes ΔF are presented as a % change from the basal fluorescence $F_0$. The grey dashed line represents the artifactual fluorescence change resulting from addition of vehicle alone to the ASD cell line. **(b)** Peak

amplitudes (ΔF) of $Ca^{2+}$ responses to 100 μM ATP normalized to the basal fluorescence ($F_0$) before stimulation in control cell lines (black and grey), FXS (red) and a sporadic ASD line (green). Bar graphs show mean of triplicate measurements after subtracting the artifactual signal resulting from addition of vehicle alone to each corresponding cell line. Data points represent individual triplicate responses. **(c)** Representative FLIPR traces showing changes in fluorescence over the basal ($\Delta F/F_0$) in response to extracellular application of 1 μM ionomycin to control (black and grey traces), FXS (red) and ASD (green) cell lines. **(d)** Mean peak $Ca^{2+}$ responses (ΔF) to 1 μM ionomycin normalized to the basal fluorescence ($F_0$) before stimulation in control cell lines (black and grey), FXS line (red) and an ASD line (green). Bar graphs show mean of triplicate measurements. Data points represent individual triplicate responses. **(e)** Mean peak ATP responses for each cell line from (**b**) expressed as a percentage of the mean ionomycin response from (**d**) in that cell line. **(f)** Mean peak responses evoked by addition of 100 μM UTP to each cell line as a percentage of the of ionomycin response for that cell line.

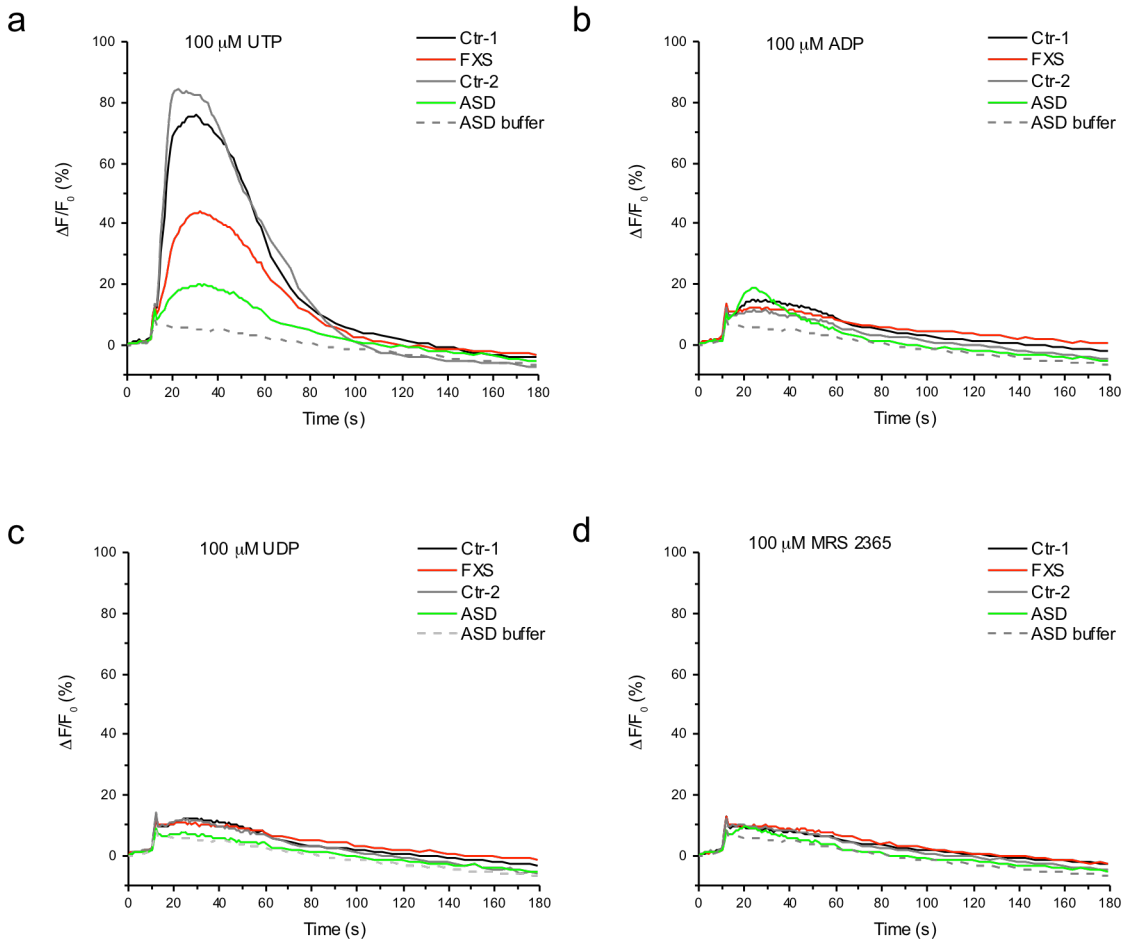


**Figure 2.6. 6 Representative $Ca^{2+}$ responses to extracellular application of different purinergic receptor agonists in absence of extracellular $Ca^{2+}$ in fibroblasts from control and ASD patients.**

**(a)** Representative FLIPR traces showing change in fluorescence over the basal ($\Delta F/F_0$) in response to extracellular application of 100 μM UTP in control (black and grey traces), FXS (red) and sporadic ASD (green) cells loaded with the $Ca^{2+}$ indicator Fluo-8. Grey dashed line represents fluorescence response of the ASD line to a vehicle addition alone. $Ca^{2+}$-free buffer

contains 1 mM EGTA. **(b)** Representative FLIPR traces showing insignificant response to extracellular application of 100 μM ADP. Color legend is the same as in (**a**). **(c)** Representative FLIPR traces showing minimal response to extracellular application of 100 μM UDP. **(d)** Representative FLIPR traces showing response to extracellular application of 100 μM MRS 2365.

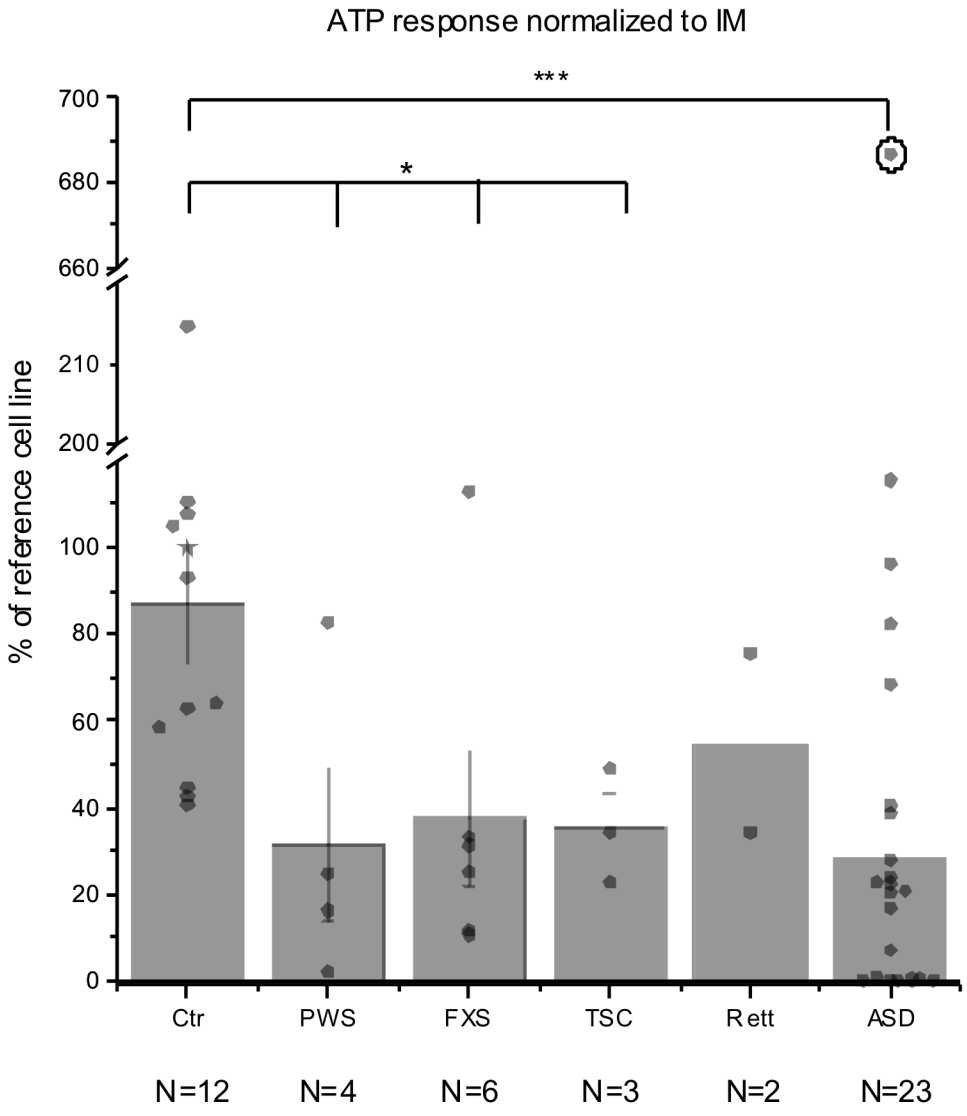


**Figure 2.6. 7 $Ca^{2+}$ response in fibroblasts from subjects with sporadic ASD as well as from controls and those with syndromic ASD.**

Average $Ca^{2+}$ response in skin fibroblasts from unaffected neurotypical controls (Ctr), Prader-Willi syndrome (PWS), fragile X syndrome (FXS), tuberous sclerosis syndrome 1 and 2 (TSC),

Rett syndrome (Rett) and from subjects with sporadic ASD (ASD). N below each cell line represents number of individuals tested. The star symbol represents the reference control cell line (GM03440). Peak $Ca^{2+}$ response ($\Delta F/F_0$) divided by the peak ionomycin response ($\Delta F/F_0$) was normalized to the mean value of the reference cell line (GM03440) run on the same FLIPR plate. Bar graphs show mean +/- s.e.m. for each group. Data points represent responses from an individual. Circled data point (AU0237-0201) was excluded from the average and statistics. * = p-value < 0.05, *** = $p < 0.001$, Mann-Whitney test.

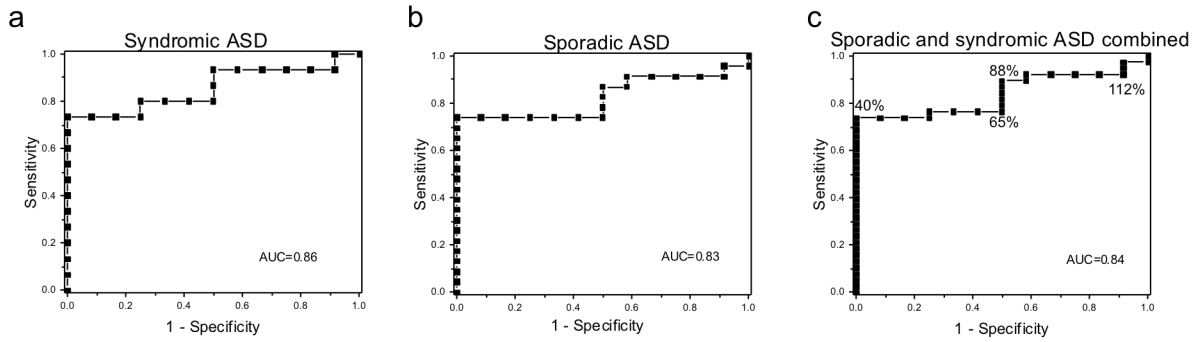


**Figure 2.6. 8 Receiver operating characteristic (ROC) curves for ATP-evoked $Ca^{2+}$ signaling in ASD.**

**(a)** ROC curve results for syndromic ASD cell lines (N=15) and unaffected neurotypical controls (N=12). Sensitivity (the true-positive rate) was plotted against (1-specificity) (the false-positive rate) for each value of $Ca^{2+}$ signaling response normalized to a reference control cell line (the data are the same as in Fig. 2.6.7). Only subjects with known identified genetic syndromes co-morbid with ASD (FXS (N=6), Rett (N=2), PWS (N=4), TSC (N=3)) were used to generate the curve. Area under the curve (AUC) is shown in each graph. **(b)** ROC curve results for sporadic ASD subjects (N=23) and unaffected neurotypical controls (N=12). **(c)** ROC results for $Ca^{2+}$ signaling in sporadic and syndromic ASD cohorts combined from (**a**) and (**b**). Numbers in % reflect $Ca^{2+}$ signaling cutoff values (presented as % of the reference cell line) to illustrate how different threshold values influence specificity and sensitivity of the ROC curve.

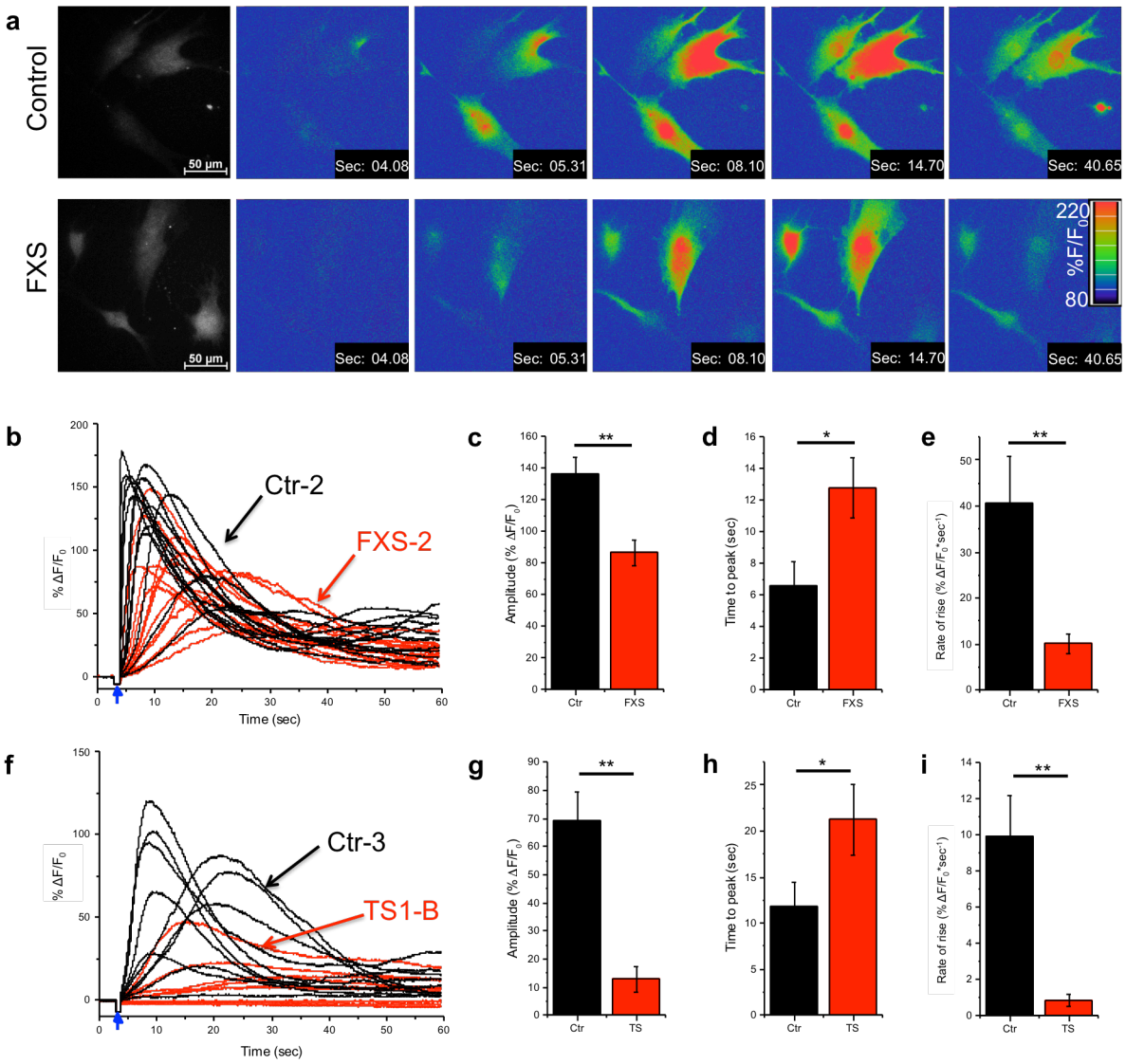


**Figure 2.6. 9 $Ca^{2+}$ release evoked by photoreleased $IP_3$ is depressed in FXS and TS cells.**

**(a)** Representative frames taken from image sequences of control (top) and FXS fibroblasts (bottom) loaded with Fluo-8 and stimulated by photorelease of i-$IP_3$. Increasing cytosolic [$Ca^{2+}$] (increasing fluorescence ratio %F/$F_0$) is depicted on a pseudocolor scale, as indicated

by the color bar. Time-stamps indicate time from beginning of the record; the photolysis flash was delivered at 3 s. The monochrome panels on the left show resting fluorescence before stimulation to indicate cell outlines. **(b)** Superimposed traces of representative global single-cell $Ca^{2+}$ responses to uncaging of i-$IP_3$ in FXS (red) and control fibroblasts (black). Traces represent average fluorescence ratio signals ($\%F/F_o$) throughout regions of interest encompassing the whole cell. Arrow indicates time of the UV flash. Data are from the cell pair labeled as FXS-2/Ctr-2 in Fig. 2.6.1c. **(c)** Mean peak amplitude of $Ca^{2+}$ responses is significantly depressed in FXS cells relative to matched controls. **(d)** Mean latency from time of photolysis flash to peak $IP_3$-evoked $Ca^{2+}$ response is prolonged in FXS fibroblasts. **(e)** Mean rate of rise of $Ca^{2+}$ fluorescence signal (peak amplitude / time to peak) is reduced in FXS cells as compared with control cells. Data in **(c-e)** are from 13 control cells and 14 FXS cells. **(f-i)** Corresponding traces (**f**), and mean values of amplitude (**g**), latency (**h**) and rate of rise **(i)** derived from cells labeled as Ctr-3 and TS1-B in Fig. 2.6.2c. Data are from 11 TS cells and 12 matched controls.

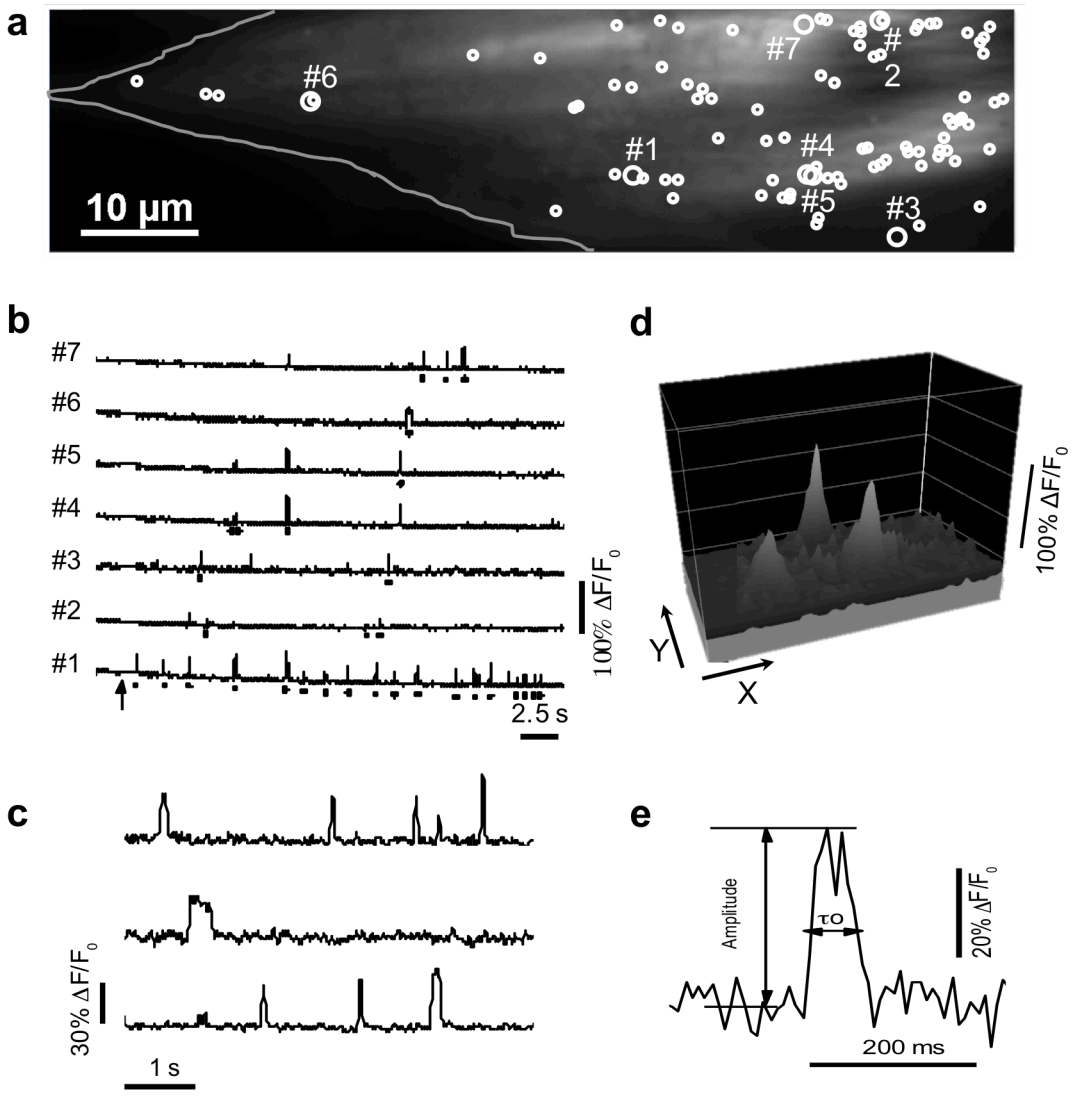


**Figure 2.6. 10 Local $IP_3$-evoked $Ca^{2+}$ events.**

**(a)** Resting Cal-520 fluorescence of a control fibroblast **(b)** (outlined) imaged by TIRF microscopy. Circles mark all sites where $Ca^{2+}$ release events were identified within a 40 sec imaging record following photorelease of i-$IP_3$ in a 128 x 512 pixel (20.48 x 81.92 µm) imaging field. Larger circles mark sites from which traces in **(b)** were obtained. Representative traces

from sites numbered in **(a)**. Dots underneath the traces mark events arising at that particular site; unmarked signals represent fluorescence bleed-through from events localized to adjacent but discrete sites. Arrow indicates the timing of the UV flash. **(c)** Examples of individual events shown on an expanded timescale to better illustrate their kinetics. **(d)** Surface intensity plot of three individual puffs near their peak times. **(e)** A single $Ca^{2+}$ event shown on an expanded scale to illustrate measurements of peak amplitude and event duration ($tau_o$) at half-maximal amplitude.

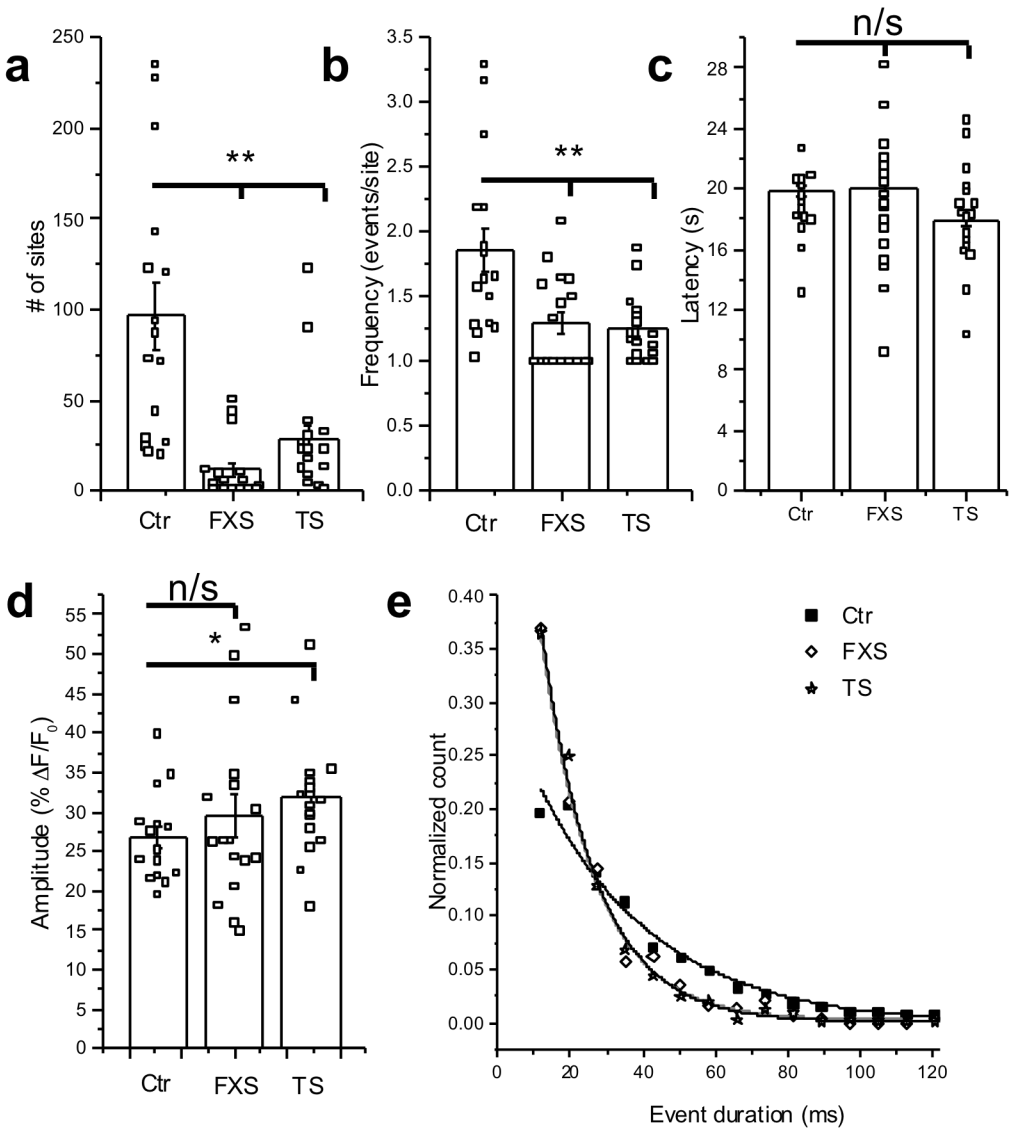


**Figure 2.6. 11 $IP_3$-mediated $Ca^{2+}$ signaling in FXS and TS fibroblasts is impaired at the level of local events.**

Data are from 17 FXS-3 cells, 17 TS1-B cells, and 16 control cells (Ctr-3) matched to both experimental groups. Open black squares in a-d represent mean measurements from individual

cells; histograms and error bars are overall means $\pm$ 1 s.e.m. across all cells in each group. **(a)** Total numbers of $Ca^{2+}$ release sites detected within cells during 40 s imaging records following uniform photorelease of i-$IP_3$. **(b)** Mean event frequency per site, calculated from the number of events observed per site throughout the recording period. **(c)** Mean latencies following the photolysis flash to the first event at each site within a cell. **(d)** Mean amplitudes of all events within each cell. **(e)** Distributions of event durations (at half maximal amplitude) derived from all events identified in FXS (open diamonds), TS (stars) and control cells (black squares). The data are fit by single-exponential distributions with time constants $t_o$ of 15 ms (both FXS and TS) and 32 ms (control). Outcomes were compared using two-sample Mann-Whitney test. * = p-value <0.05; ** = p <0.01, n/s – non-significant.

## Chapter 3. $IP_3$-mediated $Ca^{2+}$ signaling in central nervous system and peripheral tissue cells from a mouse model of FXS

### *3.1 Introduction*

My previous findings described in Chapter 2 provide strong evidence that $Ca^{2+}$ release through $IP_3Rs$ is decreased in skin fibroblasts from human patients with monogenic models and sporadic forms of ASD. Given crucial roles played by $IP_3$-mediated $Ca^{2+}$ release in the brain, I wanted to investigate if the same signaling abnormality is present in neurons.

The $IP_3R$ is a key signaling hub in the canonical metabotropic glutamate receptor (mGluR) pathway in neurons (Inoue et al. 1998; Berridge 1993). Although a complex array of downstream signals (Lüscher and Huber 2010) arising from mGluR activation has been previously reported in FXS (Bear, Huber, and Warren 2004; Repicky and Broadie 2009; Nakamoto et al. 2007), the role of downstream $Ca^{2+}$ release at the level of $IP_3Rs$ in ASD has not been determined at a molecular level.

The role of mGluR signaling gained a lot of attention when Mark Bear at Massachusetts Institute of Technology postulated a "mGluR theory of Fragile X" (Bear, Huber, and Warren 2004). This theory postulates that disrupted mGluR signaling underlies the pathogenesis of the disorder, and that hyperactivation of the group 1 mGluR receptors phenocopies a wide array of biological landmarks of FXS. As a continuation of my previous work, I wanted to expand my findings on molecular deficits in $IP_3$-mediated $Ca^{2+}$ signaling in humans with FXS to investigate if metabotropic signaling in the mouse model of FXS also manifests in decreased $Ca^{2+}$ release from the ER.

### *3.2 Materials and Methods*

#### 3.2.1 Materials.

DMEM (cat. # 11995-065) was purchased from Life Technologies, Neurobasal-A (cat. # 12349-015), B-27 supplement (cat. # 17504-044) and GlutaMax (cat. # 35050-061) were from Gibco/Thermo Fisher Scientific. 2.5% Trypsin (cat. # 25-054CI) was from Cellgro. DNase (cat. # D4527-10KU) was from Sigma-Aldrich. NPEC-caged-(1S,3R)-1-Amino-1,3-dicarboxycyclopentane (ACPD; cat. # 3331), (RS)-α-Methyl-4-carboxyphenylglycine (MCPG; cat. # 0336) were from Tocris. Fluo-8AM, Cal-520AM and Cal-630AM were purchased from AAT Bioquest, diluted in DMSO/Pluronic to a stock concentration of 2 mM and frozen until needed. Adenosine triphosphate (ATP) was purchased from Sigma Aldrich, diluted in water to a stock concentration of 100 mM and frozen as 50 µl aliquots until needed. Ionomycin was purchased from Life Technologies, diluted in DMSO to 1 mM and frozen as 10 µl aliquots until needed. GCaMP6f was obtained from the University of Pennsylvania Vector Core (Chen et al. 2013).

#### 3.2.2 Postnatal neuronal cultures.

All experiments were performed in accordance with and approved by the Institutional Animal Care and Use Committee (IACUC) at the University of California, Irvine. FVB.129P2-*Pde6b*$^{+}$ *Tyr*$^{c\text{-}ch}$ *Fmr1*$^{tm1Cgr}$/J mice were used. Females heterozygous for the *FMR1* gene were bred with wild type males to generate male littermates that were either hemizygous or wild-type for the *FMR1* gene. Postnatal day 0-2 male mouse pups were used to initiate cortical

neuron/astrocyte co-cultures. On the day of the dissection, mouse pup tails were cut for genotyping, and male pups that were either wild-type or knockout for *FMR1* gene were used. Primers were ordered from Integrated DNA Technologies: FXS primer: 5'-CAC GAG ACT AGT GAG ACG TG-3' (forward), WT primer: 5'-TGT GAT AGA ATA TGC AGC ATG TGA-3' (forward).

Brains were dissected in ice-cold dissection media (4.2 mM $NaHCO_3$, 1 mM pyruvate, 20 mM HEPES, 5.33 mM KCl, 0.44 mM $KH_2PO_4$, 137 mM NaCl, 0.33 mM $Na_2HPO_4*7H_2O$, 5.55 mM d-glucose, adjusted pH to 7.3.), and meninges were carefully removed. Cortices were dissected, minced and placed into 450 µl of ice-cold dissection media. 50 µl of pre-warmed 2.5% trypsin was added, and the mixture was incubated at $37^0$C for 15 minutes. 20 µl of DNase was added to the mixture and incubated for additional 5 minutes. 1 ml of the plating media was added to inactivate the trypsin, and after the brain tissues settled to the bottom, the media was carefully aspirated. Brain tissue was re-suspended in 1 ml of plating media and triturated with three fire-polished glass Pasteur pipettes with decreasing size 8-10 times to dissociate the cells. After cells were transferred to 50 ml conical tubes using a strainer, they were plated at 60,000/well in 0.5 ml plating media in the center part of a 35 mm glass bottom dish that was pre-treated with 0.1 mg/ml poly-d-lysine for 1 hour.

In 2-4 hours, the plating media was carefully aspirated and replaced with 2 ml of the maintenance media. 1 ml of media was changed twice a week. Neuronal cultures were used between day 14 and day 21 *in vitro*.

### 3.2.3 Mouse fibroblast cultures.

Postnatal day 0-2 male mouse pups were euthanized through decapitation. A section of skin from a flank was placed in ice-cold dissection media and cut into 1 mm pieces. 4-6 pieces of skin were placed into each well of a gelatin-coated 6-well plate. 200 µl DMEM + 10% FBS were carefully added to each well and explants were allowed to attach to the bottom of the well before adding additional 2 ml of media. Proliferating fibroblasts grow out of the explants and on average reach confluency after 7-10 days in culture before being harvested in $Ca^{2+}$- and $Mg^{2+}$-free 0.25% trypsin-EDTA (Life Technologies) and sub-cultured at 1:4 ratio. Fibroblasts were cultured in Dulbecco's Modified Eagle's Media (Gibco, 11965-092) supplemented with 10% (v/v) fetal bovine serum with penicillin/streptomycin at 37 °C in a humidified incubator gassed with 95% air and 5% $CO_2$, and used for up to 10 passages. For $Ca^{2+}$ signaling studies, cells were detached with $Ca^{2+}$- and $Mg^{2+}$-free 0.25% trypsin-EDTA, harvested in normal growth media and sub-cultured on FLIPR 96 well plates for 2 days to provide standardized conditions prior to imaging studies.

### 3.2.4 Single-cell $Ca^{2+}$ imaging.

Neuronal/astrocytic co-cultures grown in glass-bottomed 35 mm imaging dishes were loaded for imaging using membrane-permeant esters of Cal-520. Briefly, cells were incubated at room temperature in ACSF (1.8 mM $CaCl_2$, 140 mM NaCl, 5 mM KCl, 0.5 mM $MgCl_2$, 0.4 mM $MgSO_4$, 0.4 mM $KH_2PO_4$, 0.6 mM $Na_2HPO_4$, 3 $NaHCO_3$, 10 mM glucose, 10 mM HEPES, adjusted to pH 7.35 with NaOH) containing 4 µM Cal-520 AM for 45 minutes before washing three times with the ACSF solution. $[Ca^{2+}]_i$ changes were imaged using a Nikon Eclipse

microscope system with a 40x (NA=1.30) oil objective controlled by Nikon NIS Elements software. Cal-520 ot GCaMP6f fluorescence was excited by 488 nm laser light, and emitted fluorescence (l > 510 nm) was imaged at 30 frames $sec^{-1}$ using an electron-multiplied CCD Camera iXon DU897 (Andor). An arc lamp was used to emit a single flash of UV light (350-400 nm) focused to uniformly illuminate a region slightly larger than the imaging field to uncage the extracellular caged agonist ACPD, which evoked activity persisting for tens of seconds. Image data were acquired as stack .nd2 files using Nikon Elements for offline analysis. Fluorescence signals were expressed as a ratio ($\Delta F/F_0$) of change in fluorescence ($\Delta F$) relative to the mean resting fluorescence at the same region before stimulation ($F_0$). Measurement outcomes were tested for statistical significance using the Mann-Whitney non-parametric test.

A Hamamatsu W-View Gemini beam splitter was used for simultaneous Cal-630 and GCaMP6f recordings. Cal-630 fluorescence was excited by 561 nm laser light, and GCaMP6f fluorescence was excited at 488 nm. Emitted fluorescence was imaged with a Nikon quad filter cube at 30 frames $sec^{-1}$ using a CMOS camera (Hamamatsu Orca Flash 4.0LT). Cal-630 fluorescence was recorded at l > 635 nm, and GCaMP6f fluorescence was collected at l < 550 nm filters using the beam splitter. Recordings were binned by 2x2 pixels (512 x 1024 pixels, 166.4 x 332.8 μm resolution).

### 3.2.5 High-throughput $Ca^{2+}$ imaging.

Dissociated cortical cultures from newborn mouse pups were seeded in clear-bottom black 96 well plates (Greiner Bio One T-3026-16) at 1 x $10^5$ cells per well and grown for five days at 37°C in a humidified incubator gassed with 95% air and 5% $CO_2$. To promote neuronal cell

survival, cells were cultured in Neurobasal-A medium supplemented with serum-free B-27. To promote astrocytic cell survival and proliferation, cells were plated and maintained in DMEM supplemented with 10% FBS. On the day of the experiment, cells were loaded by incubation with 2 μM of the membrane-permeant $Ca^{2+}$ indicator Fluo-8 AM (Takada, Furuya, and Sokabe 2014) in ACSF for 1 h at 37 °C, then once washed with a $Ca^{2+}$ -free HBSS solution (120 mM NaCl, 4 mM KCl, 2 mM $MgCl_2$, 10 mM glucose, 10 mM HEPES, 1 mM EGTA, pH 7.4 at room temperature). The solution was replaced with 100 μl of fresh $Ca^{2+}$-free HBSS solution in each well and cells were allowed to equilibrate for 5 minutes prior to assay with a fluorometric imaging plate reader (FLIPR; Molecular Devices, Sunnyvale, CA). A basal read of fluorescence in each well (470–495 nm excitation and 515–575 nm emission, expressed in arbitrary units; AU) was read for 2 seconds at 0.4 s exposure time. Next, 100 μl of 2x ATP (to 100 μM final concentration), 100 μl of 2x DHPG (to 100 μM final concentration), or 100 μl of 2x ionomycin (to 1 μM final concentration) in $Ca^{2+}$-free HBSS was added to a given well. A single recording was obtained from each well. Ionomycin-induced fluorescence changes from wells without prior addition of agonists were used to normalize agonist-evoked responses. Recordings were performed in triplicate.

### *3.3 Results*

#### 3.3.1 Optimizing neuronal culture conditions.

Choosing a model system is a crucial first step for studying ASD-specific molecular deficits, as many signaling pathways will critically depend on when, where, and what cell type is studied. Stages of neurodevelopment are modulated dynamically by many factors, including gene

expression patterns throughout the fetal and early postnatal life, the predominant types of neurons present at different stages, the ratio of glial/neuronal cells, as well as neuromodulators and hormones. Several studies have attempted to answer the questions of when ASD susceptibility genes converge during development and which brain regions are most vulnerable to these changes. As a guide, I used two recent studies that remarkably advanced this field. One study mapped ASD risk genes onto co-expression networks that represent developmental courses and transcriptional profiles in fetal and adult cortices (Parikshak et al. 2013). In this study, multiple ASD risk-enriched modules strongly correlated with glutamatergic neurons in upper cortical layers, predicting that specific disruption of cortical-cortical connectivity is more likely to affect core ASD phenotypes such as social behavior. Genes that were combined into independent clusters revealed predominant expression peaks evident throughout fetal development and early postnatal stages. Interestingly, several modules that included ion channels and plasma membrane receptors were highly correlated with *ITPR1* gene expression and were enriched in late fetal/early postnatal life. Another independent study demonstrated a similar pattern of convergence of ASD vulnerability genes and precisely mapped it onto cortical layer 5/6 neurons, the innermost layer of neurons (Willsey et al. 2013). They identified the mid-fetal stage (post conception week 10-24 in humans) as a point of convergence in expression for high-risk ASD genes. Moreover, layer 5/6 projection neurons of the midfetal stage are among the first cortical neurons to form synaptic connections, and it is these early neural circuits that may be particularly vulnerable to a variety of genetic perturbations and related functional disturbances that may all ultimately increase the risk for ASD.

Several studies have been published that attempted to translate mammalian neurodevelopment across species (Workman et al. 2013; Clancy et al. 2007; Semple et al. 2013). Based on different models used to extrapolate ages, human mid-fetal stage translates into mouse post-conception day 17 (Clancy et al. 2007; Workman et al. 2013) to postnatal day 0 (Semple et al. 2013). Late fetal development in humans can be roughly translated into early postnatal life in mice. I therefore decided to use cortical neurons from postnatal days 0-2 mice to capture dynamic expression changes taking place in this vulnerable developmental stage. In mice, this is the period when intense gliogenesis occurs, thus providing sources for both neurons and astrocytes in the same dish that support robust and healthy neuronal cultures. This fact allows culturing without a feeder layer, thus minimizing any variation that may arise from combining cells from different animals and genotypes. To minimize any inter-litter variations, I bred female mice heterozygous for the *FMR1* gene with wild-type males that produced male mouse pups that were either hemizygous or had a wild-type copy of the *FMR1* gene in the same litter. Cultured neurons obtained with this protocol (Beaudoin et al. 2012) demonstrate great survival and develop extensive axonal and dendritic connections. By day 12-17 *in vitro,* these neurons had characteristic morphologies and expressed appropriate axonal markers (tau, tuj1; not shown). They develop robust and mature network connections, suggesting functional excitatory inputs. Moreover, these cultures are amenable to gene manipulations such as transfection.

### 3.3.2 $Ca^{2+}$ measurements in neuronal cultures.

Postnatal cortical cells yield robust cultures *in vitro* in part because they provide an astrocytic feeder layer along with neurons that supports survival and maturation of neuronal cells. By day

12 *in vitro*, astrocytes proliferate robustly and create a nearly confluent monolayer of cells on top of which neurons reside. These glial cells support the culture by secreting growth and signaling factors, as well as by regulating neuronal activity *via* neurotransmitter reuptake mechanisms. This results in culture conditions that mimic *in vivo* conditions in terms of the cell type composition. However, during the imaging process it creates certain challenges as many neuronal cells reside on top of astrocytes, thus masking the fluorescence signal and complicating analysis. The problem can be easily circumvented by delivering a $Ca^{2+}$ indicator specifically in neurons, thus making all other cell types practically "invisible" for the purposes of $Ca^{2+}$ imaging. Luckily, a large library of genetically-encoded $Ca^{2+}$ indicators that can be expressed under different promoters has been developed (Chen et al. 2013). In 2013, a new generation of highly sensitive protein $Ca^{2+}$ sensors called GCaMP6 was shown to outperform previous versions of other sensors in mice *in vivo* as well as in cultured neurons (Chen et al. 2013). They were shown to reliably detect single action potentials and record $Ca^{2+}$ transients in neuronal processes and single dendritic spines. More importantly for the purposes of this project, they can be specifically and selectively expressed using a commonly used viral delivery method, adeno-associated virus, under a neuron-specific promoter synapsin. In such configuration, the viral particles will infect and integrate into the host's DNA in all cells in the culture, but only cell types with an active synapsin promoter will produce the target protein.

Thus, I set out to test this new $Ca^{2+}$ sensing protein and compare it with the commonly used synthetic dyes that I have previously used to image global and local events in human skin fibroblasts. I chose the fast version of GCaMP6, as it was shown to have a dissociation constant ($K_d$=375 nM (Chen et al. 2013, supplementary information)) similar to that of dyes commonly

used in our lab, such as Cal-520 AM ($K_d$=320 nM, https://www.aatbio.com/products/21130) and Fluo-8 AM ($K_d$=389 nM, https://www.aatbio.com/products/21081). I used AAV1.Syn.GCaMP6f.WPRE.SV40 viral delivery vector to infect neuronal cultures and to specifically target gene expression to neuronal cells only (Kügler, Kilic, and Bähr 2003). After the initial viral particle titration step with 1:2,000, 1:20,000 and 1:200,000 dilutions, I established that the 1:20,000 dilution gave the most consistent results in terms of GCaMP6f expression (data not shown). The infection was performed at day 7-14 *in vitro*, and the protein expression was studied between days 14 and 21 *in vitro*. Neuronal cultures were routinely inspected using light microscopy before the infection and prior to any imaging experiments. Under these conditions, I was able to achieve healthy cultures with the majority of neurons showing low-level basal fluorescence with the characteristic expression pattern of a cytosolic indicator having no evidence of nuclear expression (Fig. 3.5.1(a) and 3.5.2 (a)).

To compare the performance of synthetic dyes and the genetically-encoded $Ca^{2+}$ sensor GCaMP6f, I incubated cells expressing GCaMP6f with 4 μMof Cal-630AM, a red-shifted $Ca^{2+}$ sensor, and subjected the cells to trains of field electric stimulation at 70 mV at different frequencies. The resulting action potential-induced $Ca^{2+}$ transients in the same cell detected by GCaMP6f or Cal-630 were recorded simultaneously using a dichroic beam splitter. As expected, GCaMP6f localized to neurons only and could be distinguished from Cal-630 fluorescence by an exclusively cytoplasmic expression pattern. In contrast to GCaMP6f, Cal-630 loaded indiscriminately into both neuronal and glial cells. At resting conditions, astrocytes had very low basal fluorescence with bouts of spontaneous $Ca^{2+}$ waves spreading across the imaging field. These events were observed as slow, large increases in fluorescence intensity evident in the Cal-

630 traces, but absent from the GCaMP6f traces (Fig. 3.5.1 (b), cell #4). GCaMP6f was excellent at registering slow, large events in neurons, such as the ones caused by high-frequency field stimulation (Fig. 3.5.1 (c)). These data demonstrate the wide dynamic range and large signal/basal ratio properties of the GCaMP6f sensor. However, even the fast version of this indicator appeared to be too slow to reveal fast events, such as those caused by low-frequency electric stimulation (Fig. 3.5.1 (d) demonstrates a zoomed-in portion of the full-length trace from Fig. 3.5.1 (b)). Therefore, my data show that the synthetic dye Cal-630 excels at reporting fast, transient spikes caused by single action potentials, compared to the traces of GCaMP6f that are barely distinguishable from the baseline noise, and where individual $Ca^{2+}$ spikes cannot be resolved (Fig. 3.5.1 (d), the GCaMP6f trace is offset for clarity). These results are consistent with the previous findings from our group in that GCaMP6f is inferior to small molecule dyes in detecting small events, either by the virtue of losing fast events, or by perturbing the $Ca^{2+}$ signaling itself (Lock, Parker, and Smith 2015). However, while GCaMP6f is inferior in detecting fast, transient local events, it is excellent at detecting large, slow events happening in neurons, especially in neuronal/astrocytic co-cultures without "contaminating" the signal from underlying glial cells.

Next I wanted to compare the performance of the two indicators with slower $Ca^{2+}$ wave responses that arise from activation of metabotropic receptors. I used an NPEC-caged analogue of trans-1-amino-1,3-dicarboxycyclopentane (ACPD) that can be transformed into a biologically active form upon UV light stimulation to selectively activate metabotropic glutamate receptors without complications from activating ionotropic glutamate receptors. Consistent with my previous findings on action potential-induced $Ca^{2+}$ spikes, GCaMP6f could discriminate between

neurons and astrocytes, and again the amplitude of individual spikes appeared dampened compared with the Cal-630 recordings (Fig. 3.5.2 (b)). One brief UV flash was sub-optimal in eliciting a $Ca^{2+}$ response, however, in GCaMP6f-expressing neurons it lead to an abrupt drop in fluorescence signal, presumably due to photobleaching (Fig. 3.5.2 (c)). After a short train of four UV flashes, neurons responded with a characteristic $Ca^{2+}$ wave originating in proximal dendrites and spreading into the soma, as previously reported (Nakamura, Nakamura, and Ross 1999). Comparison of the waveforms from the GCaMP6f and Cal-630 recordings (Fig. 3.5.2 (d); the GCaMP6f trace was offset to overlay the Cal-630 trace) suggested that the two indicators are similarly effective in reporting a slow $Ca^{2+}$ rise. Since the signal-to-noise ratio measured with the two indicators is similar, it appears that GCaMP6f is as effective in detecting global metabotropic signals as synthetic dyes, but has the advantage of allowing the selective targeting to neurons, without a complicating signal from the glial cells.

Based on these results, I decided to use genetically encoded GCaMP6f indicator for imaging slow $Ca^{2+}$ waves in neurons, and employ synthetic dyes for any recordings of non-neuronal cells or for fast events.

### 3.3.3 mGluR-mediated $Ca^{2+}$ signaling events in cortical neurons from FXS and wild-type mice.

The goal of the experiments presented in this chapter was to determine if $Ca^{2+}$ signaling abnormalities reported in human skin fibroblasts from patients with FXS are recapitulated in mammalian neurons with a similar lack of functional FMR1 protein. Neurons are architecturally complex cells, where spatial origin of the signal greatly influences downstream events. After

optimizing the culturing conditions and choice of indicator, I then went on to investigate whether the $Ca^{2+}$ signaling abnormality observed in human skin fibroblasts from patients with FXS was also present in mouse neurons with the *FMR1* gene deletion. $IP_3$ signaling in neurons can be stimulated by activation of plasma membrane metabotropic receptors. To stimulate $IP_3$-mediated $Ca^{2+}$ release in neurons, I used UV flash uncaging of the broad-spectrum mGluR agonist trans-ACPD, or bath application of the selective group 1 mGluR agonist, DHPG. Photoreleased ACPD elicited $Ca^{2+}$ waves originating in proximal dendrites that propagated bidirectionally and frequently invaded the soma (Fig. 3.5.3 (a)), consistent with previous reports (El-Hassar et al. 2011; Hagenston, Fitzpatrick, and Yeckel 2008). $Ca^{2+}$ waves were blocked by (RS)-α-Methyl-4-carboxyphenylglycine (MCPG), a non-selective group I/group II metabotropic glutamate receptor antagonist, suggesting that the effect of ACPD is on metabotropic, not ionotropic, glutamate receptors (data not shown).

UV uncaging of ACPD under identical conditions elicited responses in neurons from *FMR1*$^{-/y}$ and *FMR1*$^{+/y}$ mice that did not differ in their amplitude (Fig. 3.5.3 (c)), nor time after the UV flash to reach the peak amplitude (Fig. 3.5.3 (d)).

One possible explanation for these discrepancies between my findings in human skin fibroblasts and mouse neurons may lie in differential expression of of $IP_3$ receptor types. Fibroblasts express predominantly type 2 and 3 $IP_3$Rs, whereas neurons primarily express type 1. Thus, astrocytes that express mainly type 2 $IP_3$Rs may be better translatable to my previous findings in human skin fibroblast. To test this hypothesis, I measured $IP_3$-mediated $Ca^{2+}$ release using the same co-cultures that were rich in glial cells. Cells were loaded with Cal-520 and stimulated with extracellular agonists of mGluR receptors – cACPD and DHPG. Astrocytes

responded robustly to both of these agonists, however, again the amplitude of the response was not different between genotypes (Fig. 3.5.4). Finally, I used caged $IP_3$ to bypass the mGluR signaling pathway and activate $IP_3$Rs directly. This method also gives greater flexibility in the size of the elicited response. I used three different UV flash durations to stimulate sub-maximal and maximal responses to determine if there is a difference in the peak amplitude response or sensitivity to $IP_3$ in mouse astrocytes. Similar to my results with extracellular agonists, $Ca^{2+}$ responses to photoreleased $IP_3$ in wild-type astrocytes were undistinguishable from the $FMR1^{-/y}$ cells (Fig. 3.5.5).

### 3.3.4 High-throughput FLIPR assay on mouse cell cultures.

Methodological differences in how $Ca^{2+}$ signaling is being imaged may account for the apparent discrepancies between the human and mouse cells. To probe this idea, I decided to use the high-throughput $Ca^{2+}$ screening assay, FLIPR, to closely replicate imaging conditions used on human fibroblasts from the previous chapter. Cortical cells from newborn mice were plated on a 96-well plate and were allowed to grow for five days in neuronal maintenance media to promote neuronal cell survival. ATP (100 μM final concentration) was applied to activate cell-surface purinergic receptors and induce subsequent $IP_3$ production and $Ca^{2+}$ release. $Ca^{2+}$-free extracellular medium supplemented with 1 mM EGTA was used to exclude $Ca^{2+}$ entry across the cell membrane. Averaged fluorescence traces from three independent wells illustrating ATP responses in neurons from *FMR1*$^{-/y}$ or *FMR1*$^{+/y}$ mice are shown in Fig. 3.5.6. I quantified fluorescence signals as a ratio ($\Delta F/F_0$) of the fluorescence change ($\Delta F$) at each well relative to the basal fluorescence ($F_0$) before stimulation and further normalized it to the ionomycin

response to account for any possible differences in the ER store filling. Fig. 3.5.6 (b) shows mean $\Delta F/F_0$ values from these cells in response to 100 μM ATP normalized to $\Delta F/F_0$ of the ionomycin response (1 μM). FXS neuron-enriched cultures demonstrated slightly greater response to ATP compared with that of wild-type neurons. Extracellular stimulation with 100 μM DHPG demonstrated even greater increase in $Ca^{2+}$ signaling in FXS neurons (Fig. 3.5.6 (c,d))

Similarly to initiation of the neuron-enriched culture, I generated a cortical culture that was enriched with astrocytes by culturing the cells in DMEM + 10% FBS media that is accommodating for astrocyte growth and proliferation. Analogous to the results of neuron-enriched cultures, $Ca^{2+}$ responses in glial cells from knockout animals were more robust compared with those from wild-type mice (Fig. 3.5.7).

Another possibility was that the $Ca^{2+}$ signaling deficits observed in human cells are specific to peripheral tissues such as skin fibroblasts, and do not mimic signaling machinery in the central nervous system. Therefore, I decided to test mouse skin fibroblasts with the high-throughput $Ca^{2+}$ assay, thus fully replicating my early experiments on human skin fibroblasts from patients with FXS. 100 μM ATP applied to each individual well with mouse skin fibroblasts in the absence of extracellular $Ca^{2+}$ elicited a robust response. Fig.3.5.8 (a) shows fluorescence traces averaged from six independent wells in response to the agonist addition, and Fig. 3.5.8 (b) demonstrates that response normalized to the corresponding ionomycin response. As can be seen from the data, fibroblasts from the *FMR1*$^{-/y}$ did not differ in their response to ATP from the cells obtained from wild-type mice. Clearly, murine fibroblasts, not only their glia and neurons, differ from human cells.

### *3.4 Discussion*

Here I report $Ca^{2+}$ signaling results on dissociated cortical neurons, astrocytes and fibroblasts obtained from a mouse model of FXS. This work was done because it was previously discovered that non-neuronal (fibroblast) cells from human patients with FXS display a pronounced and consistent $Ca^{2+}$ signaling deficit arising at the level of $IP_3$ receptors. However, no murine cell type recapitulated the human findings.

$IP_3$-mediated $Ca^{2+}$ release is an important neuronal signaling mechanism implicated in regulation of many neuronal functions, such as neuronal firing rates and short- and long-term plasticity. It is mobilized in response to activation of various metabotropic neurotransmitter receptors, including group 1 mGluRs. Normally, stimulation of mGluRs in dendrites triggers increased local protein synthesis, ultimately resulting in AMPA receptor internalization and slowing of net synaptic maturation through mGluR-mediated LTD. The mGluR theory of FXS postulates that absence of FMRP overactivates the mGluR-mediated signaling pathway, and thus leads to features associated with FXS. Moreover, multiple studies from different groups in *Fmr1* knockout mice with pharmacological or genetic reduction of mGluR function showed correction of many of these abnormalities, further demonstrating that mGluRs play a significant role in the pathophysiology of FXS, at least in mice (Dölen et al. 2007; Darnell and Klann 2013; Yan et al. 2005). Despite the fact that overactivation of these receptors has long been implicated in pathophysiology of FXS, surprisingly little is known about the resulting $Ca^{2+}$ release upon activation of these receptors. My findings described in Chapter 2 on human skin fibroblasts show that $IP_3$-mediated $Ca^{2+}$ release is depressed in response to P2YR activation. Extrapolating these findings to mouse neurons from the same disorder suggests that $Ca^{2+}$ release from the ER

downstream of the mGluR signaling would be decreased, contrary to the widely reported increased activity at the level of the plasma membrane receptor. However, data in this chapter suggest that the mGluR-mediated $Ca^{2+}$ signaling is not diminished in neurons and astrocytes from *Fmr1* KO mice, consistent with previous reports on overactivated mGluR signaling in the mouse model of FXS (Yan et al. 2005; Osterweil et al. 2010).

Extracellular activation of the mGluRs with broad mGluR agonist t-ACPD and specific group 1 agonist DHPG did not reveal deficits in the $Ca^{2+}$ release in mouse neuronal or glial cells. A high-throughput $Ca^{2+}$ assay demonstrated increases in the $Ca^{2+}$ signaling pathway in response to activation of the $IP_3$ signaling pathway with two metabotropic agonists, ATP and DHPG in mouse cortical cultures, whereas no changes were observed in mouse skin fibroblasts.

Several factors could contribute to this seeming discrepancy. First, the human condition primarily arises from a pathogenic expansion of a CGG repeat on the X chromosome. The number of repeats predicts the pathology: in unaffected individuals with less than 40 repeats the 5'UTR portion of the *FMR1* gene is unmethylated, and the protein product is expressed normally. If the number of repeats exceeds 200, the *FMR1* becomes fully methylated and produces no protein. The mouse model represents a full genetic deletion, ultimately leading to the same phenotype at the protein level, yet it fails to capture any other possible mechanisms associated with the CGG expansion and gene methylation. The process of gene silencing in the human full mutation patients is assumed to be a static and uniform process in all cells of the body, across all developmental ages. However, one study has recently found that it may not faithfully represent the reality. Induced pluripotent stem cells (iPSCs) derived from fibroblasts from FXS patients did not necessarily replicate the CGG repeat length, the *FMR1* methylation

status or the protein expression level in the original fibroblasts. In some cases, the resulting iPSCs had reduced number of repeats, affecting epigenetic status of the *FMR1* gene promoter and ultimately altering neuronal differentiation of the resulting cell lines (Sheridan et al. 2011). Thus the *FMR1* knockout mouse model may not be appropriate for studying the condition at the epigenetic level, and may also influence many signaling pathways, such as $IP_3$ signaling.

Another possible explanation is the difference between the mouse and human proteomes. The laboratory mouse, the premier model organism for studying mammalian organism functions in biomedical research, shares a large proportion of its protein-coding genes with humans. Yet, the two mammals differ in significant ways. A massive recent mouse genome mapping study demonstrated that the expression pattern of many mouse genes show considerable divergences from their human orthologues (Yue et al. 2014). Since the *FMR1* protein has been shown to interact with at least hundreds of mRNA target transcripts in the brain (Brown et al. 2001; Darnell et al. 2011), it is likely that at least some of these targets will vary significantly from mouse to human, thus creating divergent expression profiles of these gene targets downstream of the *FMR1* regulation. Specificity and versatility of the $IP_3$ signaling pathway is ensured by a rich network of interacting proteins (Prole and Taylor 2016) that (1) may or may not be shared among humans and mice, and (2) may or may not be equally regulated by *FMR1* expression. A well-designed computational study could be capable of capturing those divergent protein interaction pathways in two different organisms and would serve as a good roadmap for guiding future studies on FXS and the translation between the two organisms. However, such a project is out of scope of the current work.

Relevant to this work, several recent FXS clinical trials have failed, including those targeted at reducing the mGluR signaling activity (Berry-Kravis et al. 2016; Jeste and Geschwind 2016). A list of possible explanations for this failure is long and includes the limitations of the outcome measures, the age of participants, and improvement of subtle changes that can only be seen in small subtypes of the heterogeneous population (Mullard 2015). However, the validity of using mouse models for modeling complex neurodevelopmental disorders such as ASD may also be questioned. For example, while the commonly used FXS mouse model replicates many behavioral and cellular phenotypes of FXS in humans, such as repetitive behavior, hypersensitivity to stimuli and dendritic spine morphology, it fails to convincingly replicate other symptoms, such as cognitive impairments and sociability seen in human patients (Kazdoba et al. 2014).

In this work, I demonstrate that at least one signaling deficit that exists in human cells is not present in the mouse model of FXS. Intriguingly, this signaling pathway is immediately downstream of the major signaling cascade commonly implicated in the mouse model pathology – mGluR. Given that the latest treatments were targeted at reducing the overactive mGluR signaling seen in mice, in human patients they may have further reduced already diminished $IP_3$-mediated $Ca^{2+}$ release downstream of mGluRs, thus making those interventions counter constructive.

Clearly, more work is needed to further understand the FXS $Ca^{2+}$ signaling phenotype in human models of the disease, but my current findings suggest that the field of the FXS may be better served if such research is done on human, not mouse cells.

### *3.5 Figures*

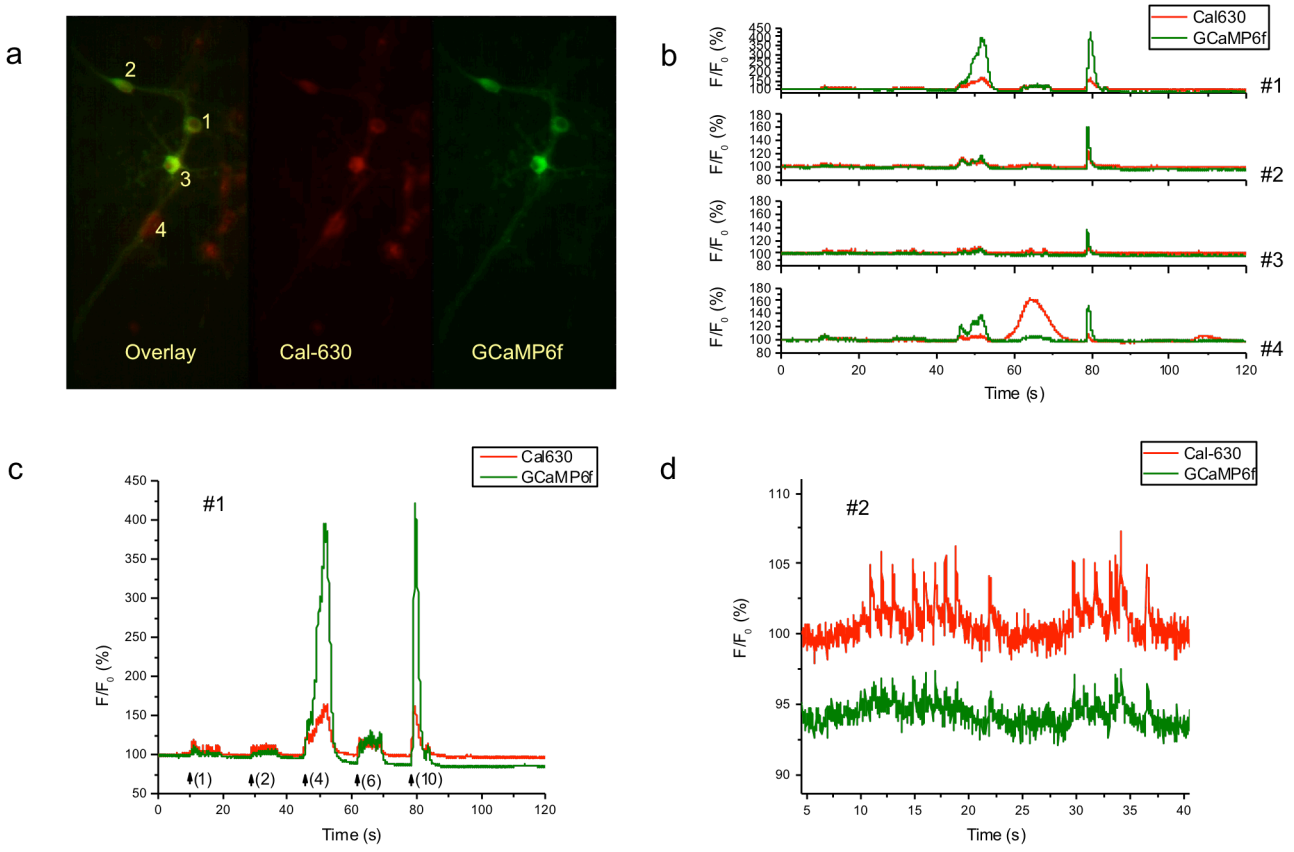


**Figure 3.5. 1 Comparison of $Ca^{2+}$ transients recorded with Cal-630 and GCaMP6f in mouse cortical neurons *in vitro*.**

**(a)** Images of neurons loaded with the $Ca^{2+}$ dye Cal-630 (red) and expressing GCaMP6f (green) composited from averaged frames of a video reveal the expression of GCaMP6f and loading of Cal-630. **(b)** Representative traces of fluorescence response ($F/F_0$) from four cells from **(a)** of Cal-630 and GCaMP6f in response to 10 spikes at 1, 2, 4, 6, and 10 Hz given at 10, 30, 45, 60, and 80 sec. Note different y-axis scale for cell #1. **(c)** Cell #1 from **(a)** and **(b)** is shown to

demonstrate a much larger $\Delta F/F_0$ change in GCaMP6f compared with Cal-630 in response to a train of 10 spikes of 70 mV at 1, 2, 4, 6, and 10 Hz (each train is represented by arrows with the frequency noted in brackets) **(d)** GCaMP6f has smaller amplitude response to a train of action potentials at 1 and 2 Hz stimulation. The GCaMP6f trace (green) is offset -5 Y units for clarity of representation.

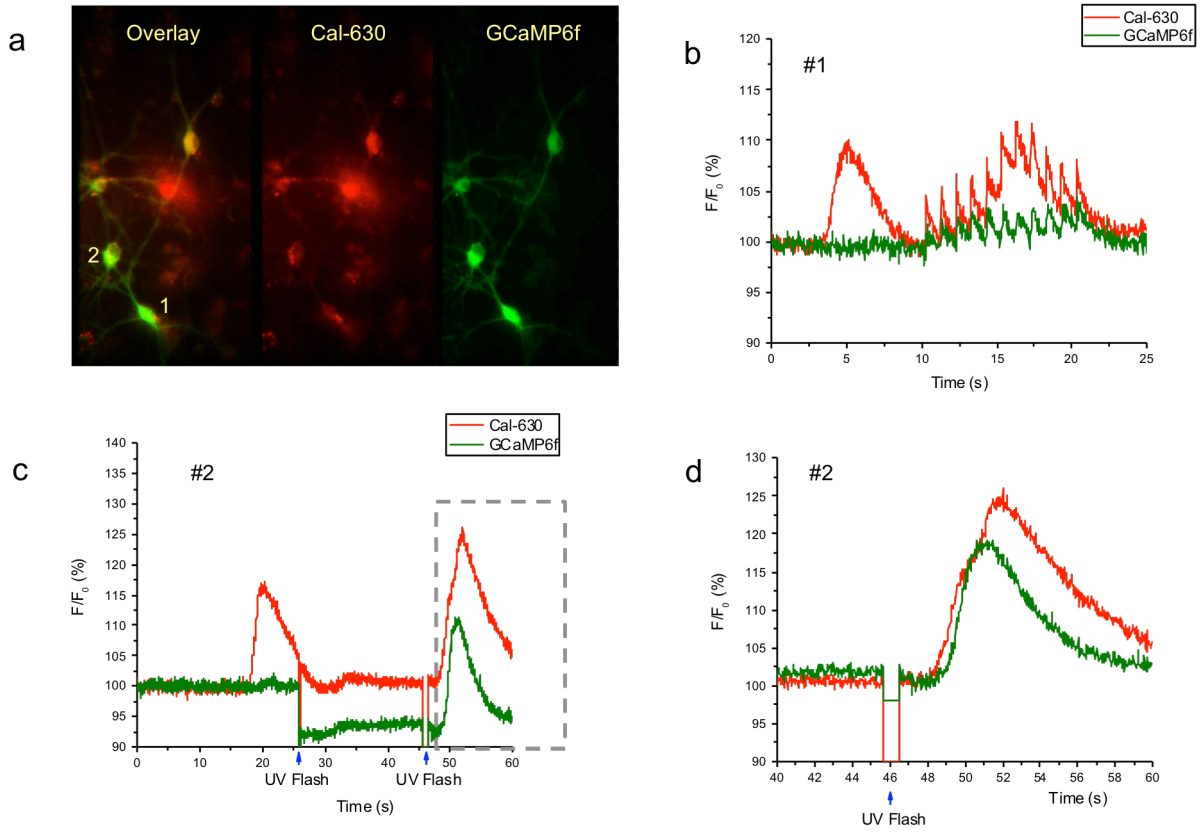


**Figure 3.5. 2 Comparison of Cal-630 and GCaMP6f performance in response to field stimulation and metabotropic activation of mGluR receptors.**

**(a)** Images of neurons loaded with the $Ca^{2+}$ dye Cal-630 (red) and expressing GCaMP6f (green) composited from averaged frames of a video reveal the expression/loading patterns of each indicator **(b)** Traces from simultaneous recording of Cal-630 (red) and GCaMP6f (green) signal in response to field stimulation-induced train of action potentials. Cal-630 signal from neuron #1 in **(a)** is "contaminated" by a slow wave response from an underlying astrocyte also loaded with Cal-630. The GCaMP6f expression is limited to neuronal cells only, thus the resulting signal does not reflect $Ca^{2+}$ changes from glial cells. **(c)** Traces derived from neuron #2 from **(a)** that

responded to uncaging of 100 μM of cACPD. UV flashes of different durations are depicted by arrows. Photobleaching of GCaMP6f signal in response to the strong UV flash is seen as an abrupt decrease in the signal level after the first flash. **(d)** An enlarged part of the trace from (c; grey dashed outline) showing kinetics of the metabotropic response. Note that the GCaMP6f signal was offset to overlap the Cal-630 signal.

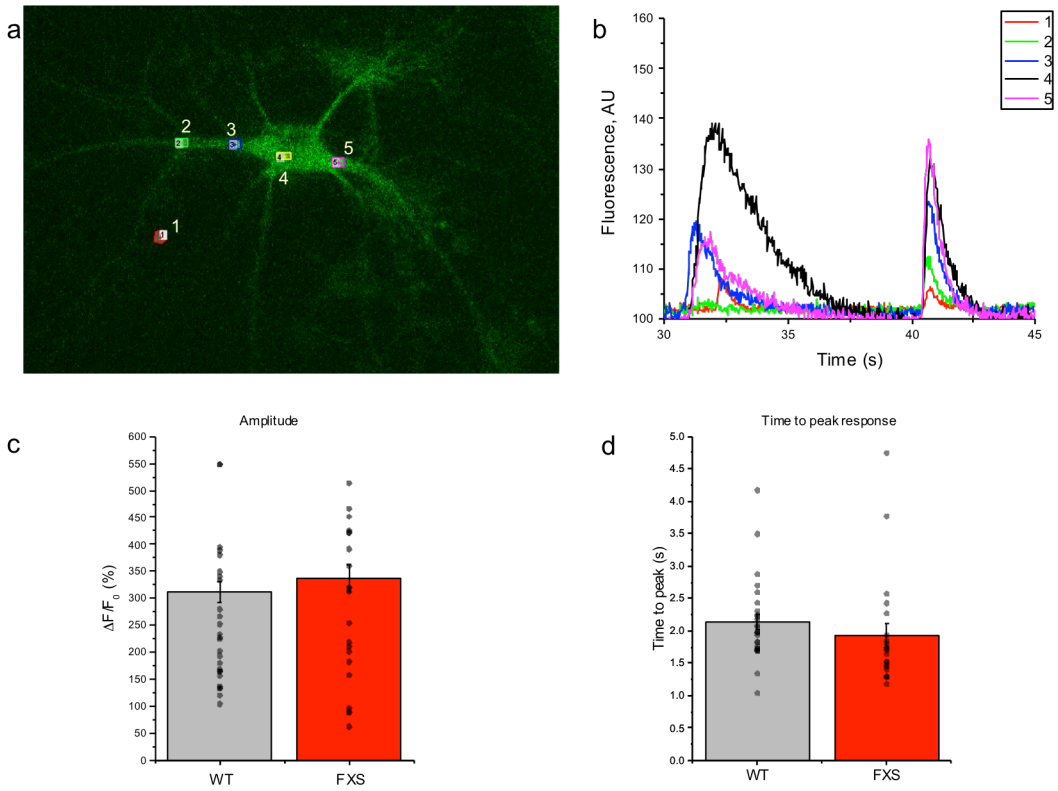


**Figure 3.5. 3 UV uncaging of t-ACPD induces $Ca^{2+}$ release in proximal dendrites of cortical neurons.**

**(a)** Averaged image of a cortical mouse neuron expressing GCaMP6f from the whole recording with 5 regions of interest (ROI). **(b)** Traces illustrating the wave formation and spread in different ROIs of a cortical neuron from **(a)**. The first event (red trace) occurs at the distal dendrite and is independent of the $Ca^{2+}$ wave invading the soma. $Ca^{2+}$ wave in response to 200 ms UV pulse uncaging induced a wave at position 3 (blue trace) that did not spread to position 2 (green trace), but initiated a somatic $Ca^{2+}$ release (position 4, black) that spread further onto the position 5 (magenta). **(c)** Mean peak amplitude of somatic $Ca^{2+}$ response does not differ statistically between FXS and WT neurons (p-value>0.05)**. (d)** Mean latency from time of

photolysis flash to peak $Ca^{2+}$ response is not different between FXS and WT neurons. All data are presented as mean ± s.e.m. Individual data points represent responses from single neurons.

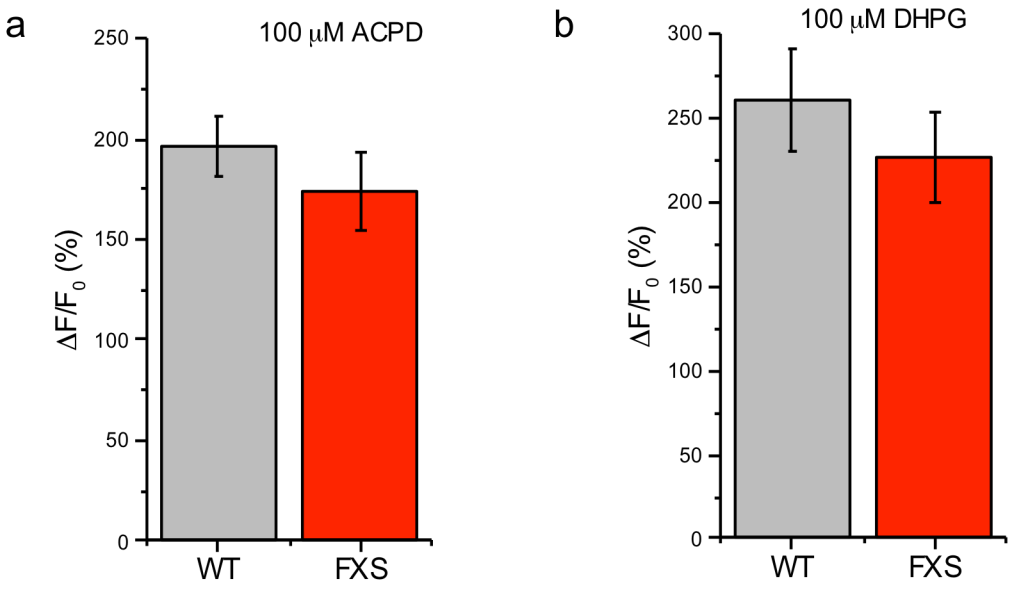


**Figure 3.5. 4 Metabotropic $Ca^{2+}$ response in astrocytes from WT or FXS mice.**

**(a)** Mean peak amplitude of $Ca^{2+}$ release in response to UV flash photolysis of 100 μM ACPD is not depressed in FXS cells relative to WT controls (p-value > 0.05). **(b)** Mean peak response to bath application of 100 μM of DHPG does not differ in astrocytes from WT or FXS mice (p-value > 0.05). All data are presented as mean ± s.e.m..

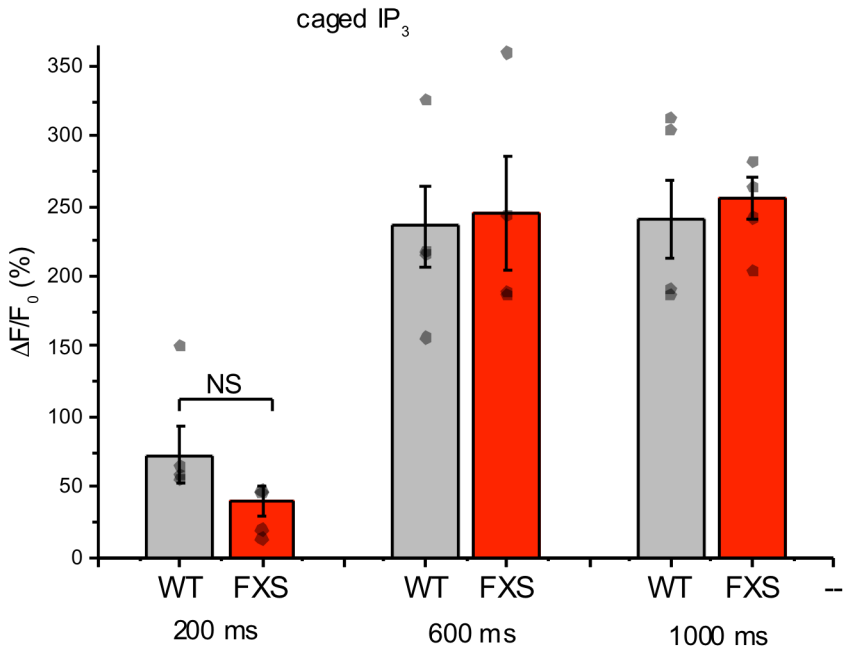


**Figure 3.5. 5 $Ca^{2+}$ release in mouse astrocytes evoked by photoreleased $IP_3$.**

$IP_3$-mediated $Ca^{2+}$ release evoked by different flash durations of the UV flash induced peak responses of similar amplitude in cultures of confluent astrocytes from WT or FXS mice. $Ca^{2+}$ responses were recorded and averaged across a confluent monolayer of the cells. All data are presented as mean ± s.e.m. Data points represent responses from individual recordings.

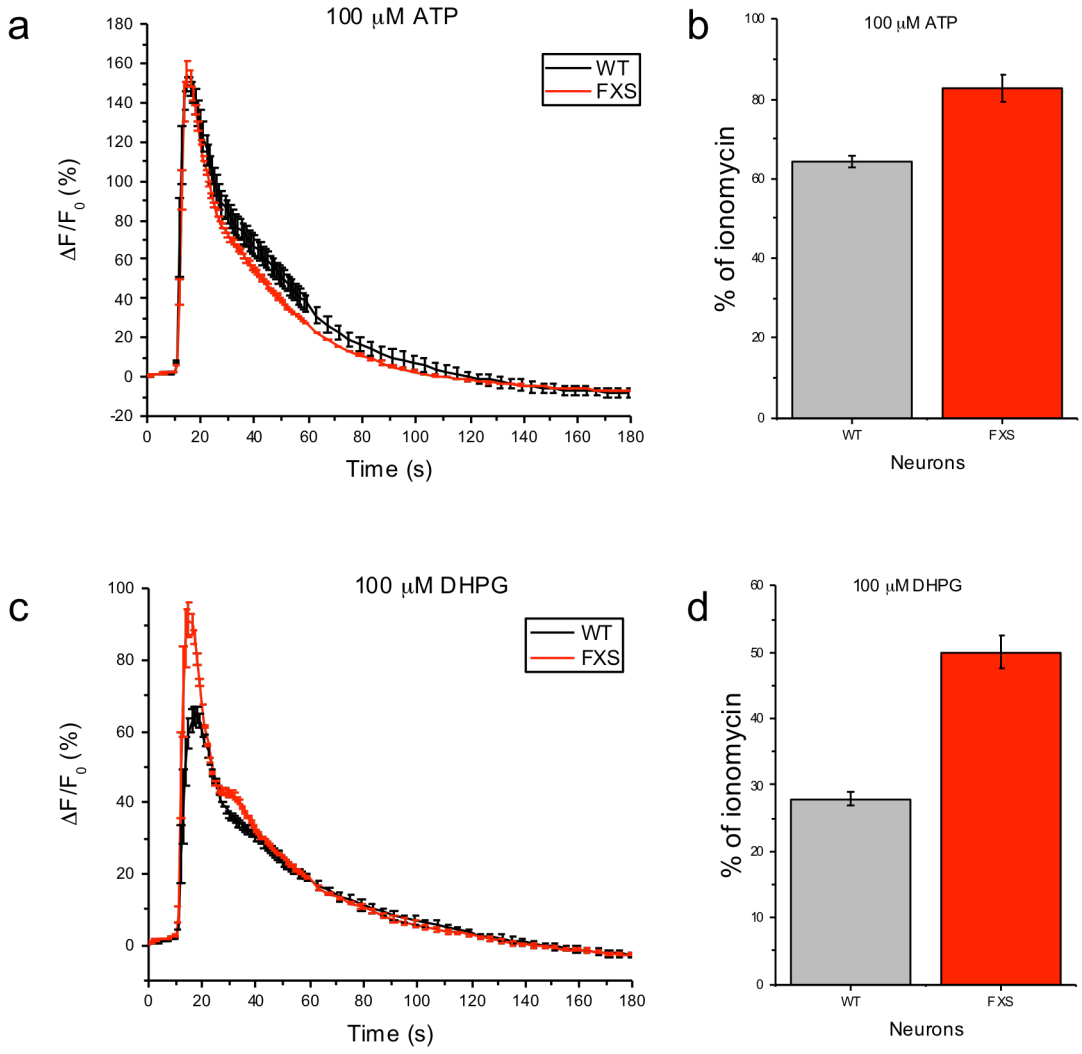


**Figure 3.5. 6 Representative $Ca^{2+}$ responses to extracellular application of purinergic agonists in absence of extracellular $Ca^{2+}$ in cultures enriched in neurons from WT or FXS P0 mice.**

**(a)** Averaged FLIPR traces from three independent wells showing changes in Fluo-8 fluorescence over the basal fluorescence ($\Delta F/F_0$) in response to extracellular application of 100

μM ATP to neuron-enriched cultures. Lines represent mean values ± s.e.m.. **(b)** Peak amplitudes (ΔF) of $Ca^{2+}$ responses to 100 μM ATP normalized to basal fluorescence ($F_0$) before stimulation are expressed as a percentage of the mean ionomycin response in neurons from WT mice (grey) or FXS (red). Bar graphs show mean of triplicate measurements after subtracting the artifactual signal resulting from addition of vehicle alone. Data are presented as mean ± s.e.m.. **(c)** Averaged FLIPR traces showing changes in Fluo-8 fluorescence over the basal fluorescence ($\Delta F/F_0$) in response to extracellular application of 100 μM DHPG to neuron-enriched cultures. **(d)** Peak amplitudes (ΔF) of $Ca^{2+}$ responses to 100 μM DHPG normalized to the basal fluorescence ($F_0$) before stimulation are expressed as a percentage of the mean ionomycin response in neurons from WT mice (grey) or FXS (red). Bar graphs show mean of triplicate measurements after subtracting the artifactual signal resulting from addition of vehicle alone. Data are presented as mean ± s.e.m..

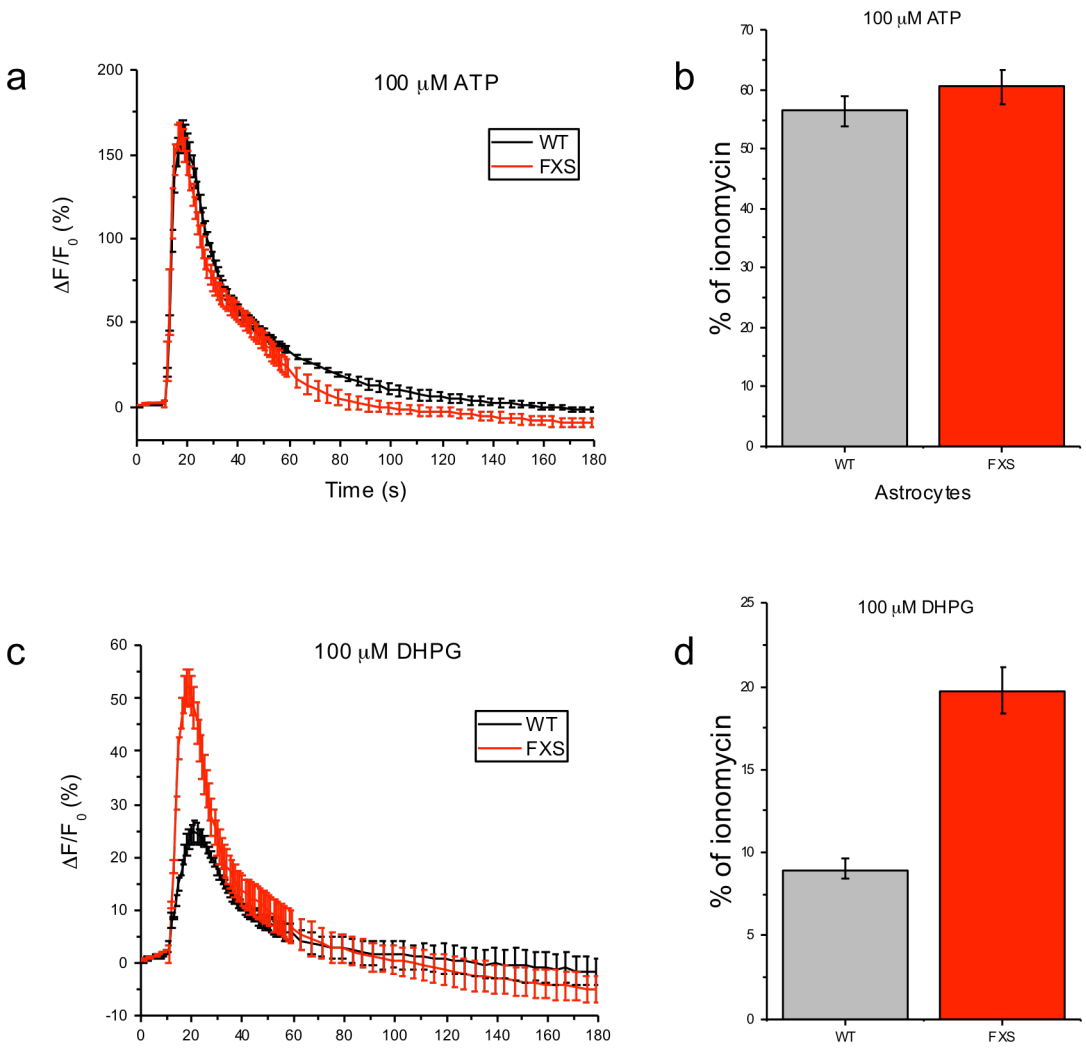


**Figure 3.5. 7 Representative $Ca^{2+}$ responses to extracellular application of purinergic agonists in absence of extracellular $Ca^{2+}$ in cultures enriched in astrocytes from WT or FXS P0 mice.**

**(a)** Averaged FLIPR traces from three independent wells showing changes in Fluo-8 fluorescence over the basal fluorescence ($\Delta F/F_0$) in response to extracellular application of 100

μM ATP to glia-enriched cultures. Lines represent mean values ± s.e.m.. **(b)** Peak amplitudes (ΔF) of $Ca^{2+}$ responses to 100 μM ATP normalized to the basal fluorescence ($F_0$) before stimulation are expressed as a percentage of the mean ionomycin response in astrocytes from WT mice (grey) or FXS (red). Bar graphs show mean of triplicate measurements after subtracting the artifactual signal resulting from addition of vehicle alone. Data are presented as mean ± s.e.m.. **(c)** Averaged FLIPR traces showing changes in Fluo-8 fluorescence over the basal fluorescence ($\Delta F/F_0$) in response to extracellular application of 100 μM DHPG to astrocyte-enriched cultures. **(d)** Peak amplitudes (ΔF) of $Ca^{2+}$ responses to 100 μM DHPG normalized to the basal fluorescence ($F_0$) before stimulation expressed as a percentage of the mean ionomycin response in astrocytes from WT mice (grey) or FXS (red). Bar graphs show mean of triplicate measurements after subtracting the artifactual signal resulting from addition of vehicle alone. Data are presented as mean ± s.e.m..

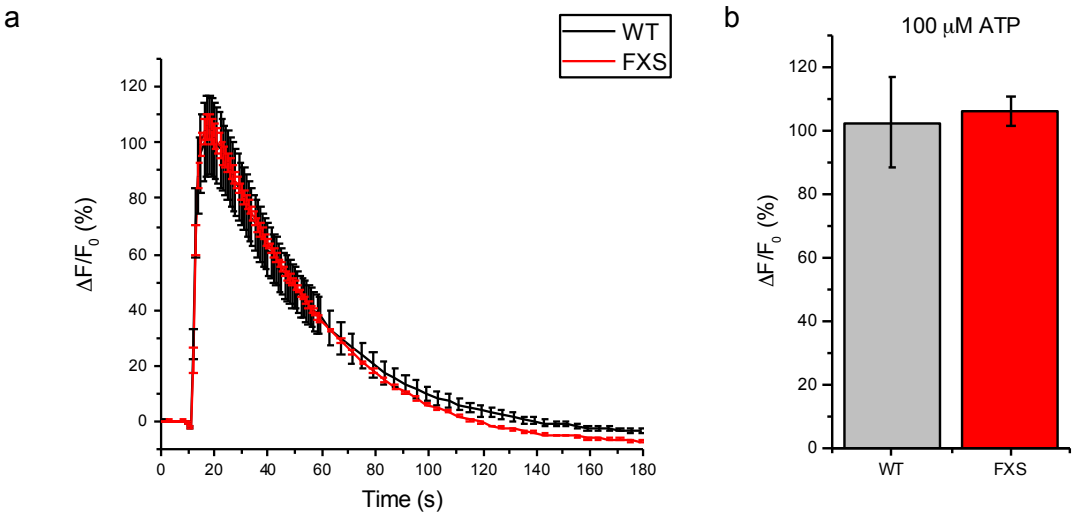


**Figure 3.5. 8 Representative $Ca^{2+}$ responses to extracellular application of ATP in absence of extracellular $Ca^{2+}$ in skin fibroblasts from WT and FXS P0 mice.**

**(a)** Averaged FLIPR traces from six independent wells showing changes in Fluo-8 fluorescence over the basal fluorescence ($\Delta F/F_0$) in response to extracellular application of 100 μM ATP in WT fibroblasts (black) and FXS cells (red). Lines represent mean values ± s.e.m.. **(b)** Peak amplitudes ($\Delta F$) of $Ca^{2+}$ responses to 100 μM ATP normalized to the basal fluorescence ($F_0$) before stimulation from WT mice (grey) or FXS (red). Bar graphs show mean of triplicate measurements after subtracting the artifactual signal resulting from addition of vehicle alone. Data are presented as mean ± s.e.m..

## Chapter 4. Discussion and implications of this work

ASD is a broad, umbrella diagnosis for a heterogeneous group of conditions encompassing several neurodevelopmental problems, along with many phenotypes and co-morbidities. Here I demonstrate that patient-derived fibroblasts from subjects with monogenic syndromes with high prevalence of ASD (FXS, TSC1, TSC2, Rett, and Prader-Willi syndromes) display depressed $Ca^{2+}$ release evoked by purinergic receptor activation of $IP_3$ signaling. I further extend these findings to fibroblast cell lines from patients with sporadic ASD without any known genetic mutations. This $Ca^{2+}$ signaling defect was identified in 85% of the subjects with sporadic ASD, suggesting that dysregulation of $IP_3$ signaling constitutes a nexus where genes altered in ASD converge to exert their deleterious effect. This decrease is not due to the defective activation and/or signaling from the membrane-bound receptors, but results from decreased $IP_3R$ activity, since the intracellular uncaging of i-$IP_3$ leads to similarly dampened response. Using the optical patch-clamp technique, I discovered that these changes may be attributed to decreased functioning of elementary single or clustered $IP_3Rs$ at the molecular level. The mean open time in human FXS fibroblasts was about one half that in wild type cells, and the numbers of definable release sites were reduced. These results suggest that the $IP_3Rs$, although carrying no mutations themselves, are functionally altered at the level of single (or small clusters of) channels in these three distinct ASD models.

### *4.1 Downstream consequences of diminished $IP_3$ $Ca^{2+}$ signaling.*

In neurons, $IP_3$-mediated $Ca^{2+}$ signaling is activated through agonist stimulation of Gq-coupled receptors such as 5HT2A or mGluR1/5 receptor subtypes found on the plasma

membrane. $IP_3R$-mediated $Ca^{2+}$ release in neurons is involved in crucial functions, including synaptic plasticity and memory (Inoue et al. 1998; Rose and Konnerth 2001), neuronal excitability (Hernandez-Lopez et al. 2000; Stutzmann, LaFerla, and Parker 2003), neurotransmitter release (Li et al. 1998; Diamant, Schwartz, and Atlas 1990), axon growth (Gomez and Spitzer 1999) and long-term changes in gene expression (Li et al. 1998), highlighting the central integrating position played by $IP_3Rs$ (Patterson, Boehning, and Snyder 2004). Both spatial and temporal features of $Ca^{2+}$ signals are crucial for the reliable signal initiation and propagation. Large signals that propagate to the soma can carry information from dendritic synapses, activating certain genes and transcription factors in the nucleus; while smaller events confined to a single synapse regulate neuronal properties at the dendritic level. $Ca^{2+}$ release from the ER dynamically regulates activity-dependent membrane excitability through the opening of small conductance $Ca^{2+}$-activated $K^+$ channels (Chandy et al. 1998; Köhler et al. 1996). This current is proportional to the $Ca^{2+}$ signal amplitude (Stutzmann, LaFerla, and Parker 2003) and underlies spike-frequency adaptation, a phenomenon where accumulating intracellular $Ca^{2+}$ reaches sufficient levels to activate hyperpolarizing $K^+$ currents and transiently suppress membrane excitability. As a result, $IP_3$-evoked $Ca^{2+}$ release transiently hyperpolarizes the cell and briefly depresses neuronal excitability, leading to a reduction in firing frequency (Stutzmann, LaFerla, and Parker 2003). Suppressed $IP_3$-mediated $Ca^{2+}$ release from the internal stores, as I report in diverse models of ASD, is thus expected to diminish the inhibitory $K^+$ conductance, and as such would tend to produce neuronal hyperexcitability, consistent with observations in several models of ASD (Repicky and Broadie 2009; Bateup et al. 2011).

Depression of $IP_3$-mediated $Ca^{2+}$ signaling may further disrupt neurodevelopment through separate mechanisms. $IP_3Rs$ have been shown to be central participants in autophagy (Cárdenas et al. 2010; Criollo et al. 2007; Hamada et al. 2014; Vicencio et al. 2009). Decreased levels of autophagy result in defective synaptic pruning, which have been repeatedly associated with ASD in humans and mouse models (Tang et al. 2014). Promotion of autophagy also rescues behavioral defects in mouse models of ASD (Tang et al. 2014). The role of mitochondria energy-deficient endophenotype has long been an active line of investigation in a subset of patients with ASD (Gargus and Imtiaz 2008; Filipek et al. 2003), and several studies have shown a link between $IP_3$-mediated $Ca^{2+}$ release and mitochondrial function (Pinton et al. 2008; Cárdenas et al. 2010; La Rovere et al. 2016; Decuypere et al. 2011). Under normal basal conditions, low-level constitutive $IP_3R$-mediated transfer of $Ca^{2+}$ from the ER to mitochondria maintains optimal cellular bioenergetics (Cárdenas et al. 2010). This ongoing transfer supports normal cellular bioenergetics by maintaining oxidative phosphorylation and ATP production. In its absence, cells undergo an energy crisis; oxidative phosphorylation is compromised, ATP levels fall and AMPK-dependent, mTOR-independent autophagy is induced as a mechanism to enable the cell to survive. Reduced mitochondrial activity likely has adverse consequences for normal neurodevelopment and neuronal function, resulting from ATP deficiency and its effects on membrane potential and neurotransmitter release, as well as production of excess reactive oxygen species (ROS).

### *4.2 $Ca^{2+}$ signaling screen as a biomarker for ASD.*

The recent development of mouse models for ASD has greatly improved our understanding of the condition. Laboratory mice can provide valuable information about neuronal networks and synaptic function in primary neurons, as human neurons are largely unavailable for laboratory research. A great deal of ASD animal work has been concentrated on the mouse model of FXS, a syndromic form of ASD in humans. Since Mark Bear coined his mGluR theory of FXS in 2004 (Bear, Huber, and Warren 2004), it has taken a central role in the FXS research field. The theory explains several cellular and molecular deficits occurring in a FXS brain by a hyperactive signaling arising from the enhanced group 1 mGluR activation. The mouse model turned out to be highly amenable to correction of many deficits with pharmacological and genetic mGluR reduction. Three pharmacological companies – Novartis, Roche and Seaside Therapeutics (that had partnered with Roche) launched independent clinical trials on mGluR antagonists in humans. All of them failed to meet their primary endpoints.

The $IP_3R$ is a key signaling hub in the canonical metabotropic glutamate receptor pathway in neurons (Inoue et al. 1998; Berridge 1993), and according to the mGluR theory of FXS (Bear, Huber, and Warren 2004), the overactive mGluR signaling cascade underlies the pathogenesis of the disorder. Surprisingly, not much is known about $Ca^{2+}$ signaling release in response to activation of the mGluR in FXS. In Chapter 2, I demonstrate that human skin fibroblasts from patients with FXS have pronounced signaling deficits at the level of $IP_3Rs$, which led me to hypothesize that $Ca^{2+}$ release resulting from activation of metabotropic receptors would be decreased in neurons from a mouse model of FXS. However, my findings in Chapter 3 demonstrate that mouse neurons did not replicate this signaling deficit. Furthermore, neither

mouse astrocytes nor skin fibroblasts from FXS mice demonstrated this signaling abnormality. In conclusion, the mouse completely fails as a model for the $IP_3R$ defect I observe in human FXS cells, providing a possible explanation for recent failures of several clinical trials for this disease.

My findings tap into an important but often overlooked topic of divergence in signaling pathways between species ((Yue et al. 2014; Seok et al. 2013), but also see (Takao and Miyakawa 2015)). The mouse brain is not simply a mini-version of a human brain, and this fact may explain poor success rates in translation between preclinical studies on rodents to clinical studies in humans, especially in the neurological field. This is well exemplified by the recent failures of two clinical FXS drug trials (Mullard 2015), and >100 failed clinical trials of Alzheimer's disease therapies (Schneider et al. 2014), all of which showed promise in mouse models.

At present, a strong emphasis is put on mapping behavioral defects seen in humans onto rodents and then correcting them in the mouse models. A different (and perhaps better) approach would be to refine biochemical or biophysical functional biomarkers as molecular readouts for validating drug targets in human cells. Biomarkers of ASD have long been sought in the hopes that they might improve outcomes for these patients and their families. A high-throughput $Ca^{2+}$ signaling assay such as the one I describe here may potentially serve as a molecular target for future drug discoveries. Indeed, the promise of cell-based approaches to ASD is underscored by the now well-established utility of going directly to human disease cells for drug discovery in instances where animal models are lacking; as was the case for cystic fibrosis where novel therapeutics were identified based on high throughput screening of patient cells for correction of

a patient's cellular biomarker phenotype (Van Goor et al. 2009; Van Goor et al. 2011; Davis, Yasothan, and Kirkpatrick 2012).

My study opens the prospect that a skin biopsy sample could become a functional cellular diagnostic and surrogate clinical trial outcome end-point measure, much as long has been the case for neurogenetic encephalopathies caused by defects in mitochondria, lysosomes and peroxisomes (Kudoh, Velkoff, and Wenger 1983; Waterham and Ebberink 2012; Ye and Hoppel 2013; Saada 2011). Using this cell-based assay, novel or repurposed candidate drugs could be rapidly screened to evaluate their efficacy on a subject's cells prior to their enrollment in a clinical trial, hopefully improving the prospects for children with autism and their families.

### *4.3 Limitations and future directions.*

Although human skin fibroblasts have advantages as a model cell system to study ASD, the central pathology of ASD lies in neuronal dysfunction. To truly understand the disease pathogenesis these studies need to be extended to examine $IP_3/Ca^{2+}$ signaling in neurons. Results in skin fibroblasts cannot be directly extrapolated to $IP_3$-mediated signaling in neurons, given that fibroblasts predominantly express type 3 $IP_3Rs$ whereas neurons predominantly express type 1 $IP_3Rs$ (Zhang et al. 2014). Nevertheless, because expression levels of all three isotypes of $IP_3Rs$ are only slightly diminished in FXS and TSC fibroblasts, I conclude that the pronounced depression of $Ca^{2+}$ signaling does not result from diminished expression of a specific isotype. Instead, the depressed $Ca^{2+}$ signals likely result from modulatory effects on $IP_3R$ function, which might extend across different isotypes.

Recent advances in stem cell biology and the advent of somatic cell reprogramming now enable the generation of patient-derived induced pluripotent stem cells (iPSCs) that can be differentiated *in vitro* into neurons, glia and other cell types (Takahashi and Yamanaka 2015). A promising approach will be to utilize neuronal and glial cells derived from fibroblasts from a selected small set of monogenic and sporadic ASD subjects as well as matched, non-affected controls. This would allow a determination of how $Ca^{2+}$ signaling may be altered in central nervous system cells from ASD subjects, how these alterations relate to the corresponding deficits in the fibroblasts from which the iPSC cells are derived, and provide a means to explore consequences for neuronal excitability.

In recent years, several iPSC cell lines from patients with FXS have been developed by different groups (Urbach et al. 2010; Sheridan et al. 2011). In light of the considerable attention that has been devoted to the mGluR theory of FXS, including several human trials, it is intriguing that there have yet to be any convincing reports of mGluR-mediated signaling abnormalities in human cells. A first goal of future studies would be to compare $IP_3$-mediated $Ca^{2+}$ signals in iPSC-derived neurons from FXS, TSC1 and TSC2 human subjects, as well as unaffected controls. Given the ubiquity of the ER $IP_3/Ca^{2+}$ signaling pathway across all cells of the body, and decades of experience with other organellar diseases, it is reasonable to expect that the deficits I observed in fibroblasts from ASD subjects would be reflected in neuronal function; however, that remains to be experimentally determined, and will be a critical achievement. The correlation between $Ca^{2+}$ signaling deficits in neurons v*s*. fibroblasts among different subjects would reveal the extent to which neuronal deficits can be inferred from measurements in fibroblasts, and whether similar correlations hold true across different monogenic and sporadic

cases of ASD. If such correlation exists, it would greatly support the view that $Ca^{2+}$ signaling deficiencies may play a causative role in ASD pathogenesis and provide an enormously powerful tool to dissect the underlying mechanisms.

### *4.5 Concluding remarks.*

In conclusion, my findings indicate that ER $IP_3R$ signaling is affected in three distinct monogenic genetic models of ASD as well as a majority of cases of sporadic ASD, pointing to the ER as a functional "hub" where different cellular signaling pathways merge to contribute to the pathogenesis of ASD. In addition to its role in $Ca^{2+}$ homeostasis, the ER serves as a key integrator of environmental stressors with metabolism and gene expression, as it mediates a host of broad ranging cell stress responses such as the heat shock and unfolded protein responses (Brostrom and Brostrom 2003). Because of the ubiquitous nature of $IP_3R$ signaling and its diverse roles in almost all cells of the body, deficits in $IP_3$-mediated $Ca^{2+}$ signaling may not be limited to neurological correlates of ASD, but may also explain other characteristic ASD-associated heterogeneous symptoms, such as those of the gastrointestinal tract (McElhanon et al. 2014; van De Sande, van Buul, and Brouns 2014) and immune system (Ziats and Rennert 2011; Wei et al. 2011). Furthermore, since the ER serves as a sensor of a host of environmental stressors, this same mechanism may contribute to the known environmental component to the ASD phenotype, and holds the potential to reveal relevant stressors. In this light it can be seen to integrate a matrix of ASD associated risk factors. $Ca^{2+}$ screening in skin fibroblasts, which are routinely acquired as clinical specimens, may thus offer a promising technique in conjunction

with behavioral testing for early detection of ASD, as well as their potential use for high-throughput screening of novel therapeutic agents.

**References**

Agulhon, Cendra, Todd A. Fiacco, and Ken D. McCarthy. 2010. "Hippocampal Short- and Long-Term Plasticity Are Not Modulated by Astrocyte Ca2+ Signaling." *Science* 327 (5970): 1250–54. doi:10.1126/science.1184821.

Amir, Ruthie E, Ignatia B Van Den Veyver, Mimi Wan, Charles Q Tran, Uta Francke, and Huda Y Zoghbi. 1999. "Rett Syndrome Is Caused by Mutations in X-Linked MECP2, Encoding Methyl-CpG-Binding Protein 2." *Nature Genetics* 23: 185–88.

Anderson, Deborah K, Jessie W Liang, and Catherine Lord. 2014. "Predicting Young Adult Outcome among More and Less Cognitively Able Individuals with Autism Spectrum Disorders." *Journal of Child Psychology and Psychiatry, and Allied Disciplines* 55 (5): 485–94. doi:10.1111/jcpp.12178.

Anney, Richard, Lambertus Klei, Dalila Pinto, Regina Regan, Judith Conroy, Tiago R Magalhaes, Catarina Correia, et al. 2010. "A Genome-Wide Scan for Common Alleles Affecting Risk for Autism." *Human Molecular Genetics* 19 (20): 4072–82. doi:10.1093/hmg/ddq307.

Association, American Psychiatric. 2016. "Diagnostic and Statistical Manual of Mental Disorders | DSM Library." *Association, American Psychiatric*. Accessed June 1. http://psychiatryonline.org/doi/book/10.1176/appi.books.9780890425596.

Autism and Developmental Disabilities Monitoring Network Surveillance Year 2010 Principal

Investigators. 2014. “Prevalence of Autism Spectrum Disorder among Children Aged 8 Years - Autism and Developmental Disabilities Monitoring Network, 2010.” *MMWR* 63 (2): 1–21. doi:24670961.

Bailey, A., A. Le Couteur, I. Gottesman, P. Bolton, E. Simonoff, E. Yuzda, M. Rutter, et al. 1995. “Autism as a Strongly Genetic Disorder: Evidence from a British Twin Study.” *Psychological Medicine* 25 (1): 63-77. doi:10.1017/S0033291700028099.

Baskys, A, and R C Malenka. 1991. “Agonists at Metabotropic Glutamate Receptors Presynaptically Inhibit EPSCs in Neonatal Rat Hippocampus.” *The Journal of Physiology* 444: 687–701. doi:10.1113/jphysiol.1991.sp018901.

Bateup, Helen S, Caroline A Johnson, Cassandra L Denefrio, Jessica L Saulnier, Karl Kornacker, and Bernardo L Sabatini. 2013. “Excitatory/inhibitory Synaptic Imbalance Leads to Hippocampal Hyperexcitability in Mouse Models of Tuberous Sclerosis.” *Neuron* 78 (3). Elsevier: 510–22. doi:10.1016/j.neuron.2013.03.017.

Bateup, Helen S, Kevin T Takasaki, Jessica L Saulnier, Cassandra L Denefrio, and Bernardo L Sabatini. 2011. “Loss of Tsc1 in Vivo Impairs Hippocampal mGluR-LTD and Increases Excitatory Synaptic Function.” *The Journal of Neuroscience,* 31 (24): 8862–69. doi:10.1523/JNEUROSCI.1617-11.2011.

Bauer, Peter O., Roman Hudec, Shoichiro Ozaki, Misako Okuno, Etsuko Ebisui, Katsuhiko Mikoshiba, and Nobuyuki Nukina. 2011. “Genetic Ablation and Chemical Inhibition of IP3R1 Reduce Mutant Huntingtin Aggregation.” *Biochemical and Biophysical Research*

*Communications* 416 (1–2). doi:10.1016/j.bbrc.2011.10.096.

Bear, Mark F, Kimberly M Huber, and Stephen T Warren. 2004. "The mGluR Theory of Fragile X Mental Retardation." *Trends in Neurosciences* 27 (7): 370–77. doi:10.1016/j.tins.2004.04.009.

Beaudoin, Gerard M J, Seung-Hye Lee, Dipika Singh, Yang Yuan, Yu-Gie Ng, Louis F Reichardt, and Jyothi Arikkath. 2012. "Culturing Pyramidal Neurons from the Early Postnatal Mouse Hippocampus and Cortex." *Nature Protocols* 7 (9): 1741–54. doi:10.1038/nprot.2012.099.

Berridge, M.J. 1997a. "Annual Review Prize Lecture Elementary and Global Aspects of Calcium Signalling." *J. Physiol.* 499 (2): 291–306.

Berridge, M.J. 1993. "Inositol Trisphosphate and Calcium Signaling." *Nature* 361: 315–25.

Berridge, M.J. 2009. "Inositol Trisphosphate and Calcium Signalling Mechanisms." *Biochimica et Biophysica Acta - Molecular Cell Research* 1793 (6): 933–40. doi:10.1016/j.bbamcr.2008.10.005.

Berridge, M.J. 2016. "The Inositol Trisphosphate/Calcium Signaling Pathway in Health and Disease." *Physiological Reviews* 96 (4): 1261–96. doi:10.1152/physrev.00006.2016.

Berridge, M J. 1997b. "Elementary and Global Aspects of Calcium Signalling." *The Journal of Physiology* 499 (2): 291–306.

Berridge, M J, P Lipp, and M D Bootman. 2000. “The Versatility and Universality of Calcium Signalling.” *Nature Reviews. Molecular Cell Biology* 1 (1): 11–21. doi:10.1038/35036035.

Berridge, M J, and N G Patel. 1968. “Insect Salivary Glands: Stimulation of Fluid Secretion by 5-Hydroxytryptamine and Adenosine-3’,5’-monophosphate.” *Science* 162 (3852): 462–63. http://www.ncbi.nlm.nih.gov/pubmed/4300804.

Berry-Kravis, Elizabeth M, David Hessl, Barbara Rathmell, Peter Zarevics, Maryann Cherubini, Karen Walton-bowen, Yi Mu, et al. 2012. “Effects of STX209 ( Arbaclofen ) on Neurobehavioral Function in Children and Adults with Fragile X Syndrome : A Randomized , Controlled , Phase 2 Trial.” *Science Translational Medicine* 4 (152).

Berry-Kravis, Elizabeth, Vincent Des Portes, Randi Hagerman, Sébastien Jacquemont, Perrine Charles, Jeannie Visootsak, Marc Brinkman, et al. 2016. “Mavoglurant in Fragile X Syndrome : Results of Two Randomized , Double-Blind , Placebo-Controlled Trials.” *Sci. Transl. Med.* 8 (321).

Bezprozvanny, I. 2011. “Role of Inositol 1,4,5-Trisphosphate Receptors in Pathogenesis of Huntington’s Disease and Spinocerebellar Ataxias.” *Neurochemical Research* 36 (7): 1186–97. doi:10.1007/s11064-010-0393-y.

Bezprozvanny, I, J Watras, and B E Ehrlich. 1991. “Bell-Shaped Calcium-Response Curves of Ins(1,4,5)P3- and Calcium-Gated Channels from Endoplasmic Reticulum of Cerebellum.” *Nature* 351 (6329): 751–54. doi:10.1038/351751a0.

Blumberg, Stephen J, and Matthew D Bramlett. 2013. “Changes in Prevalence of Parent-Reported Autism Spectrum Disorder in School-Aged U.S. Children : 2007 to 2011 – 2012.” *National Health Statistics Reports*, no. 65.

Bootman, M D, M J Berridge, and P Lipp. 1997. “Cooking with Calcium: The Recipes for Composing Global Signals from Elementary Events.” *Cell* 91 (3): 367–73.

Bradford, M M. 1976. “A Rapid and Sensitive Method for the Quantitation of Microgram Quantities of Protein Utilizing the Principle of Protein-Dye Binding.” *Analytical Biochemistry* 72 (May): 248–54.

Brostrom, Margaret A, and Charles O Brostrom. 2003. “Calcium Dynamics and Endoplasmic Reticular Function in the Regulation of Protein Synthesis: Implications for Cell Growth and Adaptability.” *Cell Calcium* 34 (4–5): 345–63. doi:10.1016/S0143-4160(03)00127-1.

Brown, V, P Jin, S Ceman, J C Darnell, W T O’Donnell, S a Tenenbaum, X Jin, et al. 2001. “Microarray Identification of FMRP-Associated Brain mRNAs and Altered mRNA Translational Profiles in Fragile X Syndrome.” *Cell* 107 (4): 477–87.

Burnstock, Geoffrey, Maria-Pia Abbracchio, Jean-Marie Boeynaems, José L. Boyer, Stefania Ceruti, Marta Fumagalli, Christian Gachet, et al. 2016. “P2Y Receptors.” *IUPHAR/BPS Guide to PHARMACOLOGY*. http://www.guidetopharmacology.org/GRAC/FamilyDisplayForward?familyId=52.

Campion, D, C Dumanchin, D Hannequin, B Dubois, S Belliard, M Puel, C Thomas-Anterion, et

al. 1999. “Early-Onset Autosomal Dominant Alzheimer Disease: Prevalence, Genetic Heterogeneity, and Mutation Spectrum.” *American Journal of Human Genetics* 65 (3): 664–70. doi:10.1086/302553.

Cao, X, L P Li, Q Wang, Q Wu, H H Hu, M Zhang, Y Y Fang, et al. 2013. “Astrocyte-Derived ATP Modulates Depressive-like Behaviors.” *Nat Med* 19 (6). 773–77. doi:10.1038/nm.3162.

Cárdenas, César, Russell A. Miller, Ian Smith, Thi Bui, Jordi Molgó, Marioly Müller, Horia Vais, et al. 2010. “Essential Regulation of Cell Bioenergetics by Constitutive InsP3 Receptor Ca2+ Transfer to Mitochondria.” *Cell* 142 (2): 270–83. doi:10.1016/j.cell.2010.06.007.

Chan, Sic L., Michael Mayne, Clark P. Holden, Jonathan D. Geiger, and Mark P. Mattson. 2000. “Presenilin-1 Mutations Increase Levels of Ryanodine Receptors and Calcium Release in PC12 Cells and Cortical Neurons.” *Journal of Biological Chemistry* 275 (24): 18195–200. doi:10.1074/jbc.M000040200.

Chandy, K G, E Fantino, O Wittekindt, K Kalman, L L Tong, T H Ho, G A Gutman, et al. 1998. “Isolation of a Novel Potassium Channel Gene hSKCa3 Containing a Polymorphic CAG Repeat: A Candidate for Schizophrenia and Bipolar Disorder?” *Molecular Psychiatry* 3 (1): 32–37.

Chen, Naiyan, Hiroki Sugihara, Jitendra Sharma, Gertrudis Perea, Jeremy Petravicz, and Chuong Le. 2012. “Nucleus Basalis-Enabled Stimulus-Specific Plasticity in the Visual Cortex Is Mediated by Astrocytes.” *Proceedings of the National Academy of Sciences* 109 (41): E2832–E2841. doi:10.1073/pnas.1206557109/-

/DCSupplemental.www.pnas.org/cgi/doi/10.1073/pnas.1206557109.

Chen, Tsai-Wen, Trevor J Wardill, Yi Sun, Stefan R Pulver, Sabine L Renninger, Amy Baohan, Eric R Schreiter, et al. 2013. "Ultrasensitive Fluorescent Proteins for Imaging Neuronal Activity." *Nature* 499 (7458): 295–300. doi:10.1038/nature12354.

Chen, Xi, Tie-Shan Tang, Huiping Tu, Omar Nelson, Mark Pook, Robert Hammer, Nobuyuki Nukina, and Ilya Bezprozvanny. 2008. "Deranged Calcium Signaling and Neurodegeneration in Spinocerebellar Ataxia Type 3." *The Journal of Neuroscience* 28 (48): 12713–24. doi:10.1523/JNEUROSCI.3909-08.2008.

Cheung, King-Ho, Lijuan Mei, Don-On Daniel Mak, Ikuo Hayashi, Takeshi Iwatsubo, David E Kang, and J Kevin Foskett. 2010. "Gain-of-Function Enhancement of IP3 Receptor Modal Gating by Familial Alzheimer's Disease-Linked Presenilin Mutants in Human Cells and Mouse Neurons." *Science Signaling* 3 (114). doi:10.1126/scisignal.2000818.

Clancy, Barbara, Barbara L. Finlay, Richard B. Darlington, and K. J S Anand. 2007. "Extrapolating Brain Development from Experimental Species to Humans." *NeuroToxicology* 28 (5): 931–37. doi:10.1016/j.neuro.2007.01.014.

Clandinin, Thomas R., John a. DeModena, and Paul W. Sternberg. 1998. "Inositol Trisphosphate Mediates a RAS-Independent Response to LET-23 Receptor Tyrosine Kinase Activation in C. Elegans." *Cell* 92: 523–33. doi:10.1016/S0092-8674(00)80945-9.

Coffee, Bradford, Krayton Keith, Igor Albizua, Tamika Malone, Julie Mowrey, Stephanie L

Sherman, and Stephen T Warren. 2009. “Incidence of Fragile X Syndrome by Newborn Screening for Methylated FMR1 DNA.” *American Journal of Human Genetics* 85 (4): 503–14. doi:10.1016/j.ajhg.2009.09.007.

Cohen, A S, and W C Abraham. 1996. “Facilitation of Long-Term Potentiation by Prior Activation of Metabotropic Glutamate Receptors.” *J Neurophysiol* 76 (2): 953–62.

Consortium, The European Chromosome 16 Tuberous Sclerosis. 1993. “Identification and Characterization of the Tuberous Sclerosis Gene on Chromosome 16.” *Cell* 75 (7): 1305–15. doi:10.1016/0092-8674(93)90618-Z.

Constantino, John N., and Tony Charman. 2015. “Diagnosis of Autism Spectrum Disorder: Reconciling the Syndrome, Its Diverse Origins, and Variation in Expression.” *The Lancet Neurology* 15 (3): 279–91. doi:10.1016/S1474-4422(15)00151-9.

Coriell. 2016. “Coriell Cell Biorepository.” https://catalog.coriell.org/0/Sections/Search/Sample_Detail.aspx?Ref=GM03440&Product=CC.

Criollo, A, M C Maiuri, E Tasdemir, I Vitale, A A Fiebig, D Andrews, J Molgó, et al. 2007. “Regulation of Autophagy by the Inositol Trisphosphate Receptor.” *Cell Death and Differentiation* 14 (5): 1029–39. doi:10.1038/sj.cdd.4402099.

Dargan, Sheila L, and Ian Parker. 2003. “Buffer Kinetics Shape the Spatiotemporal Patterns of IP3-Evoked Ca2+ Signals.” *The Journal of Physiology* 553 (3): 775–88.

doi:10.1113/jphysiol.2003.054247.

Darnell, Jennifer C., Sarah J. Van Driesche, Chaolin Zhang, Ka Ying Sharon Hung, Aldo Mele, Claire E. Fraser, Elizabeth F. Stone, et al. 2011. "FMRP Stalls Ribosomal Translocation on mRNAs Linked to Synaptic Function and Autism." *Cell* 146 (2): 247–61. doi:10.1016/j.cell.2011.06.013.

Darnell, Jennifer C, and Eric Klann. 2013. "The Translation of Translational Control by FMRP: Therapeutic Targets for FXS." *Nature Neuroscience* 16 (11). 1530–36. doi:10.1038/nn.3379.

Davis, Pamela B., Uma Yasothan, and Peter Kirkpatrick. 2012. "Ivacaftor." *Nature Reviews Drug Discovery* 11 (5): 349–50. doi:10.1038/nrd3723.

de la Torre-Ubieta, Luis, Hyejung Won, Jason L Stein, and Daniel H Geschwind. 2016. "Advancing the Understanding of Autism Disease Mechanisms through Genetics." *Nature Medicine* 22 (4). 345–61. doi:10.1038/nm.4071.

De Rubeis, Silvia, and Joseph D. Buxbaum. 2015. "Genetics and Genomics of Autism Spectrum Disorder: Embracing Complexity." *Human Molecular Genetics* 1 (8): 1–8. doi:10.1093/hmg/ddv273.

Decuypere, Jean-Paul, Kirsten Welkenhuyzen, Tomas Luyten, Raf Ponsaerts, Michael Dewaele, Jordi Molgó, Patrizia Agostinis, et al. 2011. "Ins(1,4,5)P3 Receptor-Mediated Ca2+ Signaling and Autophagy Induction Are Interrelated." *Autophagy* 7 (12): 1472–89.

Demuro, A, and I Parker. 2013. "Cytotoxicity of Intracellular abeta42 Amyloid Oligomers

Involves Ca2+ Release from the Endoplasmic Reticulum by Stimulated Production of Inositol Trisphosphate." *J Neurosci* 33 (9): 3824–33. doi:10.1523/JNEUROSCI.4367-12.2013.

Deng, Pan-Yue, David Sojka, and Vitaly a Klyachko. 2011. "Abnormal Presynaptic Short-Term Plasticity and Information Processing in a Mouse Model of Fragile X Syndrome." *The Journal of Neuroscience* 31 (30): 10971–82. doi:10.1523/JNEUROSCI.2021-11.2011.

Di Leva, Francesca, Teuta Domi, Laura Fedrizzi, Dmitry Lim, and Ernesto Carafoli. 2008. "The Plasma Membrane Ca2+ ATPase of Animal Cells: Structure, Function and Regulation." *Archives of Biochemistry and Biophysics* 476 (1): 65–74. doi:10.1016/j.abb.2008.02.026.

Diamant, S., L. Schwartz, and D. Atlas. 1990. "Potentiation of Neurotransmitter Release Coincides with Potentiation of Phosphatidyl Inositol Turnover. A Possible in Vitro Model for Long Term Potentiation." *Neuroscience Letters* 109 (1–2): 140–45. doi:10.1016/0304-3940(90)90552-K.

Dickinson, George D, Divya Swaminathan, and Ian Parker. 2012. "The Probability of Triggering Calcium Puffs Is Linearly Related to the Number of Inositol Trisphosphate Receptors in a Cluster." *Biophysical Journal* 102 (8): 1826–36. doi:10.1016/j.bpj.2012.03.029.

Dölen, Gül, Emily Osterweil, B S Shankaranarayana Rao, Gordon B Smith, Benjamin D Auerbach, Sumantra Chattarji, and Mark F Bear. 2007. "Correction of Fragile X Syndrome in Mice." *Neuron* 56 (6): 955–62. doi:10.1016/j.neuron.2007.12.001.

El-Hassar, Lynda, Anna M Hagenston, Lisa Bertetto D'Angelo, and Mark F Yeckel. 2011. "Metabotropic Glutamate Receptors Regulate Hippocampal CA1 Pyramidal Neuron Excitability via $Ca^{2+}$ Wave-Dependent Activation of SK and TRPC Channels." *The Journal of Physiology* 589 (13): 3211–29. doi:10.1113/jphysiol.2011.209783.

Elkins, Ryan C., Mark R. Davies, Stephen J. Brough, David J. Gavaghan, Yi Cui, Najah Abi-Gerges, and Gary R. Mirams. 2013. "Variability in High-Throughput Ion-Channel Screening Data and Consequences for Cardiac Safety Assessment." *Journal of Pharmacological and Toxicological Methods* 68 (1): 112–22. doi:10.1016/j.vascn.2013.04.007.

Ellefsen, Kyle L, Brett Settle, Ian Parker, and Ian F Smith. 2014. "An Algorithm for Automated Detection, Localization and Measurement of Local Calcium Signals from Camera-Based Imaging." *Cell Calcium* 56 (3): 147–56. doi:10.1016/j.ceca.2014.06.003.

Ellis, Hillary T., Michael G. Tordoff, and M. Rockwell Parker. 2013. "Itpr3 Is Responsible for the Mouse Tufted (Tf) Locus." *Journal of Heredity* 104 (2): 295–97. doi:10.1093/jhered/ess089.

Erb, Laurie, and Gary A. Weisman. 2012. "Coupling of P2Y Receptors to G Proteins and Other Signaling Pathways." *Wiley Interdisciplinary Reviews: Membrane Transport and Signaling* 1 (6): 789–803. doi:10.1002/wmts.62.

Etcheberrigaray, R, N Hirashima, L Nee, J Prince, S Govoni, M Racchi, R E Tanzi, and D L Alkon. 1998. "Calcium Responses in Fibroblasts from Asymptomatic Members of Alzheimer's Disease Families." *Neurobiology of Disease* 5: 37–45.

doi:10.1006/nbdi.1998.0176.

Fain, J N, and M J Berridge. 1979. “Relationship between Hormonal Activation of Phosphatidylinositol Hydrolysis, Fluid Secretion and Calcium Flux in the Blowfly Salivary Gland.” *The Biochemical Journal* 178 (1): 45–58.

Ferreiro, Elisabete, Catarina R. Oliveira, and Cláudia M F Pereira. 2004. “Involvement of Endoplasmic Reticulum Ca2+ Release through Ryanodine and Inositol 1,4,5-Triphosphate Receptors in the Neurotoxic Effects Induced by the Amyloid-beta Peptide.” *Journal of Neuroscience Research* 76 (6): 872–80. doi:10.1002/jnr.20135.

Filipek, Pauline A. 2013. “Medical Aspects of Autism.” In *Handbook of Autism and Pervasive Developmental Disorders*, 534–78. Hoboken, NJ, USA: John Wiley & Sons, Inc. doi:10.1002/9780470939345.ch20.

Filipek, Pauline A., Jenifer Juranek, Moyra Smith, Lee Z. Mays, Erica R. Ramos, Maureen Bocian, Diane Masser-Frye, et al. 2003. “Mitochondrial Dysfunction in Autistic Patients with 15q Inverted Duplication.” *Annals of Neurology* 53 (6): 801–4. doi:10.1002/ana.10596.

Fine, Jenny, Peter Cole, and James S Davidson. 1989. “Extracellular Nucleotides Stimulate Receptor-Mediated Calcium Mobilization and Inositol Phosphate Production in Human Fibroblasts.” *Biochem J.* 263: 371–76.

Folstein, Susan, and Michael Rutter. 1977. “Genetic Influences and Infantile Autism.” *Nature* 265 (5596): 726–28. doi:10.1038/265726a0.

Foskett, J Kevin, Carl White, King-ho Cheung, and Don-on Daniel Mak. 2007. "Inositol Trisphosphate Receptor Ca2+ Release Channels." *Physiology Reviews* 87: 593–658. doi:10.1152/physrev.00035.2006.

Fu, Ying-Hui, Derek P.A. Kuhl, Antonio Pizzuti, Maura Pieretti, James S. Sutcliffe, Stephen Richards, Annemieke J.M.H. Verkert, et al. 1991. "Variation of the CGG Repeat at the Fragile X Site Results in Genetic Instability: Resolution of the Sherman Paradox." *Cell* 67 (6): 1047–58. doi:10.1016/0092-8674(91)90283-5.

Fujii, Satoshi, Mineo Matsumoto, Kotaro Igarashi, Hiroshi Kato, and Katsuhiko Mikoshiba. 2000. "Synaptic Plasticity in Hippocampal CA1 Neurons of Mice Lacking Type 1 Inositol-1,4,5-Trisphosphate Receptors." *Learning & Memory (Cold Spring Harbor, N.Y.)* 7 (5): 312–20. doi:10.1101/lm.34100.Previous.

Gargus, J.J., and F. Imtiaz. 2008. "Mitochondrial Energy-Deficient Endophenotype in Autism." *Am J Biochem and Biotech* 4 (2): 198–207.

Gargus, J Jay. 2009. "Genetic Calcium Signaling Abnormalities in the Central Nervous System: Seizures, Migraine, and Autism." *Annals of the New York Academy of Sciences* 1151: 133–56. doi:10.1111/j.1749-6632.2008.03572.x.

Gaugler, Trent, Lambertus Klei, Stephan J Sanders, Corneliu A Bodea, Arthur P Goldberg, Ann B Lee, Milind Mahajan, et al. 2014. "Most Genetic Risk for Autism Resides with Common Variation." *Nature Genetics* 46 (8). doi:10.1038/ng.3039.

Geschwind, Daniel H, and Matthew W State. 2015. “Gene Hunting in Autism Spectrum Disorder: On the Path to Precision Medicine.” *The Lancet Neurology* 4422 (15). doi:10.1016/S1474-4422(15)00044-7.

Ghosh, Anirvan, Aubin Michalon, Lothar Lindemann, Paulo Fontoura, and Luca Santarelli. 2013. “Drug Discovery for Autism Spectrum Disorder: Challenges and Opportunities.” *Nature Reviews. Drug Discovery* 12 (10): 777–90. doi:10.1038/nrd4102.

Gibson, Jay R, Aundrea F Bartley, Seth a Hays, and Kimberly M Huber. 2008. “Imbalance of Neocortical Excitation and Inhibition and Altered UP States Reflect Network Hyperexcitability in the Mouse Model of Fragile X Syndrome.” *Journal of Neurophysiology* 100 (5): 2615–26. doi:10.1152/jn.90752.2008.

Gilman, Sarah R, Ivan Iossifov, Dan Levy, Michael Ronemus, Michael Wigler, and Dennis Vitkup. 2011. “Rare de Novo Variants Associated with Autism Implicate a Large Functional Network of Genes Involved in Formation and Function of Synapses.” *Neuron* 70 (5): 898–907. doi:10.1016/j.neuron.2011.05.021.

Girirajan, Santhosh, Megan Y Dennis, Carl Baker, Maika Malig, Bradley P Coe, Catarina D Campbell, Kenneth Mark, et al. 2013. “Refinement and Discovery of New Hotspots of Copy-Number Variation Associated with Autism Spectrum Disorder.” *American Journal of Human Genetics* 92 (2): 221–37. doi:10.1016/j.ajhg.2012.12.016.

Gomez, Timothy M, and Nicholas C Spitzer. 1999. “In Vivo Regulation of Axon Extension and Path Finding by Growth-Cone Calcium Transients.” *Nature* 397: 350–55.

Goussakov, Ivan, Megan B Miller, and Grace E Stutzmann. 2010. "NMDA-Mediated Ca 2 2 Influx Drives Aberrant Ryanodine Receptor Activation in Dendrites of Young Alzheimer ' S Disease Mice." *J Neurosci* 30 (36): 12128–37. doi:10.1523/JNEUROSCI.2474-10.2010.

Group, Cross-disorder, and Psychiatric Genomics Consortium. 2013. "Identification of Risk Loci with Shared Effects on Five Major Psychiatric Disorders: A Genome-Wide Analysis." *The Lancet* 6736 (12): 1–9. doi:10.1016/S0140-6736(12)62129-1.

Guo, Q, K Furukawa, B L Sopher, D G Pham, J Xie, N Robinson, G M Martin, and M P Mattson. 1996. "Alzheimer's PS-1 Mutation Perturbs Calcium Homeostasis and Sensitizes PC12 Cells to Death Induced by Amyloid Beta-Peptide." *Neuroreport* 8 (1): 379–83.

Guo, Qing, Weiming Fu, Bryce L. Sopher, Miles W. Miller, Carol B. Ware, George M. Martin, and Mark P. Mattson. 1999. "Increased Vulnerability of Hippocampal Neurons to Excitotoxic Necrosis in Presenilin-1 Mutant Knock-in Mice." *Nature Medicine* 5 (1): 101–6. doi:10.1038/4789.

Hagenston, Anna M, John S Fitzpatrick, and Mark F Yeckel. 2008. "mGluR-Mediated Calcium Waves That Invade the Soma Regulate Firing in Layer V Medial Prefrontal Cortical Pyramidal Neurons." *Cereb. Cortex* 18 (2): 407–23. doi:10.1093/cercor/bhm075.MGluR-Mediated.

Hamada, Kozo, Akiko Terauchi, Kyoko Nakamura, Takayasu Higo, Nobuyuki Nukina, Nagisa Matsumoto, Chihiro Hisatsune, Takeshi Nakamura, and Katsuhiko Mikoshiba. 2014. "Aberrant Calcium Signaling by Transglutaminase-Mediated Posttranslational Modification

of Inositol 1,4,5-Trisphosphate Receptors." *Proceedings of the National Academy of Sciences of the United States of America*, 111(38): E3966-75. doi:10.1073/pnas.1409730111.

Hanley, A.J., and J.B. McNeil. 1982. "The Meaning and Use of the Area under a Receiver Operating Characteristic (ROC) Curve." *Radiology* 143: 29–36. doi:10.1148/radiology.143.1.7063747.

Hara, K, A Shiga, H Nozaki, J Mitsui, Y Takahashi, H Ishiguro, H Yomono, et al. 2008. "Total Deletion and a Missense Mutation of ITPR1 in Japanese SCA15 Families." *Neurology* 71 (8): 547–51. doi:10.1212/01.wnl.0000311277.71046.a0.

Hernandez-Lopez, Salvador, Tatiana Tkatch, Enrique Perez-Garci, Elvira Galarraga, Heidi Hamm, and D James Surmeier. 2000. "D2 Dopamine Receptors in Striatal Medium Spiny Neurons Reduce L-Type Ca2+ Currents and Excitability via a Novel PLCbeta1 – IP3 – Calcineurin-Signaling Cascade." *The Journal of Neuroscience* 20 (24): 8987–95.

Hirashima, Naohide, René Etcheberrigaray, Stefania Bergamaschi, Marco Racchi, Fiorenzo Battaini, Giuliano Binetti, Stefano Govoni, and Daniel L. Alkon. 1996. "Calcium Responses in Human Fibroblasts: A Diagnostic Molecular Profile for Alzheimer's Disease." *Neurobiology of Aging* 17 (4): 549–55. doi:10.1016/0197-4580(96)00074-7.

Hosmer, David W., and Stanley Lemeshow. 2000. *Applied Logistic Regression*. Edited by David W. Hosmer and Stanley Lemeshow. Second. New York, NY: John Wiley and Sons. doi:10.1198/tech.2002.s650.

Huang, Lijia, Jodi Warman Chardon, Melissa T Carter, Kathie L Friend, Tracy E Dudding, Jeremy Schwartzentruber, Ruobing Zou, et al. 2012. "Missense Mutations in ITPR1 Cause Autosomal Dominant Congenital Nonprogressive Spinocerebellar Ataxia." *Orphanet Journal of Rare Diseases* 7 (1): 67. doi:10.1186/1750-1172-7-67.

Inoue, T, K Kato, K Kohda, and K Mikoshiba. 1998. "Type 1 Inositol 1,4,5-Trisphosphate Receptor Is Required for Induction of Long-Term Depression in Cerebellar Purkinje Neurons." *The Journal of Neuroscience* 18 (14): 5366–73.

Ito, E., K. Oka, R. Etcheberrigaray, T. J. Nelson, D. L. McPhie, B. Tofel-Grehl, G. E. Gibson, and D. L. Alkon. 1994. "Internal Ca2+ Mobilization Is Altered in Fibroblasts from Patients with Alzheimer Disease." *Proceedings of the National Academy of Sciences* 91 (2): 534–38. doi:10.1073/pnas.91.2.534.

Iwaki, A, Y Kawano, S Miura, H Shibata, D Matsuse, W Li, H Furuya, et al. 2008. "Heterozygous Deletion of ITPR1, but Not SUMF1, in Spinocerebellar Ataxia Type 16." *Journal of Medical Genetics* 45 (1): 32–35. doi:10.1136/jmg.2007.053942.

Jaffe, D. B., and T. H. Brown. 1994. "Metabotropic Glutamate Receptor Activation Induces Calcium Waves within Hippocampal Dendrites." *Journal of Neurophysiology* 72 (1).

Jensen, Laura E., Geert Bultynck, Tomas Luyten, Hozeefa Amijee, Martin D. Bootman, and H. Llewelyn Roderick. 2013. "Alzheimer's Disease-Associated Peptide Aβ42 Mobilizes ER Ca2+ via InsP3R-Dependent and -Independent Mechanisms." *Frontiers in Molecular Neuroscience* 6: 1–12. doi:10.3389/fnmol.2013.00036.

Jeste, Shafali S, and Daniel H Geschwind. 2016. “Clinical Trials for Neurodevelopmental Disorders : At a Therapeutic Frontier.” *Science Translational Medicine* 8 (321): 1–4.

Kazdoba, Tatiana M, Prescott T Leach, Jill L Silverman, and Jacqueline N Crawley. 2014. “Modeling Fragile X Syndrome in the Fmr1 Knockout Mouse.” *Intractable & Rare Diseases Research* 3 (4): 118–33. doi:10.5582/irdr.2014.01024.

Khodakhah, K, and C M Armstrong. 1997. “Induction of Long-Term Depression and Rebound Potentiation by Inositol Trisphosphate in Cerebellar Purkinje Neurons.” *Proceedings of the National Academy of Sciences of the United States of America* 94 (25): 14009–14.

Klar, Joakim, Chihiro Hisatsune, Shahid M. Baig, Muhammad Tariq, Anna C V Johansson, Mahmood Rasool, Naveed Altaf Malik, et al. 2014. “Abolished InsP3R2 Function Inhibits Sweat Secretion in Both Humans and Mice.” *Journal of Clinical Investigation* 124 (11): 4773–80. doi:10.1172/JCI70720.

Klei, Lambertus, Stephan J Sanders, Michael T Murtha, Vanessa Hus, Jennifer K Lowe, a Jeremy Willsey, Daniel Moreno-De-Luca, et al. 2012. “Common Genetic Variants, Acting Additively, Are a Major Source of Risk for Autism.” *Molecular Autism* 3 (1): 3-9. doi:10.1186/2040-2392-3-9.

Köhler, M, B Hirschberg, C T Bond, J M Kinzie, N V Marrion, J Maylie, and J P Adelman. 1996. “Small-Conductance, Calcium-Activated Potassium Channels from Mammalian Brain.” *Science* 273 (5282): 1709–14.

Kudoh, T, M A Velkoff, and D A Wenger. 1983. “Uptake and Metabolism of Radioactively Labeled Sphingomyelin in Cultured Skin Fibroblasts from Controls and Patients with Niemann-Pick Disease and Other Lysosomal Storage Diseases.” *Biochim Biophys Acta* 754 (1): 82–92.

Kügler, S, E Kilic, and M Bähr. 2003. “Human Synapsin 1 Gene Promoter Confers Highly Neuron-Specific Long-Term Transgene Expression from an Adenoviral Vector in the Adult Rat Brain Depending on the Transduced Area.” *Gene Therapy* 10 (4): 337–47. doi:10.1038/sj.gt.3301905.

La Rovere, Rita M L, Gemma Roest, Geert Bultynck, and Jan B Parys. 2016. “Intracellular Ca(2+) Signaling and Ca(2+) Microdomains in the Control of Cell Survival, Apoptosis and Autophagy.” *Cell Calcium*. 1–14. doi:10.1016/j.ceca.2016.04.005.

Larkum, Matthew E., Shigeo Watanabe, Takeshi Nakamura, Nechama Lasser-Ross, and William N. Ross. 2003. “Synaptically Activated Ca2+ Waves in Layer 2/3 and Layer 5 Rat Neocortical Pyramidal Neurons.” *The Journal of Physiology* 549 (2). doi:10.1113/jphysiol.2002.037614.

Laumonnier, Frédéric, Sébastien Roger, Pascaline Guérin, Florence Molinari, Ridha M’rad, Dominique Cahard, Ahlem Belhadj, et al. 2006. “Association of a Functional Deficit of the BKCa Channel, a Synaptic Regulator of Neuronal Excitability, with Autism and Mental Retardation.” *The American Journal of Psychiatry* 163 (9): 1622–29. doi:10.1176/appi.ajp.163.9.1622.

Lawrence, Y a, T L Kemper, M L Bauman, and G J Blatt. 2010. “Parvalbumin-, Calbindin-, and Calretinin-Immunoreactive Hippocampal Interneuron Density in Autism.” *Acta Neurologica Scandinavica* 121 (2): 99–108. doi:10.1111/j.1600-0404.2009.01234.x.

Leissring, M A, F M LaFerla, N Callamaras, and I Parker. 2001. “Subcellular Mechanisms of Presenilin-Mediated Enhancement of Calcium Signaling.” *Neurobiology of Disease* 8 (3): 469–78. doi:10.1006/nbdi.2001.0382.

Leissring, Malcolm A., Brooke A. Paul, Ian Parker, Carl W. Cotman, and Frank M. Laferla. 1999. “Alzheimer’s Presenilin-1 Mutation Potentiates Inositol 1,4,5- Trisphosphate-Mediated Calcium Signaling in Xenopus Oocytes.” *Journal of Neurochemistry* 72 (3): 1061–68. doi:10.1046/j.1471-4159.1999.0721061.x.

Li, W, J Llopis, M Whitney, G Zlokarnik, and RY Tsien. 1998. “Cell-Permeant Caged InsP3 Ester Shows That Ca2 Spike Frequency Can Optimize Gene Expression.” *Nature* 392: 936–41.

Li, Yong-xin, Yinong Zhang, Henry A Lester, Erin M Schuman, and Norman Davidson. 1998. “Enhancement of Neurotransmitter Release Induced by Brain- Derived Neurotrophic Factor in Cultured Hippocampal Neurons.” *The Journal of Neuroscience* 18 (24): 10231–40.

Lim, Jeong-A, Lishu Li, and Nina Raben. 2014. “Pompe Disease: From Pathophysiology to Therapy and Back Again.” *Frontiers in Aging Neuroscience* 6 (177): 1-14. doi:10.3389/fnagi.2014.00177.

Lipp, P, and E Niggli. 1996. “A Hierarchical Concept of Cellular and Subcellular Ca(2+)-Signalling.” *Progress in Biophysics and Molecular Biology* 65 (3): 265–96.

Liu, Jing, Tie-Shan Tang, Huiping Tu, Omar Nelson, Emily Herndon, Duong P Huynh, Stefan M Pulst, and Ilya Bezprozvanny. 2009. “Deranged Calcium Signaling and Neurodegeneration in Spinocerebellar Ataxia Type 2.” *The Journal of Neuroscience* 29 (29): 9148–62. doi:10.1523/JNEUROSCI.0660-09.2009.

Lock, Jeffrey T., Ian Parker, and Ian F. Smith. 2015. “A Comparison of Fluorescent Ca2+ Indicators for Imaging Local Ca2+ Signals in Cultured Cells.” *Cell Calcium* 58 (6). doi:10.1016/j.ceca.2015.10.003.

Loth, Eva, Will Spooren, Lindsay M. Ham, Maria B. Isaac, Caroline Auriche-Benichou, Tobias Banaschewski, Simon Baron-Cohen, et al. 2016. “Identification and Validation of Biomarkers for Autism Spectrum Disorders.” *Nature Reviews Drug Discovery* 15 (70). doi:10.1093/nrd.2015.7.

Lozano, Reymundo, Veronica Martinez-Cerdeno, and Randi J Hagerman. 2015. “Advances in the Understanding of the Gabaergic Neurobiology of FMR1 Expanded Alleles Leading to Targeted Treatments for Fragile X Spectrum Disorder.” *Current Pharmaceutical Design* 21 (34): 4972–79. doi:10.1007/978-1-4614-5915-6.

Lu, Ake Tzu-Hui, Xiaoxian Dai, Julian A Martinez-Agosto, and Rita M Cantor. 2012. “Support for Calcium Channel Gene Defects in Autism Spectrum Disorders.” *Molecular Autism* 3 (1): 18. doi:10.1186/2040-2392-3-18.

Lüscher, Christian, and Kimberly M Huber. 2010. “Group 1 mGluR-Dependent Synaptic Long-Term Depression: Mechanisms and Implications for Circuitry and Disease.” *Neuron* 65 (4). doi:10.1016/j.neuron.2010.01.016.

MacDonald, Rebecca, Diana Parry-Cruwys, Sally Dupere, and William Ahearn. 2014. “Assessing Progress and Outcome of Early Intensive Behavioral Intervention for Toddlers with Autism.” *Research in Developmental Disabilities* 35 (12), 3632–44. doi:10.1016/j.ridd.2014.08.036.

Maclennan, David H, and Elena Zvaritch. 2011. “Mechanistic Models for Muscle Diseases and Disorders Originating in the Sarcoplasmic Reticulum.” *Biochimica et Biophysica Acta* 1813 (5): 948–64. doi:10.1016/j.bbamcr.2010.11.009.

Mak, Don-On Daniel, King Ho Cheung, Patrick Toglia, J. Kevin Foskett, and Ghanim Ullah. 2015. “Analyzing and Quantifying the Gain-of-Function Enhancement of IP3 Receptor Gating by Familial Alzheimer's Disease-Causing Mutants in Presenilins.” *PLoS Computational Biology* 11 (10): 1–22. doi:10.1371/journal.pcbi.1004529.

Matsumoto, M., T. Nakagawa, T. Inoue, E. Nagata, K. Tanaka, H. Takano, J. Kuno, et al. 1996. “Ataxia and Epileptic Seizures in Mice Lacking Type 1 Inositol 1,4,5-Trisphosphate Receptor.” *Nature* 379 (6561), 168–71. doi:10.1038/379168a0.

Matsumoto, Review Mineo, and Eiichiro Nagata. 1999. “Type 1 Inositol 1,4,5-Trisphosphate Receptor Knock-out Mice: Their Phenotypes and Their Meaning in Neuroscience and Clinical Practice.” *J. Mol. Med.* 77: 406–11.

Mattson, M P, and S L Chan. 2001. “Dysregulation of Cellular Calcium Homeostasis in Alzheimer’s Disease: Bad Genes and Bad Habits.” *Journal of Molecular Neuroscience.* 17 (2): 205–24. doi:10.1385/JMN:17:2:205.

McElhanon, Barbara O, Courtney McCracken, Saul Karpen, and William G Sharp. 2014. “Gastrointestinal Symptoms in Autism Spectrum Disorder: A Meta-Analysis.” *Pediatrics*, April. doi:10.1542/peds.2013-3995.

Metz, Charles E. 1978. “Basic Principles of ROC Analysis.” *Seminars in Nuclear Medicine* 8 (4): 283–298.

Miyoshi, Y, T Yamada, M Tanimura, T Taniwaki, K Arakawa, Y Ohyagi, H Furuya, et al. 2001. “A Novel Autosomal Dominant Spinocerebellar Ataxia (SCA16) Linked to Chromosome 8q22.1-24.1.” *Neurology* 57 (1): 96–100.

Morikawa, Hitoshi, Farzin Imani, Kamran Khodakhah, and John T. Williams. 2000. “Inositol 1,4,5-Triphosphate-Evoked Responses in Midbrain Dopamine Neurons.” *Journal of Neuroscience* 20 (20).

Mullard, Asher. 2015. “Fragile X Disappointments Upset Autism Ambitions.” *Nature Reviews Drug Discovery* 14 (3), 151–53. doi:10.1038/nrd4555.

Nakamoto, Mika, Vijayalaxmi Nalavadi, Michael P Epstein, Usha Narayanan, Gary J Bassell, and Stephen T Warren. 2007. “Fragile X Mental Retardation Protein Deficiency Leads to Excessive mGluR5-Dependent Internalization of AMPA Receptors.” *Proceedings of the*

*National Academy of Sciences of the United States of America* 104 (39): 15537–42. doi:10.1073/pnas.0707484104.

Nakamura, Takeshi, Kyoko Nakamura, and William N Ross. 1999. "Synergistic Release of Ca2+ from IP3 -Sensitive Stores Evoked by Synaptic Activation of mGluRs Paired with Backpropagating Action Potentials." *Neuron* 24: 727–37.

Nelson, Sacha B., and Vera Valakh. 2015. "Excitatory/Inhibitory Balance and Circuit Homeostasis in Autism Spectrum Disorders." *Neuron* 87 (4): 684–98. doi:10.1016/j.neuron.2015.07.033.

O'Roak, Brian J, Pelagia Deriziotis, Choli Lee, Laura Vives, Jerrod J Schwartz, Santhosh Girirajan, Emre Karakoc, et al. 2011. "Exome Sequencing in Sporadic Autism Spectrum Disorders Identifies Severe de Novo Mutations." *Nature Genetics* 43 (6): 585–89. doi:10.1038/ng.835.

O'Roak, Brian J, Laura Vives, Wenqing Fu, Jarrett D Egertson, Ian B Stanaway, Ian G Phelps, Gemma Carvill, et al. 2012. "Multiplex Targeted Sequencing Identifies Recurrently Mutated Genes in Autism Spectrum Disorders." *Science* 338 (6114): 1619–22. doi:10.1126/science.1227764.

O'Roak, Brian J, Laura Vives, Santhosh Girirajan, Emre Karakoc, Niklas Krumm, Bradley P Coe, Roie Levy, et al. 2012. "Sporadic Autism Exomes Reveal a Highly Interconnected Protein Network of de Novo Mutations." *Nature* 485 (7397): 246–50. doi:10.1038/nature10989.

Ogura, Hiroo, Mineo Matsumoto, and Katsuhiko Mikoshiba. 2001. “Motor Discoordination in Mutant Mice Heterozygous for the Type 1 Inositol 1,4,5-Trisphosphate Receptor.” *Behavioural Brain Research* 122 (2): 215–19. doi:10.1016/S0166-4328(01)00187-5.

Oliet, S H, R C Malenka, and R A Nicoll. 1997. “Two Distinct Forms of Long-Term Depression Coexist in CA1 Hippocampal Pyramidal Cells.” *Neuron* 18 (6): 969–82. doi:10.1016/S0896-6273(00)80336-0.

Osterweil, Emily K, Dilja D Krueger, Kimberly Reinhold, and Mark F Bear. 2010. “Hypersensitivity to mGluR5 and ERK1/2 Leads to Excessive Protein Synthesis in the Hippocampus of a Mouse Model of Fragile X Syndrome.” *The Journal of Neuroscience* 30 (46): 15616–27. doi:10.1523/JNEUROSCI.3888-10.2010.

Palmer, M. J., A. J. Irving, G. R. Seabrook, D. E. Jane, and G. L. Collingridge. 1997. “The Group I mGlu Receptor Agonist DHPG Induces a Novel Form of LTD in the CA1 Region of the Hippocampus.” *Neuropharmacology* 36 (11–12): 1517–32. doi:10.1016/S0028-3908(97)00181-0.

Palmieri, L, V Papaleo, V Porcelli, P Scarcia, L Gaita, R Sacco, J Hager, et al. 2010. “Altered Calcium Homeostasis in Autism-Spectrum Disorders: Evidence from Biochemical and Genetic Studies of the Mitochondrial Aspartate/glutamate Carrier AGC1.” *Molecular Psychiatry* 15 (1): 38–52. doi:10.1038/mp.2008.63.

Parikshak, Neelroop N., Rui Luo, Alice Zhang, Hyejung Won, Jennifer K. Lowe, Vijayendran Chandran, Steve Horvath, and Daniel H. Geschwind. 2013. “Integrative Functional Genomic

Analyses Implicate Specific Molecular Pathways and Circuits in Autism." *Cell* 155 (5): 1008–21. doi:10.1016/j.cell.2013.10.031.

Parker, I, J Choi, and Y Yao. 1996. "Elementary Events of InsP3-Induced Ca2+ Liberation in Xenopus Oocytes: Hot Spots, Puffs and Blips." *Cell Calcium* 20 (2): 105–21.

Parker, Ian, and Ian F Smith. 2010. "Recording Single-Channel Activity of Inositol Trisphosphate Receptors in Intact Cells with a Microscope, Not a Patch Clamp." *The Journal of General Physiology* 136 (2): 119–27. doi:10.1085/jgp.200910390.

Parker, I, and Y Yao. 1996. "Ca2+ Transients Associated with Openings of Inositol Trisphosphate-Gated Channels in Xenopus Oocytes." *The Journal of Physiology* 491 (3): 663–68.

Patterson, Randen L, Darren Boehning, and Solomon H Snyder. 2004. "Inositol 1,4,5-Trisphosphate Receptors as Signal Integrators." *Annual Review of Biochemistry* 73 (January): 437–65. doi:10.1146/annurev.biochem.73.071403.161303.

Petravicz, Jeremy, Kristen M. Boyt, and Ken D. McCarthy. 2014. "Astrocyte IP3R2-Dependent Ca2+ Signaling Is Not a Major Modulator of Neuronal Pathways Governing Behavior." *Frontiers in Behavioral Neuroscience* 8 (November): 384. doi:10.3389/fnbeh.2014.00384.

Petravicz, Jeremy, Todd A Fiacco, and Ken D McCarthy. 2008. "Loss of IP3 Receptor-Dependent Ca2+ Increases in Hippocampal Astrocytes Does Not Affect Baseline CA1 Pyramidal Neuron Synaptic Activity." *The Journal of Neuroscience* 28 (19): 4967–73.

doi:10.1523/JNEUROSCI.5572-07.2008.

Pietrobon, Daniela. 2010. “CaV2.1 Channelopathies.” *Pflügers Archiv : European Journal of Physiology* 460 (2): 375–93. doi:10.1007/s00424-010-0802-8.

Pinton, P, C Giorgi, R Siviero, E Zecchini, and R Rizzuto. 2008. “Calcium and Apoptosis: ER-Mitochondria Ca2+ Transfer in the Control of Apoptosis.” *Oncogene* 27 (50): 6407–18. doi:10.1038/onc.2008.308.

Pramparo, Tiziano, Karen Pierce, Michael V. Lombardo, Cynthia Carter Barnes, Steven Marinero, Clelia Ahrens-Barbeau, Sarah S. Murray, Linda Lopez, Ronghui Xu, and Eric Courchesne. 2015. “Prediction of Autism by Translation and Immune/Inflammation Coexpressed Genes in Toddlers From Pediatric Community Practices.” *JAMA Psychiatry* 92093 (4): 386–94. doi:10.1001/jamapsychiatry.2014.3008.

Pringle, B, L J Colpe, S J Blumberg, R M Avila, and M D Kogan. 2012. “Diagnostic History and Treatment of School-Aged Children with Autism Spectrum Disorder and Special Health Care Needs.” *NCHS Data Brief*, no. 97: 1–8.

Prole, David L., and Colin W. Taylor. 2016. “Inositol 1,4,5-Trisphosphate Receptors and Their Protein Partners as Signalling Hubs.” *The Journal of Physiology* 594(11): 2849-66. doi:10.1113/JP271139.

Ramanathan, Arvind, and Stuart L Schreiber. 2009. “Direct Control of Mitochondrial Function by mTOR.” *Proceedings of the National Academy of Sciences of the United States of*

*America* 106 (52): 22229–32. doi:10.1073/pnas.0912074106.

Repicky, Sarah, and Kendal Broadie. 2009. "Metabotropic Glutamate Receptor-Mediated Use-Dependent down-Regulation of Synaptic Excitability Involves the Fragile X Mental Retardation Protein." *Journal of Neurophysiology* 101 (2): 672–87. doi:10.1152/jn.90953.2008.

Ripke, Stephan, Colm O'Dushlaine, Kimberly Chambert, Jennifer L Moran, Anna K Kähler, Susanne Akterin, and Sarah E Bergen. 2013. "Genome-Wide Association Analysis Identifies 13 New Risk Loci for Schizophrenia." *Nature Genetics* 45(10): 1150-9. doi:10.1038/ng.2742.

Rose, C R, and a Konnerth. 2001. "Stores Not Just for Storage. Intracellular Calcium Release and Synaptic Plasticity." *Neuron* 31 (4): 519–22.

Roussel, Benoit D, Antonina J Kruppa, Elena Miranda, Damian C Crowther, David a Lomas, and Stefan J Marciniak. 2013. "Endoplasmic Reticulum Dysfunction in Neurological Disease." *The Lancet. Neurology* 12 (1): 105–18. doi:10.1016/S1474-4422(12)70238-7.

Rubenstein, J. L. R., and M. M. Merzenich. 2003. "Model of Autism: Increased Ratio of Excitation/inhibition in Key Neural Systems." *Genes, Brain and Behavior* 2 (5): 255–67. doi:10.1034/j.1601-183X.2003.00037.x.

Saada, Ann. 2011. "The Use of Individual Patient's Fibroblasts in the Search for Personalized Treatment of Nuclear Encoded OXPHOS Diseases." *Molecular Genetics and Metabolism*

104 (1–2): 39–47. doi:10.1016/j.ymgme.2011.07.016.

Sakai, Yasunari, Chad A Shaw, Brian C Dawson, Diana V Dugas, Zaina Al-Mohtaseb, David E Hill, and Huda Y Zoghbi. 2011. "Protein Interactome Reveals Converging Molecular Pathways among Autism Disorders." *Science Translational Medicine* 3 (86): 86ra49. doi:10.1126/scitranslmed.3002166.

Sarkar, Sovan, Gauri Krishna, Sara Imarisio, Shinji Saiki, Cahir J. O'Kane, and David C. Rubinsztein. 2008. "A Rational Mechanism for Combination Treatment of Huntington's Disease Using Lithium and Rapamycin." *Human Molecular Genetics* 17 (2): 170–78. doi:10.1093/hmg/ddm294.

Sarkisov, Dmitry V, and Samuel S-H Wang. 2008. "Order-Dependent Coincidence Detection in Cerebellar Purkinje Neurons at the Inositol Trisphosphate Receptor." *The Journal of Neuroscience* 28 (1): 133–42. doi:10.1523/JNEUROSCI.1729-07.2008.

Sasaki, Masayuki, Chihiro Ohba, Mizue Iai, Shinichi Hirabayashi, Hitoshi Osaka, Takuya Hiraide, Hirotomo Saitsu, and Naomichi Matsumoto. 2015. "Sporadic Infantile-Onset Spinocerebellar Ataxia Caused by Missense Mutations of the Inositol 1,4,5-Triphosphate Receptor Type 1 Gene." *Journal of Neurology* 262 (5): 1278–84. doi:10.1007/s00415-015-7705-8.

Sato-Miyaoka, Mai, Chihiro Hisatsune, Etsuko Ebisui, Naoko Ogawa, Hiromi Takahashi-Iwanaga, and Katsuhiko Mikoshiba. 2012. "Regulation of Hair Shedding by the Type 3 IP3 Receptor." *The Journal of Investigative Dermatology* 132 (9): 2137–47.

doi:10.1038/jid.2012.141.

Schmunk, G, and J.J. Gargus. 2013. “Channelopathy Pathogenesis in Autism Spectrum Disorders.” *Frontiers in Genetics* 4 (222): 1-20. doi:10.3389/fgene.2013.00222.

Schneider, L. S., F. Mangialasche, N. Andreasen, H. Feldman, E. Giacobini, R. Jones, V. Mantua, et al. 2014. “Clinical Trials and Late-Stage Drug Development for Alzheimer’s Disease: An Appraisal from 1984 to 2014.” *Journal of Internal Medicine* 275 (3): 251–83. doi:10.1111/joim.12191.

Semple, Bridgette D., Klas Blomgren, Kayleen Gimlin, Donna M. Ferriero, and Linda J. Noble-Haeusslein. 2013. “Brain Development in Rodents and Humans: Identifying Benchmarks of Maturation and Vulnerability to Injury across Species.” *Progress in Neurobiology* 106–107. doi:10.1016/j.pneurobio.2013.04.001.

Seok, Junhee, H Shaw Warren, Alex G Cuenca, Michael N Mindrinos, Henry V Baker, Weihong Xu, Daniel R Richards, et al. 2013. “Genomic Responses in Mouse Models Poorly Mimic Human Inflammatory Diseases.” *Proceedings of the National Academy of Sciences of the United States of America* 110 (9): 3507–12. doi:10.1073/pnas.1222878110.

Sheridan, Steven D., Kraig M. Theriault, Surya A. Reis, Fen Zhou, Jon M. Madison, Laurence Daheron, Jeanne F. Loring, and Stephen J. Haggarty. 2011. “Epigenetic Characterization of the FMR1 Gene and Aberrant Neurodevelopment in Human Induced Pluripotent Stem Cell Models of Fragile X Syndrome.” *PLoS ONE* 6 (10). doi:10.1371/journal.pone.0026203.

Shilling, Dustin, Marioly Müller, Hajime Takano, Don-On Daniel Mak, Ted Abel, Douglas a Coulter, and J Kevin Foskett. 2014. "Suppression of InsP3 Receptor-Mediated Ca2+ Signaling Alleviates Mutant Presenilin-Linked Familial Alzheimer's Disease Pathogenesis." *The Journal of Neuroscience* 34 (20): 6910–23. doi:10.1523/JNEUROSCI.5441-13.2014.

Shirasaki, T, N Harata, and N Akaike. 1994. "Metabotropic Glutamate Response in Acutely Dissociated Hippocampal CA1 Pyramidal Neurones of the Rat." *The Journal of Physiology* 475 (3): 439–53. doi:10.1113/jphysiol.1994.sp020084.

Shuai, Jianwei, John E Pearson, J Kevin Foskett, Don-On Daniel Mak, and Ian Parker. 2007. "A Kinetic Model of Single and Clustered IP3 Receptors in the Absence of Ca2+ Feedback." *Biophysical Journal* 93 (4): 1151–62. doi:10.1529/biophysj.107.108795.

Slegtenhorst, Marjon van, Ronald de Hoogt, Caroline Hermans, Mark Nellist, Bart Janssen, Senno Verhoef, Dick Lindhout, et al. 1997. "Identification of the Tuberous Sclerosis Gene TSC1 on Chromosome 9q34." *Science* 277 (5327): 805–8.

Smith, Ian F, Brian Hitt, Kim N Green, Salvatore Oddo, and Frank M LaFerla. 2005. "Enhanced Caffeine-Induced Ca2+ Release in the 3xTg-AD Mouse Model of Alzheimer's Disease." *Journal of Neurochemistry* 94 (6): 1711–18. doi:10.1111/j.1471-4159.2005.03332.x.

Smith, Ian F, Steven M Wiltgen, and Ian Parker. 2009. "Localization of Puff Sites Adjacent to the Plasma Membrane: Functional and Spatial Characterization of Ca2+ Signaling in SH-SY5Y Cells Utilizing Membrane-Permeant Caged IP3." *Cell Calcium* 45 (1): 65–76. doi:10.1016/j.ceca.2008.06.001.

Solini, A, P Chiozzi, A Morelli, R Fellin, and F Di Virgilio. 1999. "Human Primary Fibroblasts in Vitro Express a Purinergic P2X7 Receptor Coupled to Ion Fluxes, Microvesicle Formation and IL-6 Release." *Journal of Cell Science* 112 (3): 297–305.

Solini, Anna, Paola Chiozzi, Anna Morelli, Angela Passaro, Renato Fellin, and Francesco Di Virgilio. 2003. "Defective P2Y Purinergic Receptor Function: A Possible Novel Mechanism for Impaired Glucose Transport." *Journal of Cellular Physiology* 197 (3): 435–44. doi:10.1002/jcp.10379.

Splawski, Igor, Katherine W. Timothy, Leah M. Sharpe, Niels Decher, Pradeep Kumar, Raffaella Bloise, Carlo Napolitano, et al. 2004. "CaV1.2 Calcium Channel Dysfunction Causes a Multisystem Disorder Including Arrhythmia and Autism." *Cell* 119 (1): 19–31. doi:10.1016/j.cell.2004.09.011.

Splawski, Igor, Dana S Yoo, Stephanie C Stotz, Allison Cherry, David E Clapham, and Mark T Keating. 2006. "CACNA1H Mutations in Autism Spectrum Disorders." *The Journal of Biological Chemistry* 281 (31): 22085–91. doi:10.1074/jbc.M603316200.

Srinivasan, Rahul, Ben S Huang, Sharmila Venugopal, April D Johnston, Hua Chai, Hongkui Zeng, Peyman Golshani, and Baljit S Khakh. 2015. "Ca2+ Signaling in Astrocytes from Ip3r2−/− Mice in Brain Slices and during Startle Responses in Vivo." *Nature Neuroscience*, 18 (5):708-17. doi:10.1038/nn.4001.

Strom, S P, J L Stone, J R Ten Bosch, B Merriman, R M Cantor, D H Geschwind, and S F

Nelson. 2010. “High-Density SNP Association Study of the 17q21 Chromosomal Region Linked to Autism Identifies CACNA1G as a Novel Candidate Gene.” *Molecular Psychiatry* 15 (10). 996–1005. doi:10.1038/mp.2009.41.

Stutzmann, Grace E.2007. "The Pathogenesis of Alzheimer's Disease - Is It a Lifelong 'Calciumopathy'? *The Neuroscientist* 13 (5):546-59. doi:10.1177/1073858407299730.

Stutzmann, Grace E, Antonella Caccamo, Frank M LaFerla, and Ian Parker. 2004. “Dysregulated IP3 Signaling in Cortical Neurons of Knock-in Mice Expressing an Alzheimer’s-Linked Mutation in presenilin1 Results in Exaggerated Ca2+ Signals and Altered Membrane Excitability.” *The Journal of Neuroscience* 24 (2): 508–13. doi:10.1523/JNEUROSCI.4386-03.2004.

Stutzmann, Grace E, Frank M LaFerla, and Ian Parker. 2003. “Ca2+ Signaling in Mouse Cortical Neurons Studied by Two-Photon Imaging and Photoreleased Inositol Triphosphate.” *The Journal of Neuroscience* 23 (3): 758–65.

Stutzmann, Grace E, Ian Smith, Antonella Caccamo, Salvatore Oddo, Frank M Laferla, and Ian Parker. 2006. “Enhanced Ryanodine Receptor Recruitment Contributes to Ca2+ Disruptions in Young, Adult, and Aged Alzheimer’s Disease Mice.” *The Journal of Neuroscience* 26 (19): 5180–89. doi:10.1523/JNEUROSCI.0739-06.2006.

Südhof, Thomas C. 2008. “Neuroligins and Neurexins Link Synaptic Function to Cognitive Disease.” *Nature* 455 (7215): 903–11. doi:10.1038/nature07456.

Takada, H., K. Furuya, and M. Sokabe. 2014. “Mechanosensitive ATP Release from Hemichannels and Ca2+ Influx through TRPC6 Accelerate Wound Closure in Keratinocytes.” *Journal of Cell Science* 127: 4159–71. doi:10.1242/jcs.147314.

Takahashi, Kazutoshi, and Shinya Yamanaka. 2015. “A Developmental Framework for Induced Pluripotency.” *Development (Cambridge, England)* 142 (19): 3274–85. doi:10.1242/dev.114249.

Takao, Keizo, and Tsuyoshi Miyakawa. 2015. “Genomic Responses in Mouse Models Greatly Mimic Human Inflammatory Diseases.” *Proceedings of the National Academy of Sciences* 112 (4): 1167–72.

Takata, Norio, Tsuneko Mishima, Chihiro Hisatsune, Terumi Nagai, Etsuko Ebisui, Katsuhiko Mikoshiba, and Hajime Hirase. 2011. “Astrocyte Calcium Signaling Transforms Cholinergic Modulation to Cortical Plasticity In Vivo.” *Journal of Neuroscience* 31 (49): 18155–65. doi:10.1523/JNEUROSCI.5289-11.2011.

Takechi, Hajime, Jens Eilers, and Arthur Konnerth. 1998. “A New Class of Synaptic Response Involving Calcium Release in Dendritic Spines.” *Nature* 396 (6713), 757–60. doi:10.1038/25547.

Tang, Guomei, Kathryn Gudsnuk, Sheng-Han Kuo, Marisa L. Cotrina, Gorazd Rosoklija, Alexander Sosunov, Mark S. Sonders, et al. 2014. “Loss of mTOR-Dependent Macroautophagy Causes Autistic-like Synaptic Pruning Deficits.” *Neuron* 83 (5), 1131–43. doi:10.1016/j.neuron.2014.07.040.

Tordoff, M G, and H T Ellis. 2013. “A Mouse with Bad Hair and Poor Taste.” *Appetite* 71 (2013). doi:10.1016/j.appet.2013.06.070.

Tordoff, Michael G, and Hillary T Ellis. 2013. “Taste Dysfunction in BTBR Mice due to a Mutation of Itpr3, the Inositol Triphosphate Receptor 3 Gene.” *Physiological Genomics* 45 (18): 834–55. doi:10.1152/physiolgenomics.00092.2013.

Uddin, Mohammed, Kristiina Tammimies, Giovanna Pellecchia, Babak Alipanahi, Pingzhao Hu, Zhuozhi Wang, Dalila Pinto, et al. 2014. “Brain-Expressed Exons under Purifying Selection Are Enriched for de Novo Mutations in Autism Spectrum Disorder.” *Nature Genetics* 46 (7): 742–47. doi:10.1038/ng.2980.

Urbach, Achia, Ori Bar-Nur, George Q. Daley, and Nissim Benvenisty. 2010. “Differential Modeling of Fragile X Syndrome by Human Embryonic Stem Cells and Induced Pluripotent Stem Cells.” *Cell Stem Cell* 6 (5): 407–11. doi:10.1016/j.stem.2010.04.005.

Valenti, Daniela, Lidia de Bari, Bianca De Filippis, Alexandra Henrion-Caude, and Rosa Anna Vacca. 2014. “Mitochondrial Dysfunction as a Central Actor in Intellectual Disability-Related Diseases: An Overview of Down Syndrome, Autism, Fragile X and Rett Syndrome.” *Neuroscience and Biobehavioral Reviews* 46(2): 202–17. doi:10.1016/j.neubiorev.2014.01.012.

Van De Leemput, Joyce, Jayanth Chandran, Melanie A. Knight, Lynne A. Holtzclaw, Sonja Scholz, Mark R. Cookson, Henry Houlden, et al. 2007. “Deletion at ITPR1 Underlies Ataxia in Mice and Spinocerebellar Ataxia 15 in Humans.” *PLoS Genetics* 3 (6): 1076–82.

doi:10.1371/journal.pgen.0030108.

van De Sande, Marijke M H, Vincent J van Buul, and Fred J P H Brouns. 2014. "Autism and Nutrition: The Role of the Gut-Brain Axis." *Nutrition Research Reviews*, (17): 1–16. doi:10.1017/S0954422414000110.

Van Den Bosch, L., P. Van Damme, E. Bogaert, and W. Robberecht. 2006. "The Role of Excitotoxicity in the Pathogenesis of Amyotrophic Lateral Sclerosis." *Biochimica et Biophysica Acta - Molecular Basis of Disease* 1762 (11–12): 1068–82. doi:10.1016/j.bbadis.2006.05.002.

Van Goor, Fredrick, Sabine Hadida, Peter D J Grootenhuis, Bill Burton, Dong Cao, Tim Neuberger, Amanda Turnbull, et al. 2009. "Rescue of CF Airway Epithelial Cell Function in Vitro by a CFTR Potentiator, VX-770." *Proceedings of the National Academy of Sciences of the United States of America* 106 (44): 18825–30. doi:10.1073/pnas.0904709106.

Van Goor, Fredrick, Sabine Hadida, Peter D J Grootenhuis, Bill Burton, Jeffrey H Stack, Kimberly S Straley, Caroline J Decker, et al. 2011. "Correction of the F508del-CFTR Protein Processing Defect in Vitro by the Investigational Drug VX-809." *Proceedings of the National Academy of Sciences of the United States of America* 108 (46): 18843–48. doi:10.1073/pnas.1105787108.

Vicencio, J M, C Ortiz, A Criollo, A W E Jones, O Kepp, L Galluzzi, N Joza, et al. 2009. "The Inositol 1,4,5-Trisphosphate Receptor Regulates Autophagy through Its Interaction with Beclin 1." *Cell Death and Differentiation* 16 (7): 1006–17. doi:10.1038/cdd.2009.34.

Wallace, Douglas C, Weiwei Fan, and Vincent Procaccio. 2010. "Mitochondrial Energetics and Therapeutics." *Annual Review of Pathology* 5 (January): 297–348. doi:10.1146/annurev.pathol.4.110807.092314.

Wang, Fushun, Nathan A Smith, Qiwu Xu, Takumi Fujita, Akemichi Baba, Toshio Matsuda, Takahiro Takano, Lane Bekar, and Maiken Nedergaard. 2012. "Astrocytes Modulate Neural Network Activity by $Ca^2$+-Dependent Uptake of Extracellular K+." *Science Signaling* 5 (218): ra26. doi:10.1126/scisignal.2002334.

Wang, Lulu W, Elizabeth Berry-Kravis, and Randi J Hagerman. 2010. "Fragile X: Leading the Way for Targeted Treatments in Autism." *Neurotherapeutics : The Journal of the American Society for Experimental NeuroTherapeutics* 7 (3): 264–74. doi:10.1016/j.nurt.2010.05.005.

Wang, Samuel S.-H, Alexander D Kloth, and Aleksandra Badura. 2014. "Neuron Perspective The Cerebellum, Sensitive Periods, and Autism." *Neuron* 83: 518–32. doi:10.1016/j.neuron.2014.07.016.

Waterham, Hans R, and Merel S Ebberink. 2012. "Genetics and Molecular Basis of Human Peroxisome Biogenesis Disorders." *Biochimica et Biophysica Acta* 1822 (9): 1430–41. doi:10.1016/j.bbadis.2012.04.006.

Wei, Hongen, Mazhar Malik, Ashfaq M Sheikh, George Merz, W Ted Brown, and Xiaohong Li. 2011. "Abnormal Cell Properties and down-Regulated FAK-Src Complex Signaling in B Lymphoblasts of Autistic Subjects." *The American Journal of Pathology* 179 (1): 66–74. doi:10.1016/j.ajpath.2011.03.034.

Weinreb, Neal J. 2013. “Oral Small Molecule Therapy for Lysosomal Storage Diseases.” *Pediatric Endocrinology Reviews* 11 (1): 77–90.

West, Paul R., David G. Amaral, Preeti Bais, Alan M. Smith, Laura A. Egnash, Mark E. Ross, Jessica A. Palmer, et al. 2014. “Metabolomics as a Tool for Discovery of Biomarkers of Autism Spectrum Disorder in the Blood Plasma of Children.” *PLoS ONE* 9 (11). doi:10.1371/journal.pone.0112445.

Willsey, A. Jeremy, Stephan J. Sanders, Mingfeng Li, Shan Dong, Andrew T. Tebbenkamp, Rebecca a. Muhle, Steven K. Reilly, et al. 2013. “Coexpression Networks Implicate Human Midfetal Deep Cortical Projection Neurons in the Pathogenesis of Autism.” *Cell* 155 (5): 997–1007. doi:10.1016/j.cell.2013.10.020.

Workman, Alan D, Christine J Charvet, Barbara Clancy, Richard B Darlington, and Barbara L Finlay. 2013. “Modeling Transformations of Neurodevelopmental Sequences across Mammalian Species.” *The Journal of Neuroscience* 33 (17): 7368–83. doi:10.1523/JNEUROSCI.5746-12.2013.

Wu, J., D. A. Ryskamp, X. Liang, P. Egorova, O. Zakharova, G. Hung, and I. Bezprozvanny. 2016. “Enhanced Store-Operated Calcium Entry Leads to Striatal Synaptic Loss in a Huntington’s Disease Mouse Model.” *Journal of Neuroscience* 36 (1): 125–41. doi:10.1523/JNEUROSCI.1038-15.2016.

Yan, Q J, M Rammal, M Tranfaglia, and R P Bauchwitz. 2005. “Suppression of Two Major Fragile X Syndrome Mouse Model Phenotypes by the mGluR5 Antagonist MPEP.”

*Neuropharmacology* 49 (7): 1053–66. doi:10.1016/j.neuropharm.2005.06.004.

Yang, Junhua, Hongbin Yang, Yali Liu, Xia Li, Liming Qin, Huifang Lou, Shumin Duan, and Hao Wang. 2016. "Astrocytes Contribute to Synapse Elimination via Type 2 Inositol 1,4,5-Trisphosphate Receptor-Dependent Release of ATP." *eLife* 5 (APRIL2016): 1–17. doi:10.7554/eLife.15043.

Yao, Y, J Choi, and I Parker. 1995. "Quantal Puffs of Intracellular Ca2+ Evoked by Inositol Trisphosphate in Xenopus Oocytes." *The Journal of Physiology* 482 (3): 533–53.

Yao, Yong, and Ian Parker. 1993. "Inositol Trisphosphate-Mediated Ca2+ Influx into Xenopus Oocytes Triggers Ca2+ Liberation from Intracellular Stores." *J. Physiol.* 468: 275–95.

Ye, Fang, and Charles L Hoppel. 2013. "Measuring Oxidative Phosphorylation in Human Skin Fibroblasts." *Analytical Biochemistry* 437 (1): 52–58. doi:10.1016/j.ab.2013.02.010.

Yu, Timothy W, and Elizabeth Berry-Kravis. 2014. "Autism and Fragile X Syndrome." *Seminars in Neurology* 34 (3): 258–65. doi:10.1055/s-0034-1386764.

Yue, Feng, Yong Cheng, Alessandra Breschi, Jeff Vierstra, Weisheng Wu, Tyrone Ryba, Richard Sandstrom, et al. 2014. "A Comparative Encyclopedia of DNA Elements in the Mouse Genome." *Nature* 515 (7527): 355–64. doi:10.1038/nature13992.

Yuzaki, M, and K Mikoshiba. 1992. "Pharmacological and Immunocytochemical Characterization of Metabotropic Glutamate Receptors in Cultured Purkinje Cells." *The Journal of Neuroscience* 12 (11): 4253–63.

Zaman, Sayed, Umar Yazdani, Yan Deng, Wenhao Li, Bharathi S Gadad, Linda Hynan, David Karp, et al. 2016. “A Search for Blood Biomarkers for Autism: Peptoids.” *Scientific Reports* 6, 19164. doi:10.1038/srep19164.

Zeida´n-Chulia, Fares, Jose´ Luiz Rybarczyk-Filho, Alla B. Salmina, Ben-Hur Neves de Oliveira, Mami Noda, and Jose´ Cla´udio F. Moreira. 2013. “Exploring the Multifactorial Nature of Autism Through Computational Systems Biology: Calcium and the Rho GTPase RAC1 Under the Spotlight.” *Neuromolecular Medicine* 15(2): 364-83. doi:10.1007/s12017-013-8224-3.

Zhang, Ye, Kenian Chen, Steven a Sloan, Mariko L Bennett, Anja R Scholze, Sean O Keeffe, Hemali P Phatnani, et al. 2014. “An RNA-Sequencing Transcriptome and Splicing Database of Glia, Neurons, and Vascular Cells of the Cerebral Cortex.” *The Journal of Neuroscience* 34 (36): 11929–47. doi:10.1523/JNEUROSCI.1860-14.2014.

Ziats, Mark N, and Owen M Rennert. 2011. “Expression Profiling of Autism Candidate Genes during Human Brain Development Implicates Central Immune Signaling Pathways.” *PloS One* 6 (9): e24691. doi:10.1371/journal.pone.0024691.